AD_____

GRANT NUMBER: DAMD17-95-1-5027

TITLE: Cholinesterase Structure: Identification of Residues and Domains Affecting Organophosphate Inhibition and Catalysis

PRINCIPAL INVESTIGATOR: Palmer W. Taylor, Ph.D.

CONTRACTING ORGANIZATION: University of California, San Diego
La Jolla, California 92093-0934

REPORT DATE: April 1998

TYPE OF REPORT: Annual

PREPARED FOR: U.S. Army Medical Research and Materiel Command
Fort Detrick, Frederick, Maryland 21702-5012

REPORT DOCUMENTATION PAGE

Form Approved
OMB No. 0704-0188

1. AGENCY USE ONLY (Leave blank)	2. REPORT DATE	3. REPORT TYPE AND DATES COVERED
	April 1998	Annual (6 Mar 97 - 5 Mar 98)

4. TITLE AND SUBTITLE
Cholinesterase Structure-Identification of Residues and Domains Affecting Organophosphate Inhibition and Catalysis

5. FUNDING NUMBERS
DAMD17-95-1-5027

6. AUTHOR(S)
Palmer W. Taylor, Ph.D.

7. PERFORMING ORGANIZATION NAME(S) AND ADDRESS(ES)
The University of California, San Diego
La Jolla, CA 92093-0934

8. PERFORMING ORGANIZATION REPORT NUMBER

9. SPONSORING/MONITORING AGENCY NAME(S) AND ADDRESS(ES)
U.S. Army Medical Research and Materiel Command
Fort Detrick, Frederick, MD 21702-5012

10. SPONSORING/MONITORING AGENCY REPORT NUMBER

11. SUPPLEMENTARY NOTES

12a. DISTRIBUTION/AVAILABILITY STATEMENT
Approved for public release; distribution unlimited

12b. DISTRIBUTION CODE

13. ABSTRACT (Maximum 200 words)

During the project period we have initiated a completed studies in the following areas:

1) The crystal structure of a mouse acetylcholinesterase-fasciculin 2 complex has provided an essential template for structure-function studies; progress has been made in crystallizing acetylcholinesterasein the absence of fasciculin.
2) Studies of a series of enantiomeric organophosphates reacting with acetylcholinesterase have been completed; they have yielded vital information on their binding orientation in the ground and transition states. Residues on the enzyme governing enantiomer specificity and leaving group orientation have been defined through site-specific mutagenesis.
3) The interactions of fasciculin 2 with acetylcholinesterase have been studied by kinetic and site-specific mutagenesis methods. The fasciculin2-acetylcholinesterase complex has enabled us to study entry of ligands to the active center gorge.
4) Studies in oxime reactivation of cholinesterase inhibited by the enantiomeric phosphates were undertaken using 2-PAM and HI-6 with wild-type and mutant acetylcholinesterases. These studies show two faces of attack between the oxime and the conjugated phosphonate and suggests that the efficacy of oxime reactivation depends on both oxime and conjugating phosphonate structures.

14. SUBJECT TERMS	15. NUMBER OF PAGES
Cholinesterase Structure, Organophosphate, Inhibition and Catalysis, Acetylcholinesterase, Enantiomers, Oxime Reactivators Fasciculin, X-ray Crystal Structure, Site-Specific Mutagenesis	49
	16. PRICE CODE

17. SECURITY CLASSIFICATION OF REPORT	18. SECURITY CLASSIFICATION OF THIS PAGE	19. SECURITY CLASSIFICATION OF ABSTRACT	20. LIMITATION OF ABSTRACT
Unclassified	Unclassified	Unclassified	Unlimited

NSN 7540-01-280-5500

Standard Form 298 (Rev 2-89)
Prescribed by ANSI Std Z39-18
298-102

FOREWORD

Opinions, interpretations, conclusions and recommendations are those of the author and are not necessarily endorsed by the US Army.

____ Where copyrighted material is quoted, permission has been obtained to use such material.

____ Where material from documents designated for limited distribution is quoted, permission has been obtained to use the material.

____ Citations of commercial organizations and trade names in this report do not constitute an official Department of Army endorsement or approval of the products or services of these organizations.

____ In conducting research using animals, the investigator(s) adhered to the "Guide for the Care and Use of Laboratory Animals," prepared by the Committee on Care and Use of Laboratory Animals of the Institute of Laboratory Resources, National Research Council (NIH Publication No. 86-23, Revised 1985).

____ For the protection of human subjects, the investigator(s) adhered to policies of applicable Federal Law 45 CFR 46.

__X__ In conducting research utilizing recombinant DNA technology, the investigator(s) adhered to current guidelines promulgated by the National Institutes of Health.

__X__ In the conduct of research utilizing recombinant DNA, the investigator(s) adhered to the NIH Guidelines for Research Involving Recombinant DNA Molecules.

__X__ In the conduct of research involving hazardous organisms, the investigator(s) adhered to the CDC-NIH Guide for Biosafety in Microbiological and Biomedical Laboratories.

PI - Signature 6/20/98 Date

TABLE OF CONTENTS:

Page #'s

(5) INTRODUCTION:

Our project, beginning in April of 1995 and completed in March of 1998, was directed towards examining ligand interactions, particularly organophosphates and oximes, with recombinant DNA-derived AChE by kinetic, physicochemical and computational methods. The studies are oriented to analyzing mechanisms of inhibition by organophosphates, the spontaneous hydrolysis and reactivation by oximes of AChE conjugated with organophosphates and the sites of interaction of reversible inhibitors. These studies have allowed us to not only gain an understanding of the mechanisms of AChE catalysis, inhibition and reactivation, but also develop recombinant DNA derived cholinesterases as potentially useful prophylatic agents and antidotes for organophosphate poisoning.

(6) BODY:

A. Recombinant DNA-derived Acetylcholinesterase and the Crystal Structure Template

Our studies have employed site-specific mutagenesis, kinetic analysis, X-ray crystallography, fluorescence spectroscopy and structure-guided ligand design. In the initial year, we developed procedures for production of large quantities of mammalian AChE by expression in cell culture from cDNAs to be used for crystallization of homogeneous enzyme (6P). The procedure involves selection by aminoglycoside resistance of high expressing clones from human embryonic kidney (HEK-293) cells in which the gene has been stably incorporated into chromosomal DNA, growth of cells in serum free media on multilayer plates, harvesting of the media containing secreted AChE and affinity chromatography to purify the enzyme. To date, we have purified over 2 grams of AChE and supplied it to many investigators around the world for their studies. We believe that our success in obtaining AChE with a homogeneity suitable for crystallization stems from large scale production in mammalian cells over short periods of time to minimize autolysis. With the recombinant DNA derived enzyme, we were able to solve the crystal structure of the fasciculin-AChE complex (5P). Since this is the first mammalian AChE structure to be reported, it serves as a template for the analysis of structure. Most of the mutagenesis work conducted in our laboratory and other laboratories now involves mammalian AChE, rather than *Torpedo* AChE (1,2), and this provides the impetus for structural studies on this enzyme.

In collaboration with Drs. Yves Bourne and Pascale Marchot, we have also succeeded in obtaining crystals of the mouse enzyme in the absence of fasciculin. New data have been collected on the synchrotron in Grenoble which should yield a structure at 2.8 to 3Å resolution. The initial diffraction patterns show that the back side of each AChE molecule (the small omega loop containing the Cys265-Cys272 disulfide) adopts the position on a neighboring subunit in the tetrameric unit crystal corresponding to loop II of fasciculin in the fasciculin 2-AChE complex. However, the gorge remains in its narrow or closed state. The tetramer of AChE appears as a square planar structure with about a 30° twist from planarity. It is organized as a dimer of dimers. The basic dimer is held together by the four helix bundle found with the fasciculin complex, while each dimer associates by the small omega loop inserting into the mouth of the gorge of the paired subunit. Each dimer pair lies in an antiparallel configuration with one active center occluded by the omega loop and the other exposed to solvent. Hence, the overall configuration shows two exposed and two occluded active center portals. The implications of this structure with respect to attachment of structural subunits and regulation of catalysis have yet to be fully assessed. Nevertheless, with paired open and occluded active centers in the tetramer, the ease of ligand penetration to the active centers in crystals soaked with ligand will be of interest.

B. Studies of Enantiomeric Specificity of the Organophosphates

Fig. 1: Structures of the organophosphates and Oximes Used in this study

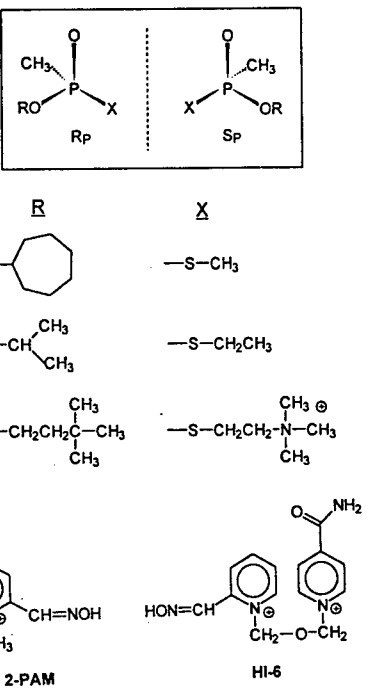

Studies examining the kinetics of reaction for a series of Rp- and Sp-alkyl methylphosphonylcholines and neutral Rp- and Sp-alkyl methylphosphonylthioates of known absolute stereochemistry (fig. 1 and Scheme I) with wild-type and mutant AChEs are now complete (Tables 1-4). Data for several charged residue and acyl pocket mutations have been analyzed by a thermodynamic mutant cycle analysis in three dimensions (X = R- and S-enantiomers; Y = charge on the leaving group thioate; Z = acyl pocket substitutions (4P,5P) (Scheme II). The data reveal that: (a) Rp and Sp chiral preference for reaction is dictated primarily by acyl pocket dimensions, restricted particularly by the 297 residue side chain. By mutation from Phe to Ile at the 297 position, the S- to R-chiral preference in reactivity inverts going from 250 to 0.3. (b) Asp74, but neither Glu202 nor Glu450, governs the enhanced reactivity of the cationic organophosphates, (c) ligand orientation in the transition state requires that: (1) the phosphonyl oxygen fit in the oxyanion hole, (2) the phosphorus be positioned for nucleophilic attack by the serine and (3) the leaving group be positioned to exit from the gorge (approximately axial to the attacking serine). Three dimensional plots of free energy change ($\Delta\Delta G^{\ddagger}$) versus enantiomer ratio and leaving group charge (fig. 2 A & B) clearly distinguish the structural determinants for enantiomeric selectivity and reactivity of cationic and neutral ligands (6P).

Scheme 1

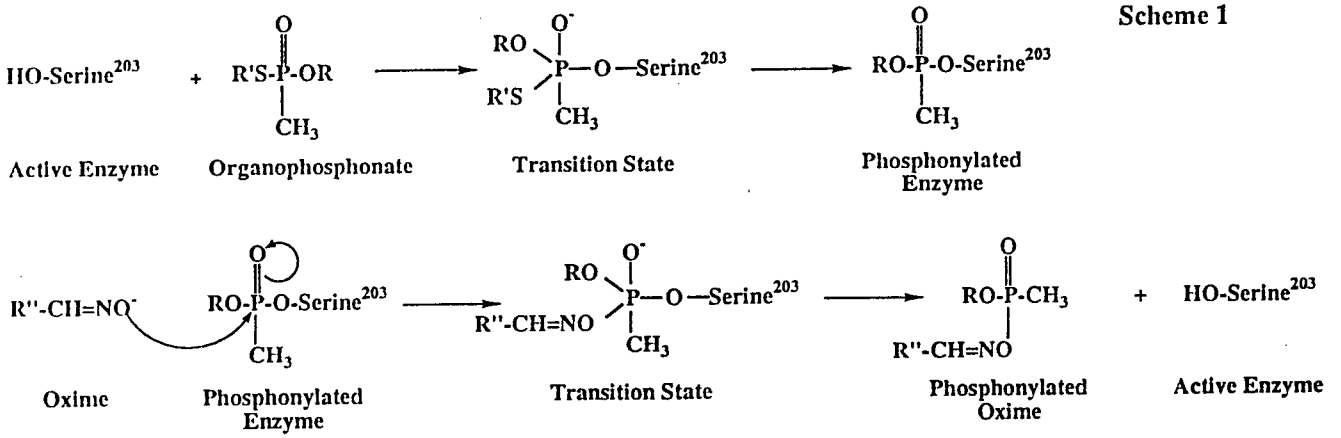

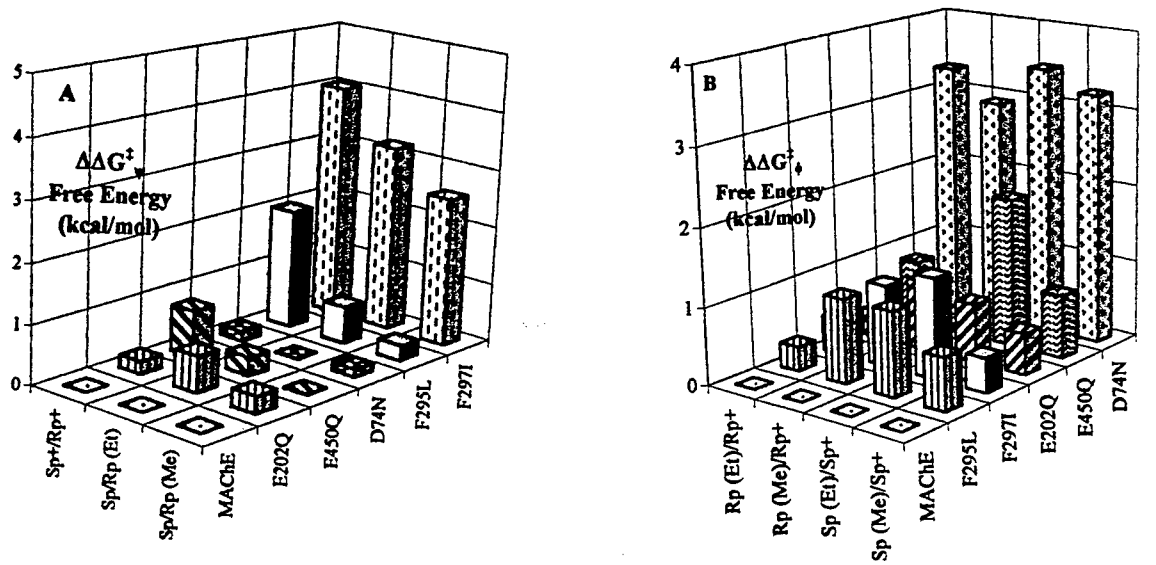

Figure 2: Relationship between the change in free energy of activation, selected mutations in acetylcholinesterase, and structures of cycloheptyl methylphosphonyl thioates. (A) Selectivity for the Sp and Rp enantiomers. (B) Selectivity for charged and uncharged jphosphonates: +, cationic cyclopheptyl methylphosphonyl thiocholine; Me, uncharged cycloheptyl methylphosphonyl thiomethane; and Et, uncharged cycloheptyl methylphosphonyl thioethane. The scheme for the thermodynamic mutant cycle analysis is shown in Scheme II and in reference 7P.

Analysis of enantiomeric selectivity is a powerful tool for understanding reaction mechanism, for the two enantiomers in the absence of a dissymmetric surface are chemically identical. The data in Tables 1-4 and in Fig. 2 1 show up to a 500-fold difference in reactivity of the Rp and Sp enantiomers and differences of this magnitude approach the chiral purity of the compounds. Over 65 years ago, Eason and Stedman (3) proposed that chiral selectivity of enzymes arose from a three point attachment of the chiral molecule with a dissymmetric surface. Applying this concept to the transition state of the organophosphates shows that: (a) insertion of the phosphonyl oxygen in the oxyanion hole, (b) the attack of the phosphorus by the γ-hydroxyl of the serine, and (c) the orientation of the leaving group out the gorge exit constitute three essential elements for a productive interaction. Moreover, spatial constraints within the acyl pocket in the absence of mutation of the acyl pocket phenylalanines to smaller side chains preclude this from being an optimal orientation for the Rp isomers since the bulky alkoxy groups show steric interference with the phenylalanines in the acyl pocket (figs. 3 and 4). The analysis has also been approached by computational docking and molecular dynamics (8P), and shows that only with the R isomer can we achieve the appropriate hydrogen bonding in the oxyganion hole and orientation of the leaving group out the gorge exit (fig. 5). These analyses are based on the X,Y plane encompassing the plane of the phosphorus-γ serine oxygen distance. Further analysis of the configuration of the conjugated phosphorus will be important for studies of oxime reactivation.

C. Studies on Modes of Ligand Entry to the Active Center of Acetylcholinesterase

The crystal structure of mouse AChE with fasciculin (Fas2) shows this 6,500 Da peptide plugs the gorge entry. The interactive surface area encompasses 1100A^2 or 28% of the surface area of fasciculin (5P). This raises the question of why residual activity in the Fas2-AChE complex remains (0.1% for ACh but higher for *p*-nitrophenylacetate) (3P,11P). Moreover, inhibitors like trifluoroacetophenones and organophosphates, can still access the active center, albeit more slowly (3P,11P). To examine the mode of ligand entry, we conducted an extensive study of the ionic strength dependence of ligand association wherein surface residues on the enzyme are modified to reduce the net negative charge on the enzyme (10P,11P). Association rates of cationic ligands (*m*-trimethylammoniotrifluoroacetophenone (TFK$^+$), echothiophate (a cationic organophosphate) and fasciculin, (a cationic peptide) decrease with an increase in ionic strength showing the masking effect of ionic strength on the electrostatic attraction between the cationic ligand and the anionic enzyme. The influence is roughly proportional to the charge on the respective ligands...fasciculin (+4) and TFK$^+$ (+1). Neutralization of anionic residues on the enzyme, aspartate and glutamate, by site-specific mutagenesis to the corresponding carboxamides, also results in

Scheme II: Free Energy Relationships for Mutant Cycle Analysis of Charged and Uncharged Analogs of Rp- and Sp-Alkoxy Methylphosphonates with Wild Type and Mutant Acetylcholinesterase.

Scheme II

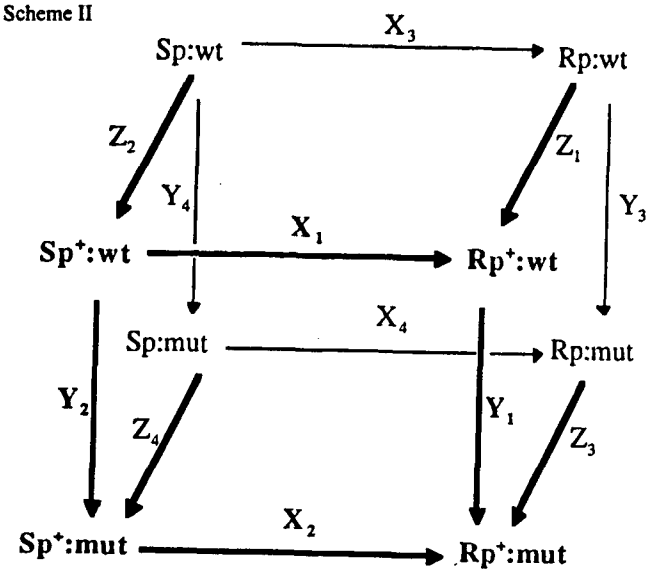

Mutant Cycle Analysis and Orientation of the Phosphonates. In Scheme II, enantiomeric selectivities of the bimolecular rate constants for organophosphonate reaction with AChE [i.e. $k(S_p{:}wt)$] in relation to the mutations (XY planes) are defined by

$$\psi_+ = \frac{S_p^+}{R_p^+} = \frac{X_1}{X_2} = \frac{Y_2}{Y_1} = \frac{k(S_p^+{:}wt)k(R_p^+{:}mut)}{k(R_p^+{:}wt)k(S_p^+{:}mut)} \quad (1)$$

$$\psi_o = \frac{S_p}{R_p} = \frac{X_3}{X_4} = \frac{Y_4}{Y_3} = \frac{k(S_p{:}wt)k(R_p{:}mut)}{k(R_p{:}wt)k(S_p{:}mut)} \quad (2)$$

The electrostatic influence of charge on the leaving group with respect to the mutations (*ZY* planes) is defined by

$$\phi_S = \frac{S_p}{S_p^+} = \frac{Z_2}{Z_4} = \frac{Y_4}{Y_2} = \frac{k(S_p{:}wt)k(S_p^+{:}mut)}{k(S_p^+{:}wt)k(S_p{:}mut)} \quad (3)$$

$$\phi_R = \frac{R_p}{R_p^+} = \frac{Z_1}{Z_3} = \frac{Y_3}{Y_1} = \frac{k(R_p{:}wt)k(R_p^+{:}mut)}{k(R_p^+{:}wt)k(R_p{:}mut)} \quad (4)$$

These values are represented as absolute values without reference to sign. They may be converted to the change in free energy of activation for the corresponding reactions, $\Delta\Delta G^{\ddagger}$, where

$$\psi_+^{\ddagger} = RT \ln \psi_+ \quad (5)$$

$$\psi_o^{\ddagger} = RT \ln \psi_o \quad (6)$$

$$\phi_S^{\ddagger} = RT \ln \phi_S \quad (7)$$

$$\phi_R^{\ddagger} = RT \ln \phi_R \quad (8)$$

and $R = 1.99 \times 10^{-3}$ kcal mol^{-1} K^{-1} and $T = 298$ K.

Table 1: Bimolecular Rate Constants (min^{-1} M^{-1}) Determined for the Inhibition of Recombinant DNA-Derived Mouse Cholinesterases by Alkyl Methylphosphonyl Thiocholine Enantiomers[a]

	cycloheptyl methylphosphonyl thiocholine			isopropyl methylphosphonyl thiocholine			3,3-dimethylbutyl methylphosphyl thiocholine		
enzyme	$S_p \times 10^6$	$R_p \times 10^6$	S_p/R_p	$S_p \times 10^6$	$R_p \times 10^6$	S_p/R_p	$S_p \times 10^6$	$R_p \times 10^6$	S_p/R_p
AChE	190 ± 30	0.81 ± 0.09	230	16 ± 1	0.14 ± 0.03	110	360 ± 10	19 ± 9	19
BuChE	470 ± 90	6.7 ± 0.7	70	10 ± 1	3.3 ± 0.1	3	500 ± 150	32 ± 16	16
F295A	290 ± 50	7.1 ± 0.7	37	16 ± 1	1.2 ± 0.1	14	530 ± 40	15 ± 0	35
F295L	66 ± 9	8.7 ± 1.1	7.6	3.4 ± 0.1	1.2 ± 0.1	3	140 ± 10	10 ± 5	14
F297A	17 ± 4	2.4 ± 0.3	7.1	1.5 ± 0.3	0.098 ± 0.012	15	56 ± 1	1.8 ± 0.1	31
F297I	16 ± 3	62 ± 3	0.3	0.95 ± 0.46	1.2 ± 0.1	0.8	56 ± 4	12 ± 4	5

[a] Data shown as means ± standard deviations.

Table 2: Bimolecular Rate Constants (k_i in min^{-1} M^{-1}) for the Inhibition of Recombinant DNA-Derived Cholinesterases by Neutral (S_p)- and (R_p)-Cycloheptyl Methylphosphonyl Thioates[a]

	leaving group					
	S-methyl			*S*-ethyl		
enzyme	$S_p \times 10^4$	$R_p \times 10^4$	S_p/R_p	$S_p \times 10^4$	$R_p \times 10^4$	S_p/R_p
AChE	31 ± 4	0.18 ± 0.07	170	7.6 ± 0.5	0.018 ± 0.002	420
BuChE	23 ± 6	0.25 ± 0.07	92	13 ± 1	0.17 ± 0.02	76
F295L	34 ± 2	0.29 ± 0.11	120	16 ± 2	0.100 ± 0.03	160
F297I	5.5 ± 0.1	2.2 ± 0.4	2.5	5.5 ± 1.3	2.6 ± 0.6	2.1

[a] Data shown as means ± standard deviations.

Table 3: Bimolecular Rate Constants (10^3 M^{-1} min^{-1})[a] Determined for the Inhibition of Recombinant DNA-Derived Mouse Cholinesterases with Mutations of Anionic Residues by (a) Alkyl Methylphosphonyl Thiocholine Enantiomers and (b) Cycloheptyl Methylphosphonyl Thioate Enantiomers

(a) alkyl substitution	cycloheptyl			isopropyl			3,3-dimethylbutyl		
enzyme	S_p	R_p	S_p/R_p	S_p	R_p	S_p/R_p	S_p	R_p	S_p/R_p
AChE	190000 ± 20000	820 ± 50	230	16000 ± 1000	150 ± 10	110	400000 ± 40000	11000 ± 1000	36
D74N	1400 ± 200	8.0 ± 0.2	180	110 ± 10	1.7 ± 0.3	65	11000 ± 2000	230 ± 20	48
E202Q	21000 ± 2000	130 ± 10	160	490 ± 20	38 ± 2	13	120000 ± 10000	2700 ± 100	44
E450Q	1400 ± 300	23 ± 3	61	180 ± 20	5.9 ± 0.3	31	12000 ± 3000	490 ± 60	24

(b) thioate substitution	SCH_3			SCH_2CH_3		
enzyme	S_p	R_p	S_p/R_p	S_p	R_p	S_p/R_p
AChE	310 ± 20	1.7 ± 0.3	180	74 ± 5	0.16 ± 0.02	460
D74N	530 ± 50	2.3 ± 0.2	230	190 ± 30	0.41 ± 0.04	460
E202Q	14 ± 1	0.060 ± 0.004	230	2.3 ± 0.3	0.014 ± 0.001	160
E450Q	9.0 ± 0.4	0.050 ± 0.002	180	14 ± 2	0.018 ± 0.004	780

[a] Data shown as means ± standard error of the mean typically from three measurements.

Table 4: Bimolecular Rate Constants (10^3 M^{-1} min^{-1})[a] Determined for the Inhibition of Recombinant DNA-Derived Mouse Cholinesterases with Mutations of Aromatic Residues by (a) Alkyl Methylphosphonyl Thiocholine Enantiomers and (b) Cycloheptyl Methylphosphonyl Thioate Enantiomers

(a) alkyl substitution	cycloheptyl			isopropyl			3,3-dimethylbutyl		
enzyme	S_p	R_p	S_p/R_p	S_p	R_p	S_p/R_p	S_p	R_p	S_p/R_p
AChE	190000 ± 20000	820 ± 50	230	16000 ± 1000	150 ± 10	110	400000 ± 40000	11000 ± 1000	36
W86A	4800 ± 1100	25 ± 5	190	43 ± 6	23 ± 7	1.9	37000 ± 14000	1700 ± 200	22
Y337A	120000 ± 10000	840 ± 40	140	24000 ± 3000	340 ± 40	71	750000 ± 20000	19000 ± 1000	39
Y337F	720000 ± 30000	3700 ± 100	190	140000 ± 10000	1000 ± 100	140	1100000 ± 100000	30000 ± 1000	37
W286A	230000 ± 20000	2000 ± 100	120	20000 ± 1000	230 ± 10	87	470000 ± 30000	13000 ± 1000	36
W286R	45000 ± 2000	350 ± 10	130	8700 ± 600	98 ± 2	89	60000 ± 1000	1800 ± 100	33

(b) thioate substitution	SCH_3			SCH_2CH_3		
enzyme	S_p	R_p	S_p/R_p	S_p	R_p	S_p/R_p
AChE	310 ± 20	1.7 ± 0.3	180	74 ± 5	0.16 ± 0.02	460
W86A	170 ± 20	0.75 ± 0.01	230	63 ± 9	0.27 ± 0.002	230
Y337A	81 ± 4	0.46 ± 0.02	180	27 ± 2	0.047 ± 0.002	570
Y337F	320 ± 10	0.94 ± 0.04	340	92 ± 8	0.13 ± 0.02	710
W286A	530 ± 40	1.6 ± 0.2	330	160 ± 10	0.43 ± 0.09	370
W286R	710 ± 30	2.1 ± 0.2	340	200 ± 30	0.35 ± 0.09	570

[a] Data shown as means ± standard error of the mean typically from three measurements.

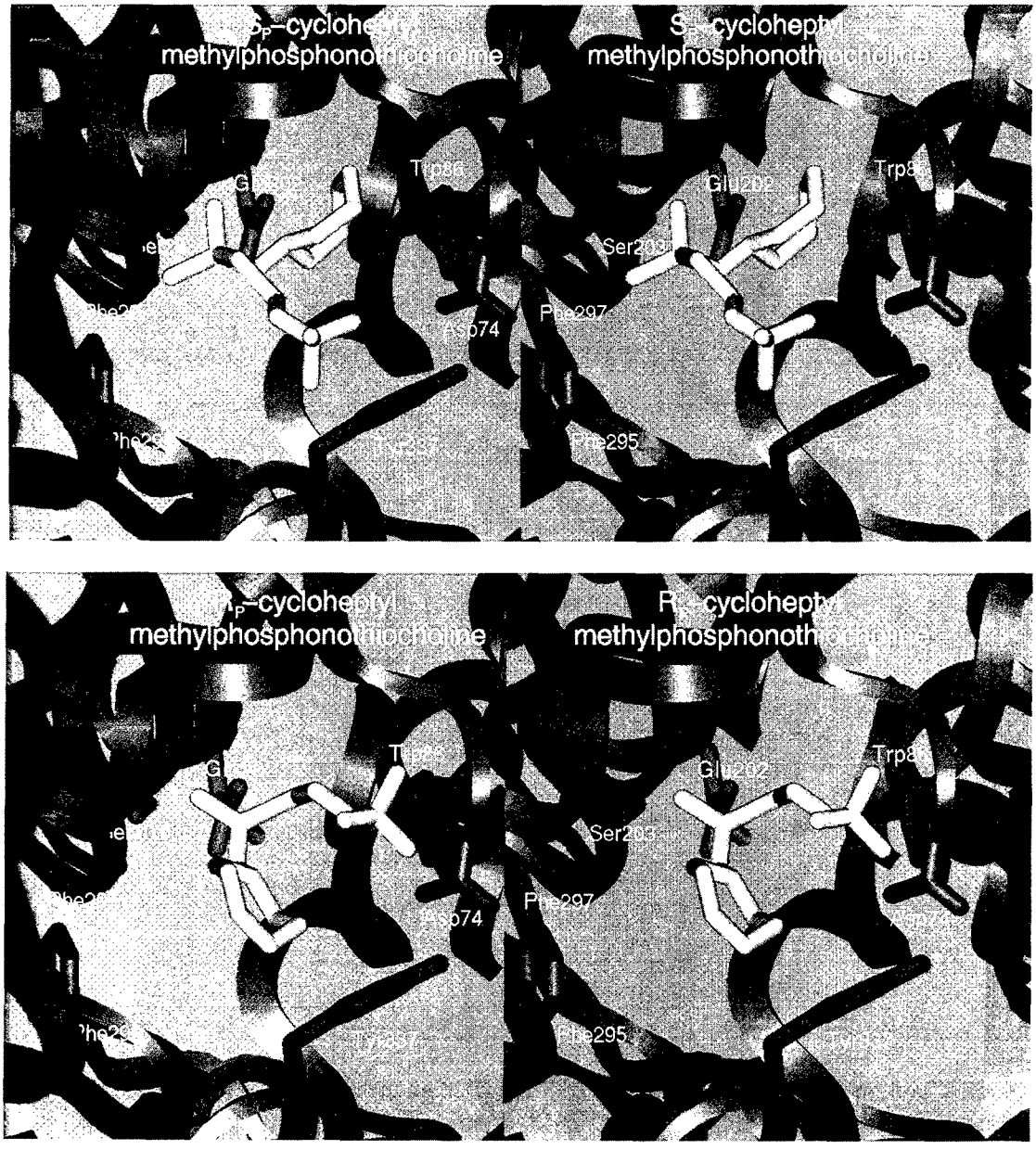

Figure 3: Stereoviews of Sp- and Rp-cycloheptyl methylphosphonothiocholine docked in the active center of mouse acetylcholinesterase. Residues of the acyl pocket (Phe 295 and 297), choline binding subsite (Trp 86, Tyr 337, Glu 202) are shown ref. 7P,8P for details). The phosphonate is positioned for attack by serine 203 and the phosphonyl oxygen is positioned in the oxyanion hole.

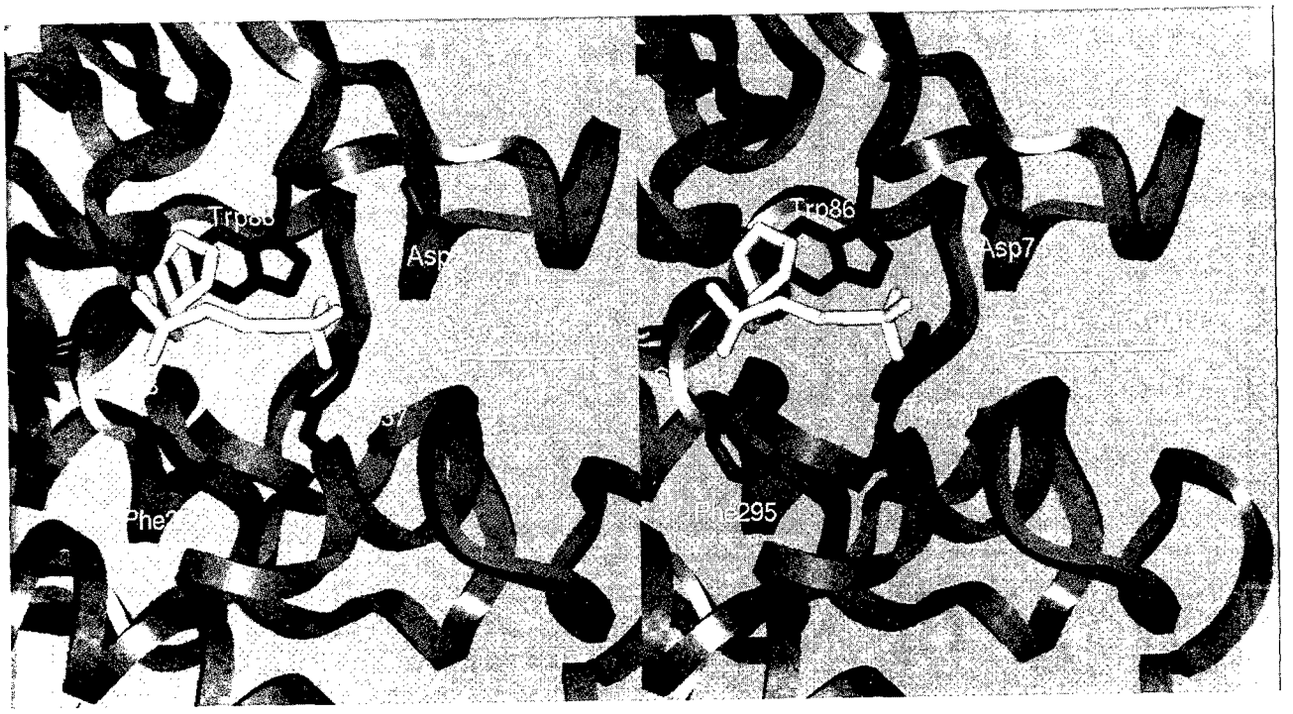

Figure 4: Stereoview of Sp-cycloheptyl methylphosphonothiocholine docked in the active center of acetylcholinesterase. The view is a side view from Figure 4 to show the orientation of the thiocholine moiety with respect to the gorge exit and Asp 74. A portion of the cholinesterase molecule on the acyl pocket side is cut away in order to show an unobstructed view of the inhibitor (cf: refs. 7P, 8P for details).

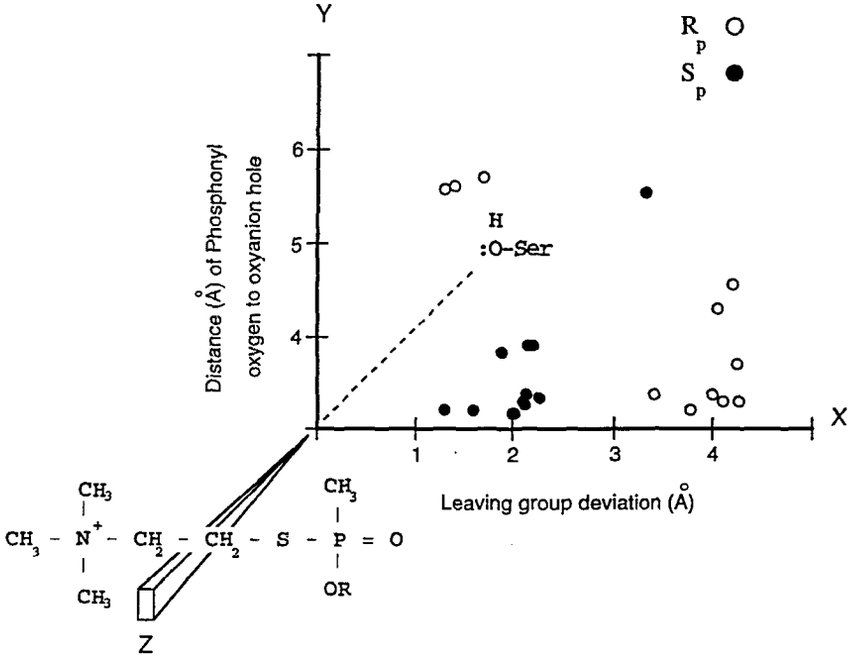

Figure 5: Molecular dynamics simulation followed by energy minimization of a docked Sp(closed circles) and Rp (open circles) cycloheptyl methylphosphonothiocholine in a reversible complex with acetylcholinesterase. The phosphorus group is docked within bonding distance with the γ-oxygen of serine 203 in the enzyme. This reaction position along the Z axis then becomes defined by the plane X, Y. A productive conformation is assumed to require: (a) the appropriate Ser-O-P distance on the Z axis (i.e., the X, Y plane); (b) insertion of the phosphonyl oxygen in the oxyanion hole (Y axis): a mean hydrogen bonding distance of 3-4 Å with the amide backbone hydrogens of Gly 121, Gly 122 and Ala 204; and (c) an orientation of the leaving group directed towards gorge entrance. The ideal position is assumed to be 180 degrees from the attacking serine oxygen placing the serine oxygen and the leaving group in apical positions and the remaining three groups in equatorial positions. The deviations reflect the difference in distances for the quaternary nitrogen between the energy minimized position and that expected for apical positioning (180°) of the serine γ-oxygen and the leaving group. Modified from reference 8P.

a predictable diminution in the electrostatic enhancement of rate (fig. 6 and Tables 5A and B). No effect of ionic strength is seen for the dissociation rates of the two ligands. The neutral isosteric, m(t-butyl)-trifluoroacetophenone (TFK°) is employed as a control to correct for ionic strength dependent changes in conformation.

Of paramount interest is the influence of bound fasciculin on the ionic strength dependence of TFK^+ association. Here the masking effect of increased ionic strength actually accelerates the reaction of TFK^+ with the fasciculin-AChE complex. Hence, the dependence of ionic strength on TFK^+ association with the fasciculin-AChE complex and with AChE alone go in opposite directions. This inverted influence is not seen when the net negative charge on the enzyme is reduced by +4 (i.e., equivalent to the charge on fasciculin) through mutation of four Glu and Asp residues to Gln and Asn (11P). The entering TFK^+ projectile path must traverse close to the bound fasciculin, and the transition state for TFK^+ diffusion into the gorge of restricted dimensions is reflected in cationic repulsion and the proximity of TFK^+ to fasciculin. Hence, TFK^+ even in the presence of fasciculin, appears not diffuse into the enzyme active center through another portal of entry. By selective mutagenesis of charged residues of the Fas2-AChE interface, we may be able to pinpoint the actual trajectory of ligand entry in the Fas2 complex.

D. Studies on Oxime Reactivation of Phosphoryl- and Phosphonyl-conjugated Cholinesterases

Having accumulated substantial data on enantiomeric selectivity for the phosphorylation reaction with wild-type and mutant enzymes, we have begun to study oxime reactivation of the enantiomeric phosphonyl-AChE conjugates (actually diastereoisomers). The data base for this is our previous work on oxime reactivation of the ethoxymethylphosponyl conjugate (1P) where an enantiomeric pair was used to give unresolved R_p and S_p-ethyl methylphosphonyl-AChE. We are now using the resolved conjugates R_p and S_p cycloheptyl-; 3,3 dimethylbutyl-; and isopropyl-methyl phosphonyl AChE (Fig. 1) to study the stereochemistry of oxime reactivation. The non-chiral dimethoxy phosphoryl enzyme is used as a frame of reference.

The chiral phosphonates are identical to those used previously and were synthesized by Dr. Harvey Berman (4,5,6). Table 6 shows some of the initial data we have accumulated for 2-PAM and HI-6 reactivation of the conjugates formed with the Sp phosphonates. First, we note that bulky residues impact the gorge and impede oxime attack. Hence, the dimethoxy phosphoryl enzyme was found to be the most susceptible to reactivation (data not shown). Moreover, the Sp compounds, which are the more reactive phsophonylating agents, are fortunately the most susceptible to reactivation. This illustrates the role for both the positioning of the phosphonyl oxygen in the oxyanion hole for the reactivation step and the interference of the gorge impacting alkoxy group in precluding access of the oxime. The insertion of the phosphonyl oxygen in the oxyanion hole is of equal importance to lowering the transition state energy for oxime attack as it is to forming the initial phosphonyl conjugate. Hence, both reactions appear to proceed through formation of pentavalent intermediates. However, it is worth noting that the acylation reaction proceeds at three to five orders of magnitude more rapidly when analyzed either as a bimolecular rate constant or as a maximum rate at saturating concentrations of ligand.

Mutation of residues in the acyl pocket also yields an interesting phenomenon where mutation of phenylalanine 297 (F297I) enhances the rate of 2-PAM reactivation while mutation of phenylalanine 295 (F295L) enhances the rate of HI-6 reactivation (Table 6). This appears to be independent of the Sp conjugating phosphonate with the influence of the mutation being more dramatic with the more bulky residue. This suggests that the attack angles of HI6 and 2PAM differ and can be optimized from mutagenesis at distinct positions for the two compounds (fig. 7).

This observation also takes on practical significance since the combination of an oxime and circulating cholinesterase is a potential scavenging pair for protection from organophosphate toxicity. A blood-borne cholinesterase at best can scavenge with a one to one stoichiometry and because of the molecular weight differences (139 for Sarin and ~75,000 for the AChE subunit), substantial quantities of AChE would have to be administered to be effective (7). To change the reaction from one of a stoichiometric nature to catalytic would reduce the amount

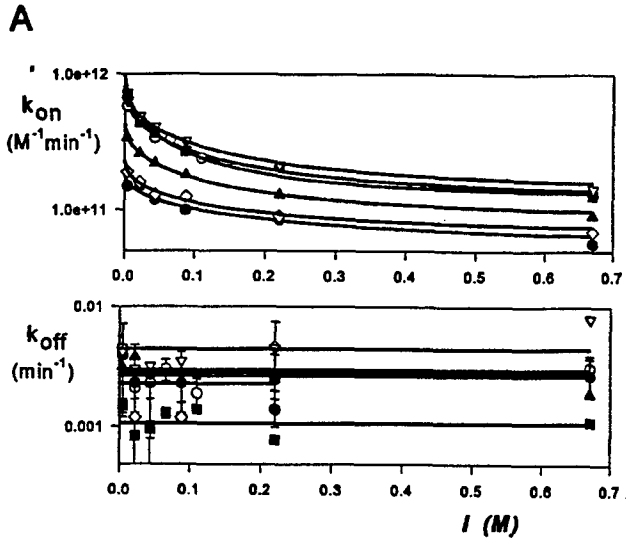

Fig 6A: Ionic strength dependence of TFK^+ second-order association rate constant (k_{on}) and first-order dissociation constant (k_{off}) with wild-type (■) and mutant mouse AChEs. All *curves* were calculated as a best fit of data to Eq. below, surface mutants: D280V (▽), D280V/D283N (○), E84Q/D280V/D283N (▲), E84Q/E91Q/D280V/D283N/D272N (◇), and E84Q/E91Q/D280V/D283N/E292Q/D372N (●). Active Center mutants: D74N (▲), E202Q (○), E450Q (●), and D74N/E202Q (◇).

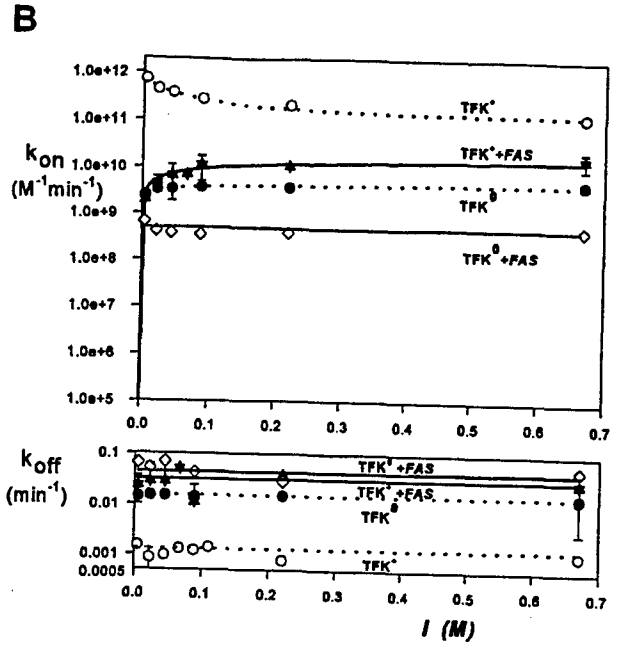

Fig. 6B: Ionic strength dependences of rate constants for ligands and AChE FAS2 complex (solid lines) and AChE alone (dashed lines). *Curves* were calculated as best fits of the data to Eq. below, association (kon) and dissociation (k_{off}) rate constants of inhibitors.

Table 5

Rate constants for TFK^+ association and dissociation with wild-type and mutant mouse AChEs in media of varying ionic strength

k_{on}^0 and k_{on}^H are second-order association rate constants at 0 and 670 mM ionic strength, respectively. z_E and z_I are charges of the enzyme and ligand, respectively, involved in interaction. Constants k_{on}^0 and z_E were obtained by nonlinear regression analysis of Equation 2 using fixed values of k_{on}^H and z_I, from experimental data presented in Fig. 5. k_{on}^0 and k_{on}^H were corrected for TFK^+ hydration. First-order dissociation rate constants k_{off} were calculated as means of values obtained at different ionic strengths.

	Enzyme	k_{on}^0	k_{on}^H	z_I	z_E	k_{off}
		$10^{11}\ M^{-1}\ min^{-1}$	$10^{11}\ M^{-1}\ min^{-1}$			$10^{-3}\ min^{-1}$
A	Wild type	9.8 ± 0.6	1.3	+1	−2.3 ± 0.2	1.1 ± 0.3
		Surface mutants				
	D280V	8.2 ± 2.0	1.5	+1	−1.7 ± 0.1	4.8 ± 2.8
	D280V/D283N	7.6 ± 0.3	1.3	+1	−1.8 ± 0.1	2.6 ± 0.4
	E84Q/E91Q/D280V/D283N	4.3± 0.8	0.92	+1	−1.7 ± 0.1	1.7 ± 0.8
	E84Q/E91Q/D280V/D283N/D372N	2.3± 0.1	0.70	+1	−1.5 ± 0.2	2.3 ± 2.0
	E84Q/E91Q/D280V/D283N/E292Q/D372N	1.8± 0.1	0.57	+1	−1.2 ± 0.2	2.8 ± 1.4
		Active center mutants				
	D74N	0.39 ± 0.01	0.055	+1	−3.2 ± 0.1	5.5 ± 4.4
	E202Q	7.9 ± 0.4	0.77	+1	−2.6 ± 0.2	59 ± 5
	E450Q	1.2 ± 0.1	0.31	+1	−1.3 ± 0.1	123 ± 23
	D74N/E202Q	0.14 ± 0.01	0.016	+1	−2.5 ± 0.4	94 ± 28
	D74N/E202Q/E450Q	≤0.14	≤0.016	+1	—	≥94
		Active center and surface mutants				
	D74N/D280V/D283N	3.1± 0.2	0.90	+1	−2.6 ± 0.3	2.3 ± 0.7

Rate constants for association and dissociation of inhibitors and for turnover of substrates with wild-type mouse AChE · FAS2 complex in media of varying ionic strength

k_{on}^0 and k_{on}^H are inhibitor second-order association rate constants at 0 and 670 mM ionic strengths, respectively. $(k_{cat}/K_m)^0$ and $(k_{cat}/K_m)^H$ are second-order reaction rate constants for substrate turnover at 0 and 670 mM ionic strengths, respectively. z_E and z_I are charges of the enzyme and ligand, respectively, involved in the interaction. Constants k_{on}^0 and z_E for TFK^+ were obtained by nonlinear regression analysis of Equation 2 using fixed values of k_{on}^H and z_I, from experimental data presented in Fig 7. k_{on}^0 and k_{on}^H were corrected for TFK^+ and TFK^0 hydration. The first-order dissociation rate constant k_{off}, constants k_{on}^0 and k_{on}^H for TFK^0 and constants $(k_{cat}/K_m)^0$ and $(k_{cat}/K_m)^H$ for substrates were calculated as a mean of values obtained at different ionic strengths. Dashes indicate indeterminant parameters.

	Ligand	k_{on}^0	k_{on}^H	z_I	z_E	k_{off}
		$10^9\ M^{-1}\ min^{-1}$	$10^9\ M^{-1}\ min^{-1}$			$10^{-3}\ min^{-1}$
B	TFK^+	≤2	17	+1	+0.9 ± 0.2	30 ± 11
	TFK^0	0.46 ± 0.11	0.46	0	—	52± 14
	Substrate	$(k_{cat}/K_m)^0$	$(k_{cat}/K_m)^H$	z_I	z_E	
		$10^6\ M^{-1}\ min^{-1}$	$10^6\ M^{-1}\ min^{-1}$			
	ATCh	2.7 ± 2.8	2.7	+1	0	
	PNPhAc	0.52 ± 0.08	0.52	0	—	

of cholinesterase required (7). Since the organophosphate-AChE reaction is rapid, the rate limitation is recovery of oxime regenerated enzyme, completing a full turnover cycle. By mutation of the acyl pocket residues we are able to increase this efficiency by more than an order of magnitude, but the mutated residue conferring the greatest efficacy for enhancing oxime attack differs for HI-6 and 2-PAM.

Oxime	Enzyme	Alkoxy substitution	k_r ($M^{-1}min^{-1}$)	% Reactivation
2-PAM	Sp-AChE	cycloheptyl	0.46	70
	Sp (F295L) AChE		1.39	76
	Sp (F297I) AChE		9.2	74
2-PAM	Sp-AChE	3,3-dimethylbutyl	0.24	103
	Sp (F295L) AChE		1.11	103
	Sp (F297I) AChE		30	102
2-PAM	Sp-AChE	isopropyl	155	99
	Sp (F295L) AChE		116	107
	Sp (F297I) AChE		1260	92
HI-6	Sp-AChE	cycloheptyl	186	96
	Sp (F295L) AChE		2520	94
	Sp (F297I) AChE		353	127
HI-6	Sp-AChE	3,3-dimethylbutyl	181	97
	Sp (F295L) AChE		1230	93
	Sp (F297I) AChE		254	120
HI-6	Sp-AChE	isopropyl	2160	91
	Sp (F295L) AChE		3320	104
	Sp (F297I) AChE		2400	102

Table 6: Rate Constants Determined for Oxime Reactivation of Mouse Acetylcholinesterase Inhibited with Enantiomeric Methylphosphonates

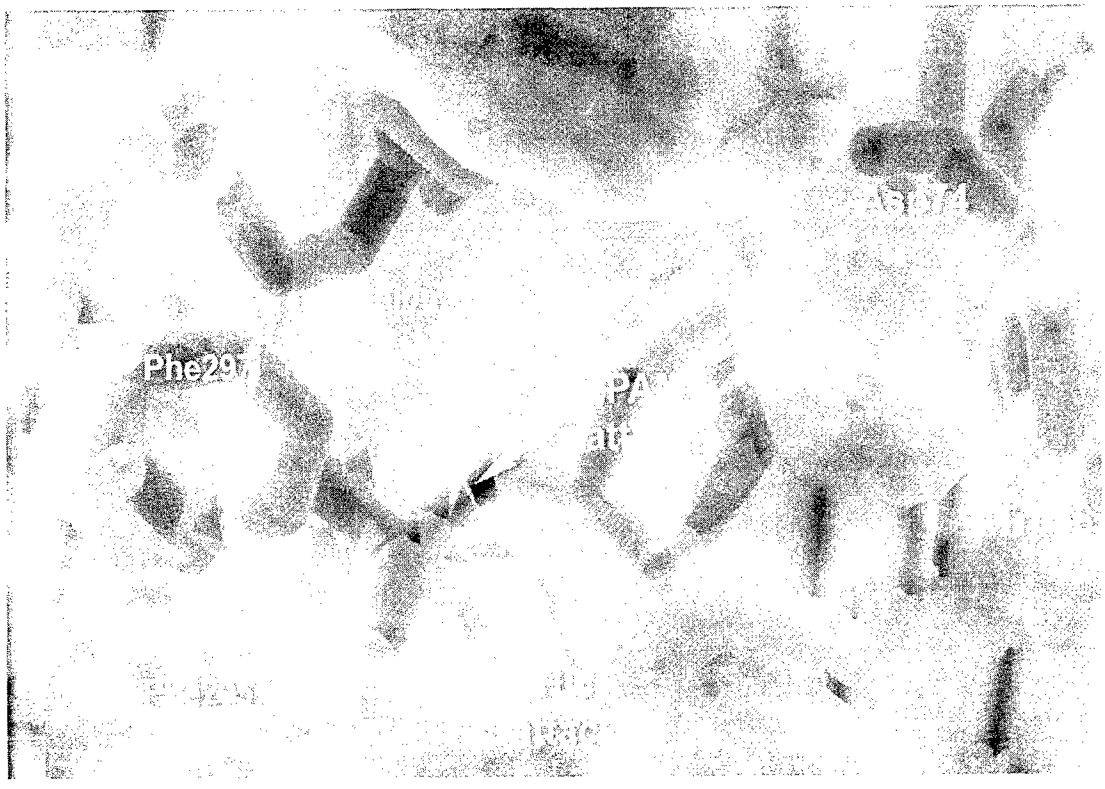

Figure 7:Structure of the active center gorge with the Sp-cycloheptyl methylphosphonyl moiety conjugated to the serine. The likely angles of attack for 2PAM and HI-6 are shown for the respective mutant enzyme. Critical residues within and Connolly surfaces of the active center gorge are shown.

Although our analysis is less complete, oxime reactivation of the Rp phosphonate conjugates is far more resistant to 2-PAM and HI-6. Virtually no reactivation is noted over a period of 2-3 days with the bulky cycloheptyl methyl phosphonyl enzyme. On the other hand, we have found that obidoxime is effective in cases where HI-6 and 2-PAM were ineffective. Current studies are directed to examining these structure-activity relationships in more depth by comparing kinetic parameters and ligand docking to the phosphonyl enzymes.

What these basic observations point to is formation of an associative intermediate of rather similar orientation to that expected for the acylation reaction. Formation of a phosphonyl-oxime appears to be an initial step in the reaction, and the reaction is facilitated by polarization of the phosphonyl oxygen bond in the oxyanion hole (24P). Less than optimal geometry for interaction is achieved with the oximes for two reasons: (1) oxime entry to the point of optimal reaction is impacted by the spatial constraints of the gorge, (2) and steric limitations intrinsic to the oxime moiety itself. Accordingly the gorge dimensions preclude the attacking nucleophile and scissile bond being apically positioned. These factors are likely to account for reactions with oximes being far slower than phosphonylation. The two oxime nucleophiles studied to date, 2-PAM and HI-6, appear to show distinctive preferred entry routes for attack of the phosphonyl moiety. 2-PAM being the smaller molecule is likely to have additional degrees of freedom and finds entry near the exit side of the acyl pocket. By contrast, HI-6 appears to have its oxime attack from deep in the gorge (fig. 7). This may arise from the two quaternary ammoniums in HI-6 and its distal end being tethered to a locus near the gorge mouth.

The face of attack of the conjugated phosphonate may be described in terms the four faces of the tetrahedron defined by the tetrahedral phosphorus. The geometric confines of the gorge and steric factors intrinsic to the oxime

itself are likely to dictate the preferential face of reactivity. Hence, optimization of the reaction rate will be both phosphonate and oxime dependent and details on optimizing this reaction are not yet fully understood. Future analyses will be extended for a large number of oximes and phosphonates and will be a subject of our continuing research.

CONCLUSIONS:

Large quantities of mammalian acetylcholinesterase have been purified to homogeneity and crystallized. This has yielded the first crystal structures of mammalian AChE as a fasciculin complex and as an apoenzyme. This structure has become an important template for mutagenesis studies and the recombinant source should allow us to use similar procedures for crystallization of mutant enzymes. Our studies of chiral phosphonate reactions with AChE have taken advantage of enantiomer (chiral) selectivity to analyze the mechanism and likely transition state of the reaction. The acyl pocket dictates chiral preference, and aspartate 74 is the primary determinant for enhancing the reaction with charged organophosphates. This analysis originating from mutagenesis studies allows one to position the critical groups in the pentavalent transition state.

Analysis of ligand entry in the fasciculin capped enzyme was completed with diffusion limited substrates, ie: acetylthiocholine, less efficient substrates such as *p*-nitrophenylacetate, and cationic and neutral trifluoro-acetophenones. Analysis of the ionic strength dependence suggests that the quaternary ligands traverse a cationic barrier in the case of the fasciculin capped enzyme, but not the apoenzyme. Analysis with mutant fasciculins where charge is neutralized or reversed should further delineate the path of ligand entry.

While oxime studies are still in progress, several trends with oxime reactivation are evident: (1) large enantiomeric preferences are seen for reactivation with the S_P enantiomers being more susceptible to reactivation, (2) opening of the acyl pocket can enhance reactivation provided the direction of geometric access is correct, (3) the oxyanion hole stabilizes the transition state in the reactivation reaction, (4) attack by the oximes can occur from at least two directions (ie two faces of the conjugated phosphonate), and (5) the efficiency of reactivation by different oximes depends on the structure of the conjugated phosphonate.

The combination of an oxime and plasma-retained AChE may prove to be a superior prophylatic agent in the prevention of organophosphate toxicity. Oximes themselves have relatively slow rates of regeneration of the active enzyme, and once aging has occurred, the conjugate is refractory to reactivation. Use of plasma-retained cholinesterases is limited by their formation of a stable conjugate; hence scavenging is stoichiometric rather than catalytic (7). With most organophosphates having molecular weights between 139 and 300 and a single AChE subunit having a mass of ~70,000 Daltons, large amounts of enzyme are necessary for scavenging. If the scavenger can be made catalytic, then its dose requirements would be markedly reduced. Oximes will also facilitate the turnover of the scavenging enzyme and we show we can enhance oxime turnover by factors of 10 to 50 with selected mutants. Hence, the mutants would be superior to wild-type enzyme for this purpose. The alternative to this procedure is to develop an AChE or phosphatase with a capacity to turn over the organophosphate as a hydrolytic reaction. This has been elegantly accomplished by Broomfield, Lockridge and their colleagues with a glycine 117 histidine mutation located in the oxyganion hole (8). The principal limitation that arises with the Gly117His mutation is the slow rate of reaction of the mutant enzyme with the organophosphate. Slow kinetics allow the offending organophosphate to distribute into tissues before it can be scavenged. Fortunately, the acyl pocket mutations maintain high reactivity with organophosphates. Pursuing the efficacy of the oxime plus mutant AChE combination in prophylaxis is an obvious future goal.

Publications in 1995 to April 1998 arising from these studies:

1P. Ashani, Y., Radić, Z., Tsigelny, I., Vellom, D.C., Pickering, N.A., Quinn, D.M., Doctor, B.P. and Taylor, P. Amino Acid Controlling Reactivation of a Chiral Organophosphonyl Conjugate of Acetylcholinesterase by Mono- and Bisquaternary Oximes. *J. Biol. Chem.* 270:6370-6380 (1995).

2P. Van den Born, H.K.L., Radic', Z., Marchot, P., Taylor, P. and Tsigelny, I. Theoretical Analysis of the Structure of the Peptide Fasciculin and its Docking to Acetylcholinesterase. *Protein Science* 4:703-715 (1995)

3P. Radić, Z., Quinn, D.M., Vellom, D.C., Camp, S. and Taylor, P. Allosteric Control of Acetylcholinesterase Catalysis by Fasciculin, *J. Biol. Chem.* 270:20391-20399 (1995).

4P. Hosea, N.A., Berman, H.A. and Taylor, P. Specificity and Orientation of Trigonal Carboxyl Esters and Tetrahedral Alkylphosphonyl Esters in Cholinesterases, *Biochemistry* 34:11528-11536 (1995).

5P. Bourne, Y., Taylor, P. and Marchot, P. Acetylcholinesterase Inhibition by Fasciculin: Crystal Structure of the Complex. *Cell* 83:502-512 (1995).

6P. Marchot, P., Ravelli, R.B.G., Raves, M.L., Bourne, Y., Vellom, D.C., Kanter, J., Camp, S., Sussman, J.L. and Taylor, P. Soluble Monomeric Acetylcholinesterase from Mouse: Expression, Purification, and Crystallization in Complex with Fasciculin. *Protein Science* 5:672-679 (1996).

7P. Hosea, N.A., Radić, Z., Tsigelny, I., Berman, H.A., Quinn, D.M. and Taylor, P. Aspartate 74 as a Primary Determinant in Cholinesterase Governing Specificity to Cationic Organophosphates. *Biochemistry* 35:10995-11004 (1996).

8P. Taylor, P., Hosea, N.A., Tsigelny, I., Radić, Z. and Berman, H.A. Determining Ligand Orientation and Transphosphonylation Mechanisms on Acetylcholinesterase by Rp, Sp Enantiomer Selectivity and Site-Specific Mutagenesis. *Enantiomer* 2:249-260 (1997).

9P. Marchot, P., Prowse, C.N., Kanter, J. Camp, S., Ackermann, E., Radić, Z., Bougis, P.E. and Taylor, P. Expression and Inhibitory Activity of Fasciculin, a Peptidic Acetylcholinesterase Inhibitor from Mamba Venom. *J. Biol. Chem.*, 272:3502-3510 (1997).

10P. Tara, S., Kirchhoff, P., Radic, Z., Taylor, P. and McCammon, J.A. Rapid Binding of a Cationic Inhibitor to Wild-Type and Mutant Acetylcholinesterase: A Brownian Dynamics Simulation, Biopolymers. In Press.

11P. Radić, Z., Kirchhoff, P., Quinn, D.M., McCammon, J.A. and Taylor, P. Electrostatic Influence on the Kinetics of Ligand Binding to Acetylcholinesterase: Distinctions Between Active Center Ligands and Fasciculin. *J. Biol. Chem.*, 272, 23265-23277, 1997.

12P. Saxena, A., Maxwell, D.M., Quinn, D.M., Radić, Z., Taylor, P. and Doctor, B.P. Mutant Acetylcholinesterases as Potential Detoxification Agents for Organophosphate Poisoning. *Biochem. Pharm.*, 53, 269-274, 1997.

Invited Contributions

13P. Taylor, P., Radić, Z., Kreienkamp, H.-J., Luo, Z. and Camp, S. Gene Expression and Ligand Specificity in the Cholinergic Synapse: A Comparison Between Acetylcholinesterase and the Nicotinic Acetylcholine Receptor. In: *Enzymes of the Cholinesterase Family.* (D. Quinn, B.P. Doctor and P. Taylor, Eds.) Plenum Press, N.Y., 15-22 (1995).

14P. Radić, Z., Quinn, D.M. and Vellom, D.C. Amino Acid Residues in Acetylcholinesterase Which Influence Fasciculin Inhibition. In: *Enzymes of the Cholinesterase Family.* (D. Quinn, B.P. Doctor and P. Taylor, Eds.) Plenum Press, N.Y., 183-188 (1995).

15P. Marchot, P., Camp. S., Radić, Z., Bougis, P.E. and Taylor, P. Structural Determinants of Fasciculin Specificity for Acetylcholinesterase. In: *Enzymes of the Cholinesterase Family.* (D. Quinn, B.P. Doctor and P. Taylor, Eds.) Plenum Press, N.Y., 197-202.

16P. Taylor, P., Ross, E.M., Sigler, P.B. and Sykes, B.D. Foundations and Future of Molecular Pharmacology. In: *Pharmacological Sciences: Perspectives for Research and Therapy in the Late 1990's.* Edited by A.C. Cuello and B. Collier, Birkhauser Verlag, Basel, Switzerland. pp. 59-66 (1995).

17P. Taylor, P., Acetylcholinesterase. In: *Encyclopedia of Neuroscience,* in press. Computer Disc Published.

18P. Quinn, D.M., Seravalli, J., Nair, H.K., Medhekar, R., Husseini, B., Radić, Z., Vellom, D.C., Hosea, N.A. and Taylor, P. The Function of Electrostatics in Acetylcholinesterase Catalysis. In: *Enzymes of the Cholinesterase Family* (D. Quinn, B.P. Doctor and P. Taylor, eds.) Plenum Press, N.Y., pp.203-206 (1995).

19P. Ashani, Y., Radić, Z., Tsigelny, I., Vellom, D.C., Hosea, N.A., Quinn, D.M., Doctor, B.P. and Taylor, P. Amino Acids that Control Mono- and Bisquaternary Oxime-Induced Reactivation of O-Ethyl Methylphosphonylated Cholinesterase. In: *Enzymes of the Cholinesterase Family* (D. Quinn, B.P. Doctor, and P. Taylor, eds.) Plenum Press, N.Y., pp.133-140 (1995).

20P. Taylor, P., Radić, Z., Hosea, N.A., Camp, S., Marchot, P. and Berman, H.A. Structural Bases for the Specificity of Cholinesterase Catalysis and Inhibition. In: *Toxicology Letters*. 82/83, 453-458 (1995).

21P. Taylor, P., Hosea, N., Marchot, P., Radić, Z., and Berman, H.A. The Cholinesterases at Atomic Resolution: Application of Structural Studies to Mechanisms of Inhibition. *Medical Defense Bioscience Review Proceedings* Vol. 1, pp. 1-12 (1996).

22P. Bourne, Y., Taylor, P. and Marchot, P. Acetylcholinesterase, "Recombinant, Monomeric (mouse)/Fasciculin 2 (mamba) Complex. In: *Macromolecular Structures,* 1997 (W. Hendrickson, ed.,) Current Biology Ltd., In Press.

23P. Taylor, P., Radic, Z., Hosea, N., Wong, L., Bruggemann, R., Marchot, P. and Berman, H.A. Uncovering Inhibition and Reactivation Mechanisms of the Cholinesterases by Selective Ligands and Analysis of Structure. Proc. 3rd Int. Conference on Enzymes Hydrolyzing Organophosphates. *Chem. Biol. Interactions,* In Press.

24P. Radic, Z. and Taylor, P. The Influence of Peripheral Site Ligands on the Raction of Symmetric and Chiral Organophosphates with Wild-Type and Mutant Acetylcholinesterases, Proc. 3rd Int. Conference on Enzymes Hydrolyzing Organophosphates. *Chem. Biol. Interactions*, In Press.

25P. Marchot, P., Bourne, Y., Prowse, C.N., Bougis, P.E. and Taylor, P. Inhibition of Mouse Acetylcholinesterase by Fasciculin: Crystal Structure of the Complex and Mutagenesis of Fasciculin. *Toxicon*, In Press 1998.

References

1. Taylor, P. and Radic, Z. The cholinesterases: from genes to proteins. *Ann. Rev. Pharmacol. &* Toxicol. 34, 281-320 (1993).
2. Shafferman, A., Kronman, C. and Ordentlich, A. Compilation of evaluated mutants of cholinesterases,in *Enzymes of the Cholinesterase Family*. D.M. Quinn, A.S. Balasubramanian, B.P. Doctor and P. Taylor, eds. Plenum Press, New York, NY, pp. 481-488 (1995).
3. Eason, L.M. and Stedman, E. Studies on the relation between chemical constitution and physiological action. *Biochem. J.* 27, 1257-1266 (1933).
4. Berman, H.A. and Decker, M.M. Kinetic, equilibrium and spectroscopic studies on dealkylation of alkyl organophosphonyl acetylcholinesterase. *J. Biol. Chem.* 261, 10646-10652 (1986).
5. Berman, H.A. and Leonard, K- Chiral reactions of acetylcholinesterase probed with enantiomeric methylphosphonothioates: non-covalent determinants of enzyme chirality. *J. Biol. Chem.* 264 3942-3950 (1989).
6. Berman, H.A. and Decker, M.M. Chiral nature of covalent methylphosphonyl conjugates of acetylcholinesterase. *J. Biol. Chem.* 264, 3951-3956 (1989).
7. Saxena, A., Ashani, Y., Raveh, L., Stevenson, D., Patel, T. and Doctor, B.P. Role of oligosaccharides in the pharmacokinetics of tissue derived and genetically engineered cholinesterases. *Mol. Pharmacol.* 53, 112-122 (1998).
8. Lockridge, O., Blong, R.M., Masson, P., Froment, M-T., Millard, C.B., and Broomfield, C.A. A single amino acid substitution, Gly 117 His, confers phosphotriesterase activity in human utyrylcholinesterase. *Biochemistry* 36, 786-795 (1997).

THE JOURNAL OF BIOLOGICAL CHEMISTRY
Vol. 272, No. 37, Issue of September 12, pp. 23265–23277, 1997
Printed in U.S.A.

Electrostatic Influence on the Kinetics of Ligand Binding to Acetylcholinesterase

DISTINCTIONS BETWEEN ACTIVE CENTER LIGANDS AND FASCICULIN*

(Received for publication, April 16, 1997, and in revised form, June 19, 1997)

Zoran Radić‡, Paul D. Kirchhoff§, Daniel M. Quinn¶, J. Andrew McCammon‡§, and Palmer Taylor‡

From the Departments of ‡Pharmacology and of §Chemistry and Biochemistry, University of California San Diego, La Jolla, California 92093-0636 and the ¶Department of Chemistry, University of Iowa, Iowa City, Iowa 52242

To explore the role that surface and active center charges play in electrostatic attraction of ligands to the active center gorge of acetylcholinesterase (AChE), and the influence of charge on the reactive orientation of the ligand, we have studied the kinetics of association of cationic and neutral ligands with the active center and peripheral site of AChE. Electrostatic influences were reduced by sequential mutations of six surface anionic residues outside of the active center gorge (Glu-84, Glu-91, Asp-280, Asp-283, Glu-292, and Asp-372) and three residues within the active center gorge (Asp-74 at the rim and Glu-202 and Glu-450 at the base). The peripheral site ligand, fasciculin 2 (FAS2), a peptide of 6.5 kDa with a net charge of +4, shows a marked enhancement of rate of association with reduction in ionic strength, and this ionic strength dependence can be markedly reduced by progressive neutralization of surface and active center gorge anionic residues. By contrast, neutralization of surface residues only has a modest influence on the rate of cationic *m*-trimethylammoniotrifluoroacetophenone (TFK^+) association with the active serine, whereas neutralization of residues in the active center gorge has a marked influence on the rate but with little change in the ionic strength dependence. Brownian dynamics calculations for approach of a small cationic ligand to the entrance of the gorge show the influence of individual charges to be in quantitative accord with that found for the surface residues. Anionic residues in the gorge may help to orient the ligand for reaction or to trap the ligand. Bound FAS2 on AChE not only reduces the rate of TFK^+ reaction with the active center but inverts the ionic strength dependence for the cationic TFK^+ association with AChE. Hence it appears that TFK^+ must traverse an electrostatic barrier at the gorge entry imparted by the bound FAS2 with its net charge of +4.

The high catalytic efficiency of acetylcholinesterase (AChE,[1] EC 3.1.1.7) as well as the rapid rates of reaction of selective AChE inhibitors are primarily addressed with cationic ligands. The physiological and most rapidly hydrolyzed substrate of AChE, acetylcholine, as well as its highest affinity inhibitors, *m*-trimethylammoniotrifluoroacetophenone (TFK^+) and fasciculin 2 (FAS2), carry one or more positive charges.

Inhibition of AChE by small cationic reversible inhibitors like *N*-methylacridinium appears diffusion limited (1) as is conjugation of the active serine by cationic TFK^+ (2). Initial rates of acetylcholine hydrolysis by *Electrophorus electricus* AChE also appear limited by the initial diffusion-controlled association of reactants (3, 4). Early kinetic studies suggested a net negative charge at the active center, a finding borne out from an overall analysis of ionizable groups (5, 6) in the three-dimensional structure of *Torpedo californica* AChE (7) and mouse AChE (8). In addition, the net negative charges on the enzyme appear to be strategically distributed for rapid catalysis. Theoretical calculations based on the crystal structure of *Torpedo* AChE (9, 10) suggest the presence of a strong electrostatic field that directs cations into the active center gorge of the enzyme.

The existence of such a field has been recently supported experimentally by analysis of electrooptical properties of snake AChE in strong, external electric fields (11). A comprehensive mutagenesis study of human AChE was undertaken to analyze the kinetic contributions of seven surface anionic charges influencing the electric field of AChE (12). Those surface residues outside of the active center gorge had only a small influence on catalytic efficiency for both cationic and neutral substrates. Recent theoretical calculations predict that anionic residues peripheral to the active center gorge exhibit only a minor influence on catalysis rates since the directing field is the result of a large number of contributions from the protein (13, 14).

Inhibition of AChE is achieved by competing ligands binding to the active center region of AChE, which is located in the center of the subunit at the base of a narrow gorge some 18–20 Å in depth. A separate set of ligands, which includes the organic cation, propidium (15), and the peptide FAS2 (16), binds to a site peripheral to the active center gorge. Inhibition of this site results from the ligand impeding substrate entry to the active center and exerting an allosteric influence on the conformation of the enzyme (15–18).

In this study, we have neutralized a series of anionic side chains through site-specific mutagenesis to distinguish the influence of electrostatics on the kinetics of inhibitor and substrate binding at the active center from that at the peripheral site. We also investigated the influence of bound FAS2 on the kinetics of entry of cationic and neutral ligands into the active center gorge.

MATERIALS AND METHODS

Enzymes—Mutations of mouse AChE were generated from a cDNA inserted into Bluescript II SK(+) (Stratagene, San Diego, CA) or directly in expression vectors pRC/CMV or pCDNA3 (Invitrogen, San Diego, CA) using M13K07 helper phage (New England Biolabs, Beverly, MA) to obtain single-stranded DNA. Oligonucleotides were synthesized (Life Technologies, Inc.; Genosys, Woodlands, TX) to encode the muta-

* This work was supported in part by grants from the National Science Foundation Supercomputer Centers MetaCenter Program and by U. S. Public Health Service Grants GM18360 and DAMD 17-95-I5027 (to P. T.), GM31749 (to J. A. M.), and NS21334 (to D. M. Q.). The costs of publication of this article were defrayed in part by the payment of page charges. This article must therefore be hereby marked "*advertisement*" in accordance with 18 U.S.C. Section 1734 solely to indicate this fact.

[1] The abbreviations used are: AChE, acetylcholinesterase; FAS2, fasciculin 2; TFK^+, *m*-trimethylammoniotrifluoroacetophenone; TFK, *m*-*tert*-butyltrifluoroacetophenone; PhAc, phenylacetate; pNPhAc, *p*-nitrophenylacetate; ACTh, acetylthiocholine.

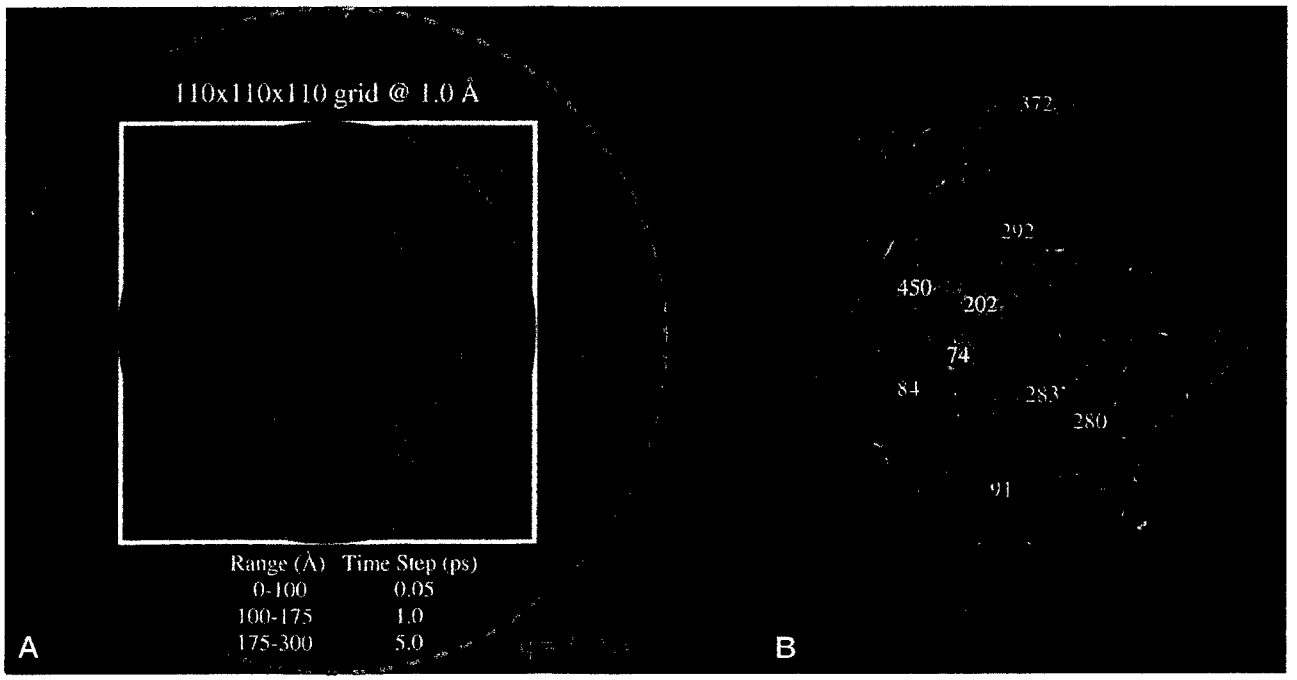

FIG. 1. **Brownian dynamics simulation of diffusion of cationic ligand into the AChE active center.** *A*, surface of the enzyme accessible to the diffusing ligand (*green*), reactive surface (*blue*), and some of parameters for the simulation. *B*, position of selected anionic residues in three-dimensional structure of mouse AChE, studied in simulations and in *in vitro* experiments.

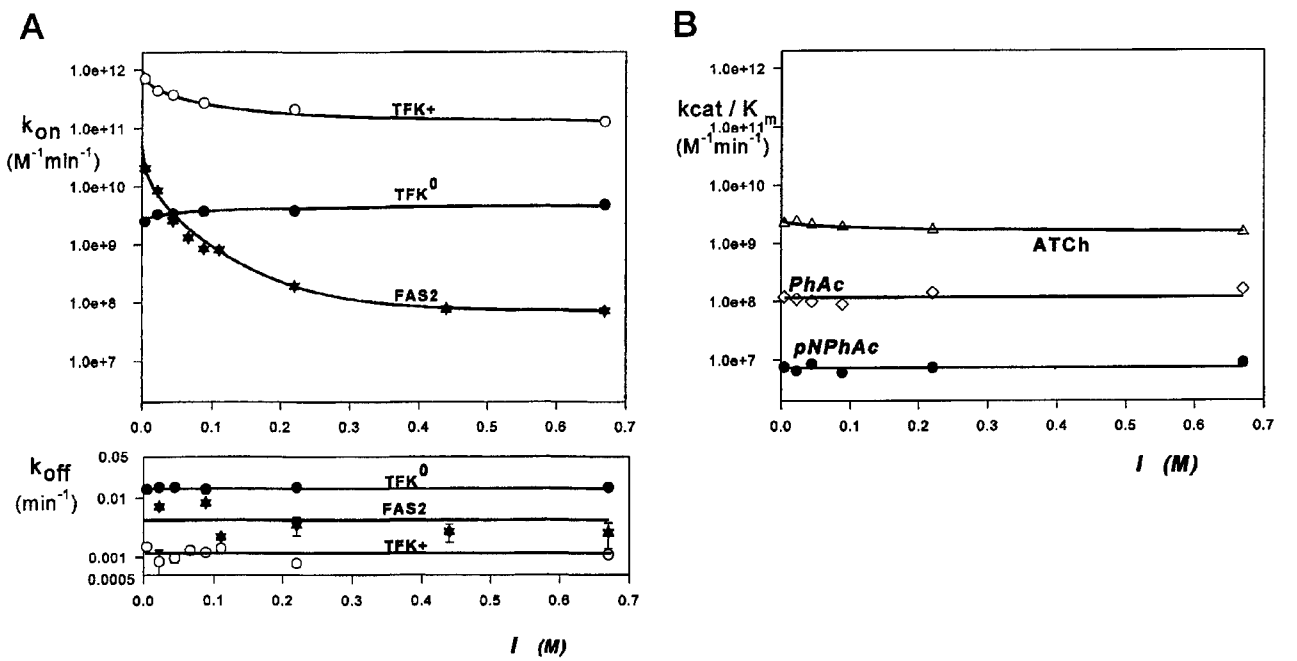

FIG. 2. **Ionic strength dependence of rate constants for ligands and mouse AChE.** *Curves* were calculated as a best fit of data to Eq. 2. *A*, association (k_{on}) and dissociation (k_{off}) rate constants of inhibitors. *B*, second-order rate constants (k_{cat}/K_m) for substrate turnover.

tion of interest and produce restriction sites that enabled screening of mutants. Multiple mutants were generated by subcloning several cDNA fragments containing single site mutations into the construct. Fragments were selected by the positions of the suitable restriction sites. Constructs were finally sequenced in the expression vector to confirm the mutation. Wild-type and mutant mouse AChEs were expressed in HEK-293 cells following transfection of the cells with the encoding cDNA as described previously (19). AChE was concentrated from the serum-free medium in which the expressing cells were grown.

Inhibitors—Purified and lyophilized FAS2 was kindly provided by Dr. Carlos Cerveñansky, Instituto de Investigaciones Biologicas, Montevideo, Uruguay, and Dr. Pascale Marchot, CNRS, University of Marseille, France. Concentrations of FAS2 stock solutions were determined by absorbance (ϵ_{276} = 4900 M^{-1} cm^{-1}) (20). *m-tert*-Butyltrifluoroacetophenone (TFK^0) and *m*-trimethylammoniotrifluoroacetophenone (TFK^+) were synthesized as described earlier (21).

Enzyme Activity—Hydrolysis of ATCh, phenylacetate, and *p*-nitrophenylacetate was measured spectrophotometrically at 412 nm for thiocholine (22) or by measuring phenol or *p*-nitrophenol release at 270 and 405 nm, respectively. Kinetic constants for hydrolysis of the above substrates by wild-type and mutant AChEs were determined as described previously (23).

Enzyme Inhibition—The second-order rate constants for FAS and trifluoroacetophenone association and the first-order constants of dis-

TABLE I

Rate constants for association and dissociation of inhibitors and for turnover of substrates with wild-type mouse AChEs in media of varying ionic strength

k_{on}^0 and k_{on}^H are second-order association rate constants for inhibitor at zero and 670 mM ionic strengths, respectively. $(k_{cat}/K_m)^0$ and $(k_{cat}/K_m)^H$ are second-order rate constants for substrate turnover at zero and 670 mM ionic strengths, respectively. z_E and z_I are charges of the enzyme and ligand, respectively, involved in the interaction. Constants k_{on}^0 for inhibitors, $(k_{cat}/K_m)^0$ for substrates and z_E were obtained by nonlinear regression analysis of Equation 2 using fixed values of k_{on}^H, $(k_{cat}/K_m)^H$ and z_I, from experimental data presented in Fig 2. Dashes denote indeterminant parameters. The first-order dissociation rate constants, k_{off}, appeared independent of ionic strength and were calculated as a mean of values obtained at different ionic strengths.

Ligand	k_{on}^0	k_{on}^H	z_I	z_E	k_{off}
	$10^9\ M^{-1}\ min^{-1}$	$10^9\ M^{-1}\ min^{-1}$			$10^{-3}\ min^{-1}$
TFK^+	980[a] ± 60	130[a]	+1	−2.3 ± 0.2	1.1 ± 0.3
TFK^0	2.2[a] ± 0.3	4.8[a]	ND[b]	ND[b]	15 ± 1
FAS2	49 ± 3	0.071	+4	−1.2 ± 0.1	4.4 ± 2.6
Substrate	$(k_{cat}/K_m)^0$	$(k_{cat}/K_m)^H$	z_I	z_E	
	$10^9\ M^{-1}\ min^{-1}$	$10^9\ M^{-1}\ min^{-1}$			
ATCh	2.5 ± 0.2	1.5	+1	−1.1 ± 0.4	
PhAc	0.12 ± 0.03	0.12	0	—	
PNPAc	0.0075 ± 0.0011	0.0075	0	—	

[a] Corrected for TFK^+ and TFK^0 hydration (*cf.* 35).

[b] Due to nonlinearity of the k_{on} *versus* I dependence, only a composite parameter $(z_I z_E) = 1.1 \pm 0.2$ was determined, instead of individual charges.

TABLE II

Catalytic parameters for hydrolysis of ATCh by wild-type and mutant mouse AChEs in 0.1 M phosphate buffer, pH 7.0

Constants were obtained by nonlinear regression analysis of the following equation:

$$v = \frac{(1 + bS/K_{ss})}{(1 + S/K_{ss})} \cdot \frac{V}{(1 + K_m/S)}$$

where S denotes the substrate concentration, K_m and K_{ss} Michaelis-Menten and substrate inhibition constants, and b the productivity ratio of the ternary SES complex to the ES complex (*cf.*, Radić *et al.* (19)). Values are means of 2–5 separate measurements.

Enzyme	K_m	K_{ss}	k_{cat}	b	k_{cat}/K_m
	μM	mM	$10^5\ min^{-1}$		$10^9\ M^{-1}\ min^{-1}$
Wild type[a]	46 ± 3	15 ± 2	1.4 ± 0.1	0.23 ± 0.01	3.0
		Surface mutants			
E84Q	120 ± 31	12 ± 7	1.8 ± 0.3	0.23 ± 0.03	1.5
E91Q	69 ± 3	11 ± 2	1.5 ± 0.1	0.24 ± 0.05	2.2
D280V	73 ± 4	10 ± 1	1.2 ± 0.2	0.23 ± 0.03	1.6
D283N	84 ± 2	14 ± 6	1.8 ± 0.5	0.17 ± 0.01	2.1
E292Q	85 ± 50	14 ± 9	1.6 ± 0.3	0.33 ± 0.11	1.9
D372N	62 ± 10	9.4 ± 0.3	1.2 ± 0.1	0.26 ± 0.03	1.9
E84Q/E91Q	131 ± 20	16 ± 2	1.2 ± 0.1	0.17 ± 0.05	0.92
D280V/D283N	60 ± 9	18 ± 2	1.4 ± 0.2	0.23 ± 0.11	2.3
E84Q/E91Q/D280V/D283N	240 ± 52	11 ± 4	1.1 ± 0.1	0.23 ± 0.04	0.46
E84Q/E91Q/D280V/D283N/D372N	162 ± 6	17 ± 7	0.82 ± 0.36	0.24 ± 0.09	0.51
E84Q/E91Q/D280V/D283N/E292Q/D372N	230 ± 32	14 ± 7	0.54 ± 0.06	0.38 ± 0.00	0.23
		Active center mutants			
D74N[a]	1,300 ± 140	530 ± 170	0.84 ± 0.11	0	0.065
E202Q	200 ± 40	140 ± 12	0.85 ± 0.06	0	0.43
E450Q[b]	140 ± 10	59 ± 22	0.034 ± 0.004	1.8 ± 0.1	0.024
D74N/E202Q	700 ± 29	18 ± 2	0.24 ± 0.03	4.9 ± 2.2	0.034
D74N/E202Q/E450Q	18,000 ± 2,500		0.04 ± 0.01		0.00022
		Active center and surface mutants			
D74N/D280V/D283N	1,600 ± 320	390 ± 131	0.36 ± 0.10	0	0.023

[a] Data of Radić *et al.* (19).

[b] Data of Hosea *et al.* (37).

sociation were determined, by monitoring the time course of reaction, from Equation 1 (*cf.* Ref. 16).

$$f = \frac{k_{on}[L]}{k_{on}[L] + k_{off}}(1 - e^{-(k_{on}[L] + k_{off})t}) \qquad \text{(Eq. 1)}$$

where f is a fraction of enzyme inhibition at time t and ligand concentration [L]. The second-order rate constants for formation of the inhibitory complex (k_{on}), the first-order rate constants for its dissociation (k_{off}), and substrate catalytic constants were plotted as a function of ionic strength of the reaction medium using the Debye-Huckel limiting law implemented within the transition state theory by Glasstone *et al.* (24, *cf.* Ref. 2); see Equation 2.

$$k_{on} = (k_{on}^0 - k_{on}^H)10^{-1.18|z_E z_I| \cdot \sqrt{I}} + k_{on}^H \qquad \text{(Eq. 2)}$$

where k_{on}, k_{on}^0, and k_{on}^H are second-order association rate constants at the specified ionic strength I, zero ionic strength, and infinite ionic strength, respectively. z_E and z_I are the charges of enzyme and inhibitor involved in the interaction.

Buffers—Enzyme activities in catalysis and inhibition were measured in media of varying ionic strength, generated by varying the

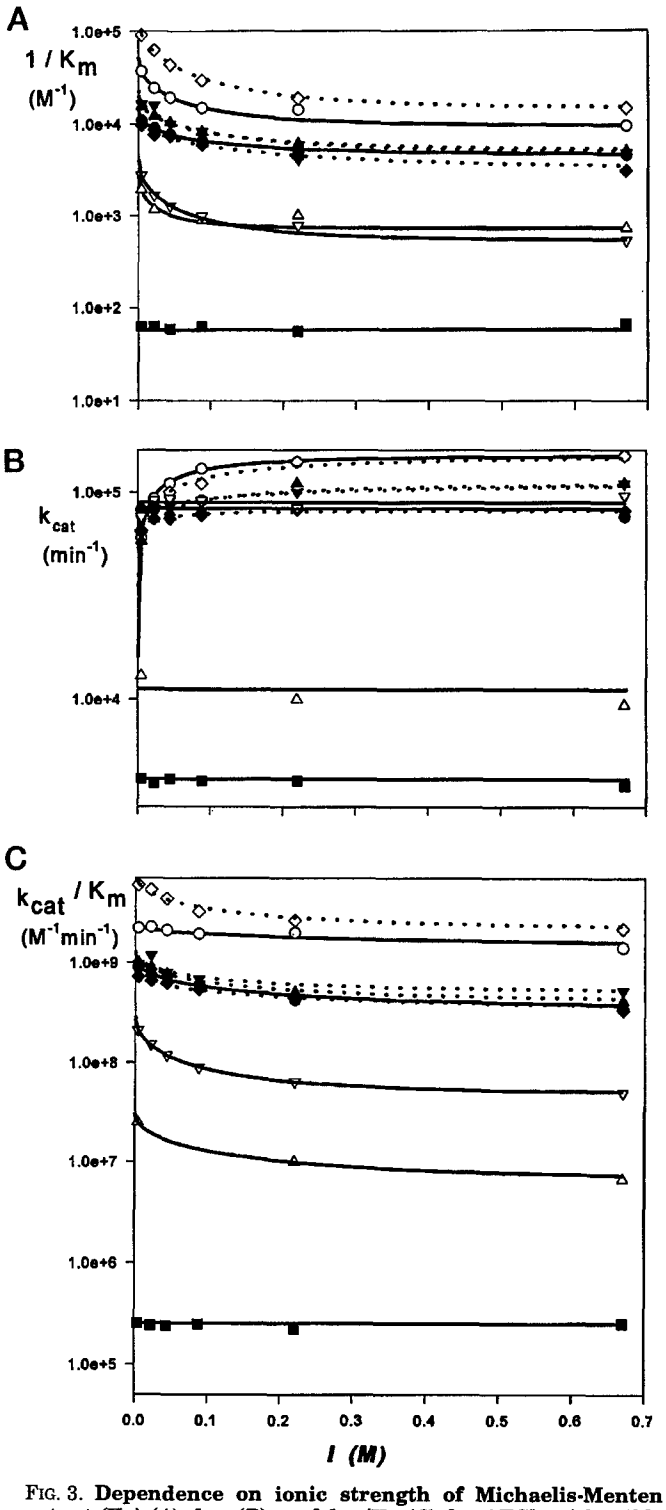

FIG. 3. **Dependence on ionic strength of Michaelis-Menten constant (K_m) (*A*), k_{cat} (*B*), and k_{cat}/K_m (*C*) for ATCh with wild-type (○) and the following mutant mouse AChEs.** D280V/D283N (◇), E84Q/E91Q/D280V/D283N (▲), E84Q/E91Q/D280V/D283N/D372N (▼), E84Q/E91Q/D280V/D283N/E292Q/D372N (◆), D74N (▽), E202Q (●), D74N/E202Q (△), and D74N/E202Q/E450Q (■). *Dashed lines* denote surface mutants, and *solid lines* denote active center mutants. All curves were calculated as best fits of data to Eq. 2.

concentration of phosphate buffer, pH 7.0, between 2 and 300 mM.

Brownian Dynamics Simulations—To conduct the Brownian dynamics simulations, the structure for the mouse AChE·FAS2 complex was obtained from the Brookhaven Protein Data Bank (8). Coordinates for the missing residues Glu-1, Gly-2, Arg-3, Pro-258, Pro-259, Gly-260, Gly-261, Ala-262, Gly-263, and Gly-264 were built in using QUANTA (25). CHARMM22 with its all-atom parameter set was used to build in the protons and missing side chains (26). Coordinates for the protons and residues 1–3 and 258–264 were relaxed using 500 steps of Adopted-Basis Newton Raphston minimization.

Ionization states of the residues were modeled to represent physiological conditions. Arg and Lys residues were modeled as protonated with an overall charge of +1. Asp and Glu residues were modeled as deprotonated with an overall charge of −1. The protonation states of the His residues were determined by inspection of the availability of hydrogen bonds. All His residues were modeled as HSD (protonated at the ND1 site) except for residue 432 which was modeled as HSE (protonated at the NE2 site) and residue 447 which was modeled as HSP (doubly protonated at the ND1 and NE2 sites). The charge on the unliganded, wild-type AChE used for the simulations was −8.0.

A reactive surface was placed at the gorge entrance. To do this the center of the mouth of the gorge and the gorge axis were first defined. In similar fashion to previous work with *T. californica* AChE (13, 27–29), the center of the mouth of the gorge was defined by determining the geometric center of four selected atoms from residues near the gorge entrance: Tyr-72:OH, Asp-74:OD1, Phe-297:CE1, and Tyr-341:CD2. The gorge axis was then defined as the line running from Ser-203:C to the geometric center. For the reactive surface at the gorge entrance, a 12-Å reactive sphere was centered on the gorge axis 2 Å above the center of the mouth of the gorge to completely cap the entrance.

Atomic charges of anionic side chains mutated to the corresponding amides were set to 0 in the AChE model to generate the corresponding mutants. Neither steric nor conformational changes potentially arising from the mutations were considered.

All calculations involved in the Brownian dynamics simulations were carried out using the University of Houston Brownian Dynamics software package UHBD (30). The simulations were conducted using a 110 × 110 × 110 grid with 1-Å spacing centered on the Ser203:C atom. Hydrodynamic radii of 35.0 and 3.5 Å were used for AChE and diffusing cationic ligand, respectively. An excluded radius of 2.0 Å was used for the ligand. Fig. 1 illustrates the reactive surface available to the diffusing ligand and several other parameters used in the simulations. The protein and solvent were assigned dielectric values of 4.0 and 78.0, respectively, with a Stern layer radius of 2.0 Å. A probe-accessible surface was used with a 1.4-Å probe radius and 300 surface points per atom. The boundary potential was determined using a single Debye-Huckel sphere of 35 Å radius and molecular charge of −8 for the AChE molecule. A step size of 0.05 ps was used for diffusion between 0 and 100 Å, 1 ps between 100 and 175 Å, and 5 ps between 175 and 300 Å from the grid center.

The rate constants of enzyme-ligand encounter were calculated from large numbers of Brownian trajectories of the substrate in the neighborhood of the enzyme (30–33). The substrate moves under the influence of the electrostatic field of the enzyme and the random bombardment of solvent molecules. Trajectories are initiated on the surface of a sphere of radius b, the b surface, around the center of coordinates of the enzyme. This sphere is made sufficiently large so that the electrostatic forces between the ligand and the enzyme are approximately centrosymmetric for $r > b$. Each trajectory is continued until the substrate satisfies a predefined encounter criterion or reaches an outer spherical surface of radius q, the quit-surface. The fraction of trajectories that finish with encounters is corrected to include the additional encounters that would have occurred if the trajectories had not been truncated at the quit-surface and is then multiplied by the rate constant for the encounter of ligand with the b surface to yield the bimolecular diffusion-controlled rate constant, k_{on} (34).

For this study, Brownian dynamics trajectories were started randomly on a b surface 55.0 Å from Ser203:C atom. A trajectory was terminated when one of three criteria were met. 1) The ligand made contact with the reactive surface. 2) The diffusing ligand reached the quit-surface, a distance greater than 300 Å from the Ser203:C atom. 3) The ligand made more than 1×10^7 steps. For the wild-type and each of the nine mutants, 3000 trajectories were conducted at 0 and 670 mM ionic strengths.

RESULTS

Effect of Ionic Strength on Rate Constants for Ligand Binding to Wild-type Acetylcholinesterase—Catalytic parameters for substrates, second-order association rate constants, and first-order dissociation rate constants for cationic and neutral ligands with wild-type AChE, measured as a function of ionic strength of reaction medium, are shown in Fig. 2. The cationic inhibitors TFK^+ and FAS2 associate with AChE significantly

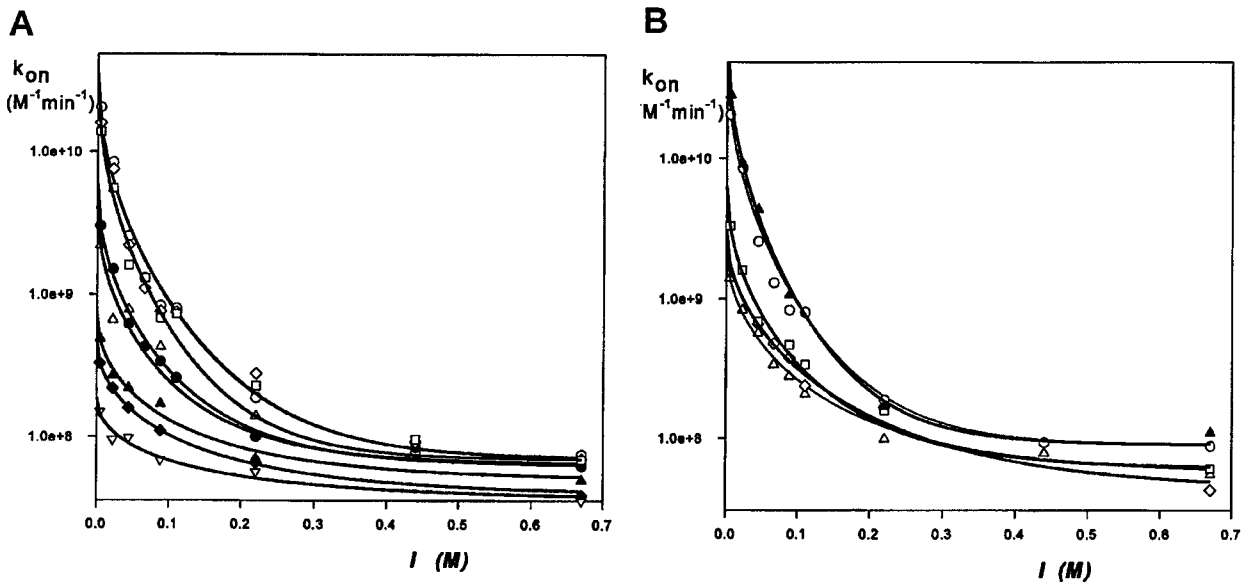

FIG. 4. **Ionic strength dependence of FAS2 second-order association rate constant (k_{on}), with wild-type (○) and mutant mouse AChEs.** All *curves* were calculated as a best fit of data to Eq. 2.*A*, surface mutants: D280V (◇), D283N (□), D280V/D283N (●), E84Q/E91Q (△), E84Q/E91Q/D280V/D283N (▲), E84Q/E91Q/D280V/D283N/D372N (◊), and E84Q/E91Q/D280V/D283N/E292Q/D372N (▽). *B*, active center mutants: E202Q (▲), D74N (□), D74N/D280V/D283N (△), and D74N/E202Q/E450Q (◇).

TABLE III

Rate constants for FAS2 association and dissociation with wild-type and mutant mouse AChEs in media of varying ionic strength

k_{on}^0 and k_{on}^H are second-order association rate constants at zero and 670 mM ionic strength, respectively. z_E and z_I are charges of the enzyme and ligand, respectively, involved in the interaction. Constants k_{on}^0 and z_E were obtained by nonlinear regression analysis of Equation 2 using fixed values of k_{on}^H and z_I, from experimental data presented in Fig. 4. First-order dissociation rate constants k_{off} were calculated as means of values obtained at different ionic strengths. k_{off} constants for two triple mutants were too large to be determined under our experimental conditions.

Enzyme	k_{on}^0	k_{on}^H	z_I	z_E	k_{off}
	10^{10} M^{-1} min^{-1}	10^7 M^{-1} min^{-1}			10^{-3} min^{-1}
Wild type	4.9 ± 0.3	8.8	+4	−1.2 ± 0.1	4.4 ± 2.6
	Surface mutants				
D280V	3.6 ± 0.3	7.0	+4	−1.1 ± 0.1	3.9 ± 2.8
D283N	3.2 ± 0.1	6.9	+4	−1.2 ± 0.1	5.5 ± 3.4
D280V/D283N	0.59 ±0.03	6.2	+4	−0.94 ± 0.04	5.2 ± 1.6
E84Q/E91Q	0.41 ± 0.08	6.4	+4	−0.90 ± 0.20	3.7 ± 0.8
E84Q/E91Q/D280V/D283N	0.072± 0.005	4.9	+4	−0.61 ± 0.06	9.3 ± 2.0
E84Q/E91Q/D280V/D283N/D372N	0.048 ±0.001	3.8	+4	−0.56 ± 0.02	5.6 ± 1.0
E84Q/E91Q/D280V/D283N/E292Q/D372N	0.019± 0.002	3.5	+4	−0.45 ± 0.07	6.6 ± 1.9
	Active center mutants				
D74N	0.63 ± 0.03	6.0	+4	−0.90 ± 0.05	42 ± 17
E202Q	7.3 ± 0.1	9.0	+4	−1.3 ± 0.2	4.5 ± 0.6
D74N/E202Q/E450Q	0.31± 0.06	5.0	+4	−0.71 ± 0.07	—
	Active center and surface mutants				
D74N/D280V/D283N	0.23± 0.01	5.5	+4	−0.69 ± 0.03	—

faster in buffers of low than high ionic strength (Table I). The increase in rates over this ionic strength range approaches 1 order of magnitude for the TFK^+ monocation and exceeds 2 orders of magnitude for FAS2, a 6.5-kDa peptide that bears net charge of +4 at pH 7.0. The association rate constants for FAS2 at low ionic strength approach the values for TFK^+. Both values at a low ionic strength are within the range of rate constants predicted for diffusion controlled reactions. For the cationic substrate ATCh, the ratio k_{cat}/K_m increased only 2-fold at low ionic strength indicating that the diffusion and chemical steps in catalysis by mouse AChE may be of similar magnitude. The rates of association of neutral ligands do not increase with a reduction in ionic strength. Hydrolysis rates of neutral substrates, PhAc and *p*NPhAc, being 1 and 2 orders of magnitude slower than ATCh hydrolysis, also were not influenced by the change in ionic strength. The association rate constants for the neutral inhibitor TFK^0, which are about 2 orders of magnitude slower than TFK^+, exhibit a modest decrease in rate with a reduction in ionic strength (Table I). This decrease was assumed to be consequence of indirect electrostatic interaction as in the case of the k_{cat} *versus* I dependence for ATCh and PhAc; only the composite parameter ($z_I z_E$) was therefore determined, instead of individual charges. Rates of dissociation of both the charged and neutral TFKs and fasciculin were largely independent of the ionic strength.

Effect of Ionic Strength on Substrate Hydrolysis by Wild-type and Mutant Acetylcholinesterases—The catalytic constants for hydrolysis of ATCh by wild-type and mutant mouse AChEs determined in 100 mM phosphate buffer, pH 7.0, are listed in Table II. Of the 17 mutants studied, mutations of aspartyl and glutamyl residues located on the enzyme surface to their corresponding amidated residues produced less than 5-fold varia-

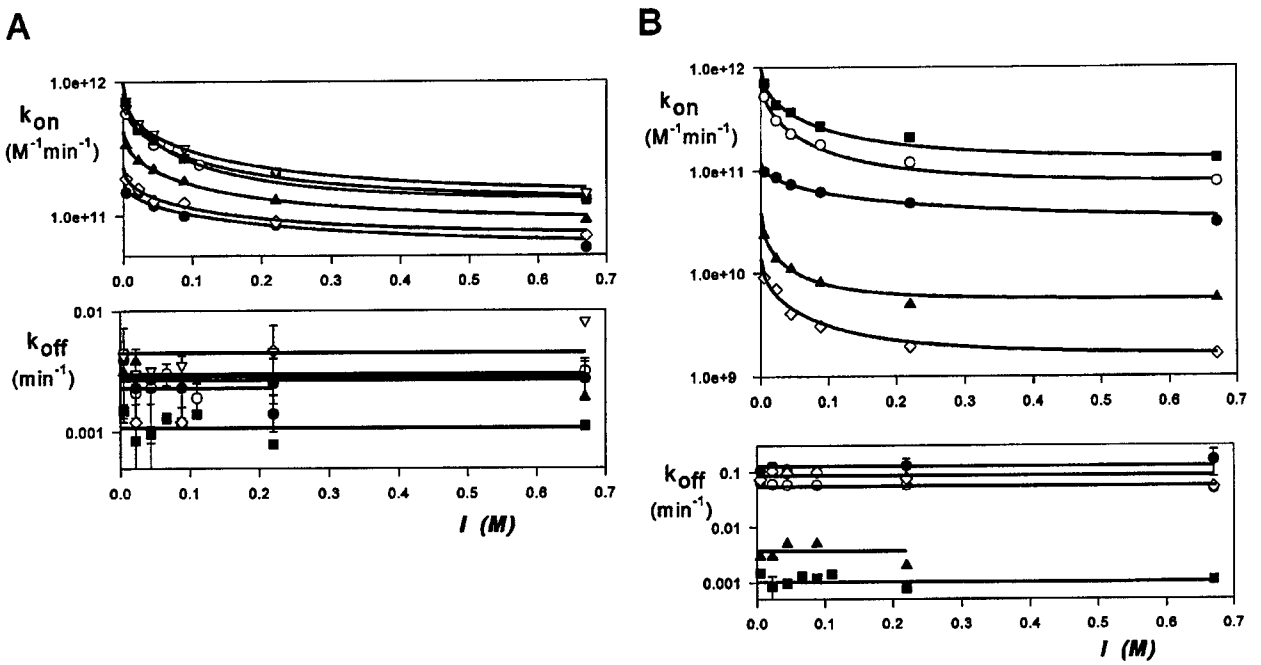

FIG. 5. **Ionic strength dependence of TFK$^+$ second-order association rate constant (k_{on}) and first-order dissociation constant (k_{off}) with wild-type (■) and mutant mouse AChEs.** All *curves* were calculated as a best fit of data to Eq. 2.*A*, surface mutants: D280V (▽), D280V/D283N (○), E84Q/E91Q/D280V/D283N (▲), E84Q/E91Q/D280V/D283N/D372N (◇), and E84Q/E91Q/D280V/D283N/E292Q/D372N (●). *B*, active center mutants: D74N (▲), E202Q (○), E450Q (●), and D74N/E202Q (◇).

TABLE IV

Rate constants for TFK$^+$ association and dissociation with wild-type and mutant mouse AChEs in media of varying ionic strength

k_{on}^0 and k_{on}^H are second-order association rate constants at 0 and 670 mM ionic strength, respectively. z_E and z_I are charges of the enzyme and ligand, respectively, involved in interaction. Constants k_{on}^0 and z_E were obtained by nonlinear regression analysis of Equation 2 using fixed values of k_{on}^H and z_I, from experimental data presented in Fig. 5. k_{on}^0 and k_{on}^H were corrected for TFK$^+$ hydration (*cf.* 35). First-order dissociation rate constants k_{off} were calculated as means of values obtained at different ionic strengths.

Enzyme	k_{on}^0	k_{on}^H	z_I	z_E	k_{off}
	10^{11} M^{-1} min^{-1}	10^{11} M^{-1} min^{-1}			10^{-3} min^{-1}
Wild type	9.8 ± 0.6	1.3	+1	−2.3 ± 0.2	1.1 ± 0.3
	Surface mutants				
D280V	8.2 ± 2.0	1.5	+1	−1.7 ± 0.1	4.8 ± 2.8
D280V/D283N	7.6 ± 0.3	1.3	+1	−1.8 ± 0.1	2.6 ± 0.4
E84Q/E91Q/D280V/D283N	4.3 ± 0.8	0.92	+1	−1.7 ± 0.1	1.7 ± 0.8
E84Q/E91Q/D280V/D283N/D372N	2.3 ± 0.1	0.70	+1	−1.5 ± 0.2	2.3 ± 2.0
E84Q/E91Q/D280V/D283N/E292Q/D372N	1.8 ± 0.1	0.57	+1	−1.2 ± 0.2	2.8 ± 1.4
	Active center mutants				
D74N	0.39 ± 0.01	0.055	+1	−3.2 ± 0.1	5.5 ± 4.4
E202Q	7.9 ± 0.4	0.77	+1	−2.6 ± 0.2	59 ± 5
E450Q	1.2 ± 0.1	0.31	+1	−1.3 ± 0.1	123 ± 23
D74N/E202Q	0.14 ± 0.01	0.016	+1	−2.5 ± 0.4	94 ± 28
D74N/E202Q/E450Q	≤0.14	≤0.016	+1	—	≥94
	Active center and surface mutants				
D74N/D280V/D283N	3.1 ± 0.2	0.90	+1	−2.6 ± 0.3	2.3 ± 0.7

tions in kinetic constants. In all cases, K_m increases. By contrast, the active center mutations, except for E202Q, produced substantial changes in catalytic parameters including increases in K_m of up to nearly 3 orders of magnitude and decreases in k_{cat} of more than an order of magnitude. The ionic strength dependences of catalytic parameters for ATCh with wild-type and seven mutants are presented in Fig. 3.

The Michaelis constant was found to increase, with ionic strength for wild-type and all mutants resulting in a decrease in k_{cat}/K_m. A modest increase in k_{cat} for all the surface mutants and wild-type AChE was evident, whereas k_{cat} for active center mutants was independent of ionic strength. Catalytic parameters for hydrolysis of neutral substrates (data not shown) did not show a dependence on ionic strength, with exception of K_m and k_{cat} for PhAc which show a slight increase at high ionic strength for wild-type AChE. The catalytic constants for active center mutants were similar to the constants for wild-type, with the exception of k_{cat} which was reduced about an order of magnitude in the mutants.

Of the three substrates, ATCh and PhAc have similar k_{cat} values that are significantly higher than k_{cat} for *p*NPhAc, indicating a common rate-limiting step in the chemical step of catalysis, presumably deacylation. The acylation step appears slower than deacylation for *p*NPhAc (3). Substitution of active center anionic residues reduces k_{cat} for ATCh and PhAc to the levels of *p*NPhAc indicating a shift in the rate-limiting step to

TABLE V

Rate constants for TFK^0 association and dissociation with wild-type and mutant mouse AChEs in media of varying ionic strength

k_{on}^0 and k_{on}^H are second-order association rate constants at 0 and 670 mM ionic strength, respectively. z_E and z_I are charges on the enzyme and ligand, respectively, involved in the interaction. Constants k_{on}^0 and z_E were obtained by nonlinear regression analysis of Equation 2 using fixed values of k_{on}^H and z_I. k_{on}^0 and k_{on}^H were corrected for TFK^0 hydration (*cf.* 35). Dashes indicate indeterminant parameters. First-order dissociation rate constants k_{off} were calculated as means of values obtained at different ionic strengths.

Enzyme	k_{on}^0	k_{on}^H	z_I	z_E	k_{off}
	$10^9\ M^{-1}\ min^{-1}$	$10^9\ M^{-1}\ min^{-1}$			$10^{-3}\ min^{-1}$
Wild-type	2.2 ± 0.3	4.8	ND[a]	ND[a]	15 ± 1
Surface mutants					
E84Q/E91Q/D280V/D283N/D372N	2.3± 0.8	8.9	ND[a]	ND[a]	26 ± 6
E84Q/E91Q/D280V/D283N/E292Q/D372N	6.4± 1.9	6.4	0		46 ± 9
Active center mutants					
D74N	3.9 ± 0.3	3.9	0		22 ± 3
E202Q	3.3 ± 0.5	3.3	0		640 ± 66
E450Q	2.2 ± 0.1	2.2	0		680 ± 220

[a] Due to nonlinearity of the k_{on} *versus* I dependence, only a composite parameter ($z_I z_E$) was determined (+1.5 ± 0.2 for wild-type and +1.4 ± 0.3 for E84Q/E91Q/D280V/D283N/D372N mutant), instead of individual charges.

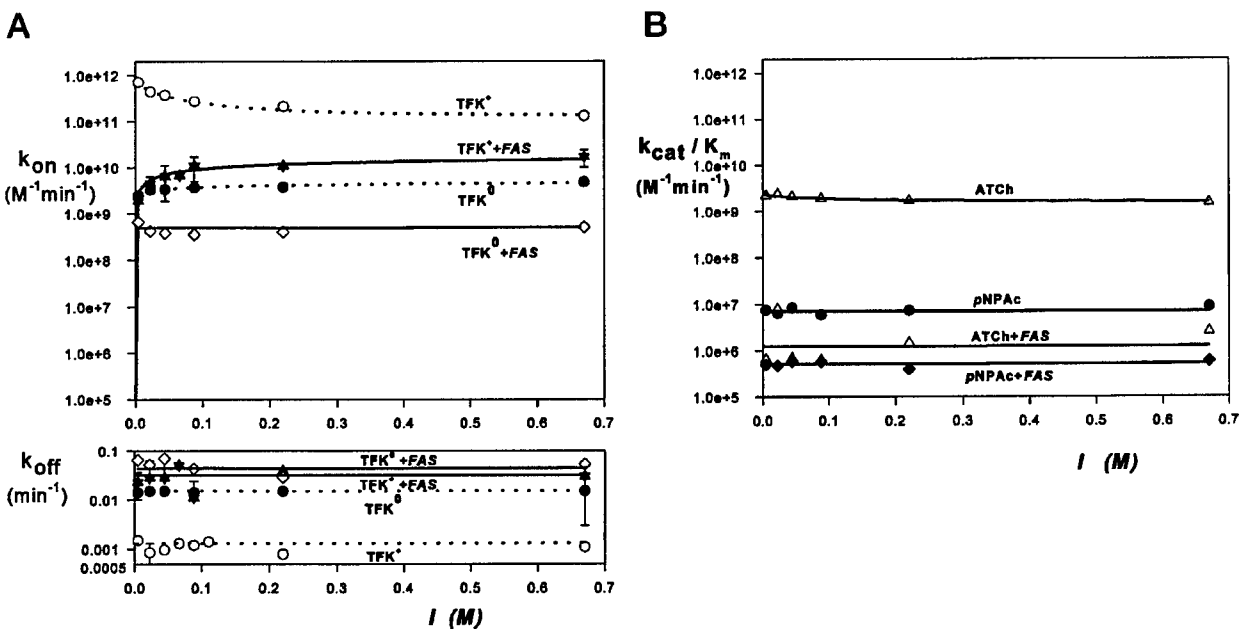

FIG. 6. **Ionic strength dependences of rate constants for ligands and AChE-FAS2 complex (*solid lines*) and AChE alone (*dashed lines*).** *Curves* were calculated as best fits of the data to Eq. 2. *A*, association (k_{on}) and dissociation (k_{off}) rate constants of inhibitors. *B*, second-order rate constants for turnover (k_{cat}/K_m) of substrates.

the acylation step for these substrates, with a concomitant loss of the ionic strength dependence. This suggests that the increases of k_{cat} for ATCh and PhAc at higher ionic strengths are due to an enhanced deacylation step of hydrolysis. Rates of deacetylation of mouse AChE thus depend on solvent-accessible charged moieties in the AChE active center, whereas the acetylation reaction does not show this dependence.

Effect of Ionic Strength on Rate Constants for Fasciculin Binding to Wild-type and Mutant Acetylcholinesterases—The second-order rate constants of FAS2 association to wild-type and mutant AChEs and the first-order rate constants for FAS2 dissociation were measured by following the approach of the inhibition reaction to equilibrium in buffers of varying ionic strength (Fig. 4).

The second-order reaction rate constants extrapolated to zero ionic strength decreased significantly upon introduction of multiple mutations to AChE diminishing the charge, either on the enzyme surface or in its active center, whereas the rate constants were only moderately affected at high ionic strength (Table III). A six-residue substitution of the surface anionic residues by the corresponding amidated amino acids resulted in a 260-fold reduction in k_{on}^0 and only 2.5-fold change in k_{on}^H. Thus, the pronounced dependence of rates of FAS2 association with wild-type AChE on ionic strength, resulting in 560-fold rate acceleration at zero ionic strength compared with high ionic strength, is virtually eliminated by neutralization of six anionic residues on the enzyme surface, and significantly reduced by neutralization of three anionic residues of the active center. This illustrates the importance of AChE anionic residues in the rate-limiting step of association of FAS2 with the enzyme.

However, except for the D74N mutant, since these residues did not affect k_{off}, they do not appear to affect the activation barrier for dissociation of the complex.

Effect of Ionic Strength on Rate Constants for Trifluoroacetophenone Binding to Wild-type and Mutant Acetylcholinesterases—The second-order association rate constant and the first-order dissociation rate constants for TFK$^+$ and wild-type and mutant AChEs were measured by following the approach of the inhibition reaction to equilibrium at varying ionic strengths

TABLE VI

Rate constants for association and dissociation of inhibitors and for turnover of substrates with wild-type mouse AChE · FAS2 complex in media of varying ionic strength

k_{on}^0 and k_{on}^H are inhibitor second-order association rate constants at 0 and 670 mM ionic strengths, respectively. $(k_{cat}/K_m)^0$ and $(k_{cat}/K_m)^H$ are second-order reaction rate constants for substrate turnover at 0 and 670 mM ionic strengths, respectively. z_E and z_I are charges of the enzyme and ligand, respectively, involved in the interaction. Constants k_{on}^0 and z_E for TFK^+ were obtained by nonlinear regression analysis of Equation 2 using fixed values of k_{on}^H and z_I, from experimental data presented in Fig 7. k_{on}^0 and k_{on}^H were corrected for TFK^+ and TFK^0 hydration (*cf.* 35). The first-order dissociation rate constant k_{off}, constants k_{on}^0 and k_{on}^H for TFK^0 and constants $(k_{cat}/K_m)^0$ and $(k_{cat}/K_m)^H$ for substrates were calculated as a mean of values obtained at different ionic strengths. Dashes indicate indeterminant parameters.

Ligand	k_{on}^0	k_{on}^H	z_I	z_E	k_{off}
	$10^9\ M^{-1}\ min^{-1}$	$10^9\ M^{-1}\ min^{-1}$			$10^{-3}\ min^{-1}$
TFK^+	≤2	17	+1	+0.9 ± 0.2	30 ± 11
TFK^0	0.46 ± 0.11	0.46	0	—	52 ± 14

Substrate	$(k_{cat}/K_m)^0$	$(k_{cat}/K_m)^H$	z_I	z_E
	$10^6\ M^{-1}\ min^{-1}$	$10^6\ M^{-1}\ min^{-1}$		
ATCh	2.7 ± 2.8	2.7	+1	0
PNPhAc	0.52 ± 0.08	0.52	0	—

TABLE VII

The second-order rate constants for association of a spherical cation with AChE calculated using Brownian dynamics simulation and the measured second-order rate constants for TFK^+ association with mouse AChE

Rate constants were determined at 0 (k_{on}^0) and 670 mM (k_{on}^H) ionic strengths. The ratios of mutant to wild-type rate constants are given in parentheses.

Mouse AChE	k_{on}^0		k_{on}^0/k_{on}^H	
	Calculated	Measured	Calculated	Measured
	$10^{11}\ M^{-1}\ min^{-1}$			
		Surface mutants		
Wild type	9.1	9.8	4.7 (1)	7.5 (1)
D280V	8.1	8.2	4.0 (0.9)	5.7 (0.8)
D280V/D283N	7.0	7.6	3.7 (0.8)	5.8 (0.8)
E84Q/E91Q/D280V/D283N/D372N	4.0	2.3	2.5 (0.5)	3.3 (0.4)
E84Q/E91Q/D280V/D283N/E292Q/D372N	2.9	1.8	1.7 (0.4)	3.2 (0.4)
		Active center mutants		
Wild type	9.1	9.8	4.7 (1)	7.5 (1)
D74N	7.9	0.39	4.7 (1)	7.1 (0.9)
E202Q	8.4	7.9	4.3 (0.9)	10 (1.3)
E450Q	8.4	1.2	4.2 (0.9)	3.9 (0.5)
D74N/E202Q	6.9	0.14	3.7 (0.8)	8.8 (1.2)
D74N/E202Q/E450Q	6.2	<0.14	3.2 (0.7)	16 (≥1)

(Fig. 5). Association rate constants for the wild-type and all mutant enzymes increased significantly with a reduction in ionic strength. The ratio between the second-order constant extrapolated to zero ionic strength k_{on}^0 and the rate constant at the highest measured ionic strength k_{on}^H decreased only slightly for the multiple mutants. Since the total difference in k_{on}^0 and k_{on}^H for the wild-type was much smaller for TFK^+ than for FAS2, charge neutralization exerted a far smaller influence than for FAS2. The extrapolated k_{on}^0 values for mutants of the surface anionic residues decreased by a factor of 5 with the simultaneous substitution of six surface residues (Table IV). By contrast both k_{on}^0 and k_{on}^H for the active center mutants decreased by almost 2 orders of magnitude upon neutralization of the three anionic residues in the active center gorge, yielding at high ionic strength a rate constant comparable in magnitude with that found for TFK^0 (Table V). Hence, anionic residues within the active center gorge, particularly Asp-74 which resides near its rim, influence the TFK^+ reaction in specific ways in addition to a long range electrostatic attraction; the anionic side chains may trap the cationic ligand within the gorge or help orient the cationic ligand in the active center to optimize the conjugation reaction.

The dissociation rate constants were only modestly enhanced upon substitution of surface residues with the amidated amino acids but were increased more than 2 orders of magnitude upon substitution of active center residues supporting a role for these residues in stabilization of TFK^+-AChE conjugate. Quantitatively similar effects were observed for the dissociation rate constants for TFK^0-AChE conjugate.

The rate constants of association for the neutral trifluoroacetophenone TFK^0 were, however, virtually unaffected by charge neutralization through mutation or charge masking by ionic strength.

Effect of Ionic Strength on Rate Constants for Substrate and TFK Binding to Acetylcholinesterase-Fasciculin 2 Complex—The association rate constants for both cationic and neutral ligands for AChE·FAS2 complex were substantially reduced compared with the unligated AChE with the greater influence exerted on the charged substrate or inhibitor (Fig. 6 and Ref. 23). The most pronounced effect on FAS2 was on k_{cat}/K_m of ATCh with a decrease of more than 3 orders of magnitude (Table VI). k_{cat}/K_m showed little dependence on ionic strength.

The ionic strength dependence of the second-order association rate constant was, however, inverted for TFK^+ association with FAS2·AChE complex where the rate constant actually decreases at low ionic strength. Accordingly the rate constants for TFK^+ association with the FAS2 complexed and free AChE differ by nearly 3 orders of magnitude at low ionic strength. The inverted dependence of ionic strength on the rate constant of the FAS2·AChE complex suggests that the bound FAS2 confers both a steric and electrostatic barrier to TFK^+ entry to the gorge. The two barriers combined slow the reaction by nearly 3 orders of magnitude (at zero ionic strength), of which about 1 order of magnitude corresponds to the steric barrier

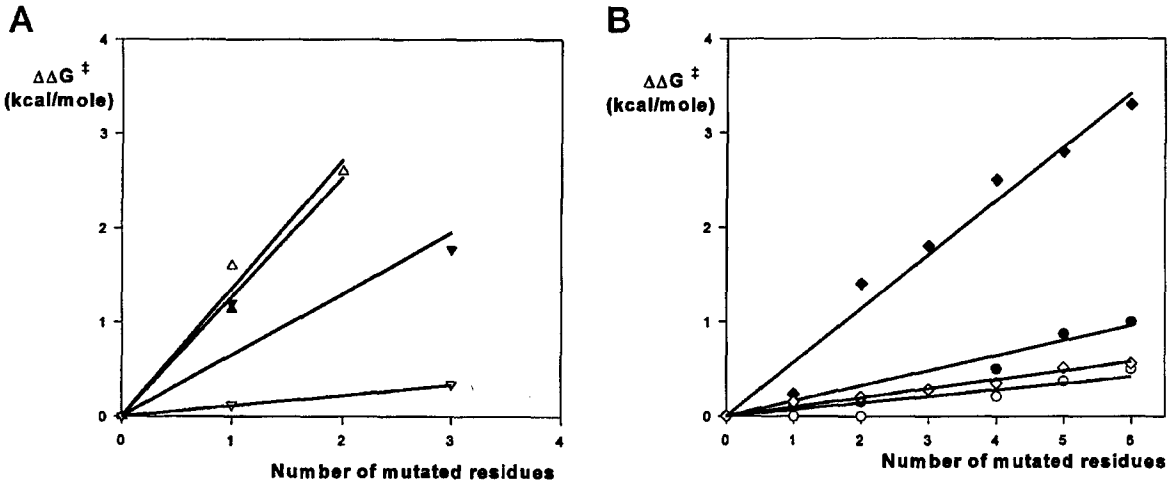

FIG. 7. **The difference of the change in free energy ($\Delta\Delta G^{\ddagger}$) between mutant and wild-type mouse AChE for association of TFK^+ and FAS2 with the mutant mouse AChEs at 0 and 670 mM ionic strength.** *A*, active center mutants: FAS2 at I = 0 mM (▼) and I = 670 mM (▽); TFK^+ at I = 0 mM (▲) and I = 670 mM (△). *B*, surface mutants: FAS2 at I = 0 mM (◆) and (◇) I = 670 mM (◇); TFK^+ at I = 0 mM (●) and I = 670 mM (○).

(difference at high ionic strength), and the remaining 2 orders to the electrostatic barrier. The rate constants of TFK^+ and TFK^0 dissociation from the AChE·FAS2 complex were increased by 30- and 3-fold, respectively, suggesting that FAS2 allosterically influences the stability of the trifluoroacetophenone conjugates with AChE.

Brownian Dynamics Simulations of Cationic Ligand Encounter with Acetylcholinesterase—The second-order rate constants for the encounter of a spherical cation with the entrance to the gorge of mouse AChE at 0 and 670 mM ionic strength were calculated using a Brownian dynamics simulations. Results for wild-type enzyme and a set of nine single and multiple mutants were compared with constants experimentally measured for TFK^+ (Table VII).

The rate constants calculated for wild-type enzyme at low and high ionic strengths were in very good agreement with the experimental values. Individual replacements of surface anionic residues resulted in a progressive reduction of the calculated rate constants. The decreases in rates found in the experiment for TFK^+ were in good accord with the calculated values. By contrast, the Brownian dynamics calculations did not reflect the reductions in rate constants seen upon neutralization of active center anionic residues. For example, an active center mutant, in which three anionic residues within the active center gorge were neutralized, showed only a 32% decrease in the rate constant calculated from Brownian dynamics, whereas the experimentally measured constant decreased more than 2 orders of magnitude. Simulations that probe the behavior of cationic ligands within the gorge would be expected to reflect these reductions (5).

Ratios of rate constants calculated for the reaction at 0 and 670 mM ionic strengths were also analyzed. This ratio decreased with an increasing number of amino acid substitutions and fell to 40% of the wild-type value upon substitution to six neutral residues on the enzyme surface. The three-residue mutant of the active center exhibited a decrease of the ratio to 70% of the wild-type value. The experimentally determined ratios for TFK^+ were essentially identical to the calculated ones. The close agreement of calculated constants with experimental values for TFK^+ association with AChE provides additional support for the electrostatic influence of AChE surface anionic residues in the rate-limiting step of this reaction. Active center anionic residues, where substantial disparity exists between experiment and computation, likely influences TFK^+ reactivity with the active serine, in addition to their long range electrostatic influence. Since the computations treat the ligand as an isotropic sphere that only moves outside of the gorge, factors influencing translation within the gorge or orientation of the ligand on the efficiency of the reaction will not be accounted for in the computations.

TABLE VIII

The differences in change in free energy ($\Delta\Delta G^{\ddagger}$) per mutated residue between mutant and wild-type AChE for association of TFK^+ and FAS2 with the enzyme at low (0 mM) and high (670 mM) ionic strength

The difference is given separately for residues mutated at the active center and on the surface. The value of ($\Delta\Delta G^{\ddagger}$) is calculated as slope of the lines from Fig. 7.

Ligand	Mutants	I	($\Delta\Delta G^{\ddagger}$) per residue
		mM	*kcal mol*$^{-1}$
TFK^+	Surface	0	0.16 ± 0.01
		670	0.069 ± 0.009
	Active center	0	1.3 ± 0.1
		670	1.4 ± 0.1
FAS2	Surface	0	0.57 ± 0.02
		670	0.096 ± 0.003
	Active center	0	0.65 ± 0.13
		670	0.11 ± 0.00

DISCUSSION

Our findings show that the multiple anionic residues on the AChE surface make modest incremental contributions to enhancing the rate of reaction of cationic ligands such as TFK^+ with the active center of the enzyme, whereas the contributions of the three anionic residues within the gorge are far larger. Trifluoroketones are known to react with the active center serine forming a hemiketal conjugate (35, 36). In the case of the cationic congener, TFK^+, the reaction appears rate-limited by diffusional entry to the gorge rather than the conjugation reaction forming the hemiketal. The influence of surface residues, as well as the absolute rate of ligand association, can be predicted with Brownian dynamics simulations. The simulations reported here, which use a spherical cationic TFK^+ that remains outside the gorge, appropriately account for the long range electrostatic influences but underestimate the influence of anionic residues within the gorge. Anionic residues within the gorge are likely to be critical for trapping cationic ligands that have entered the gorge and for achieving the reactive orientation of cationic ligands, factors not considered in the current Brownian dynamics simulations.

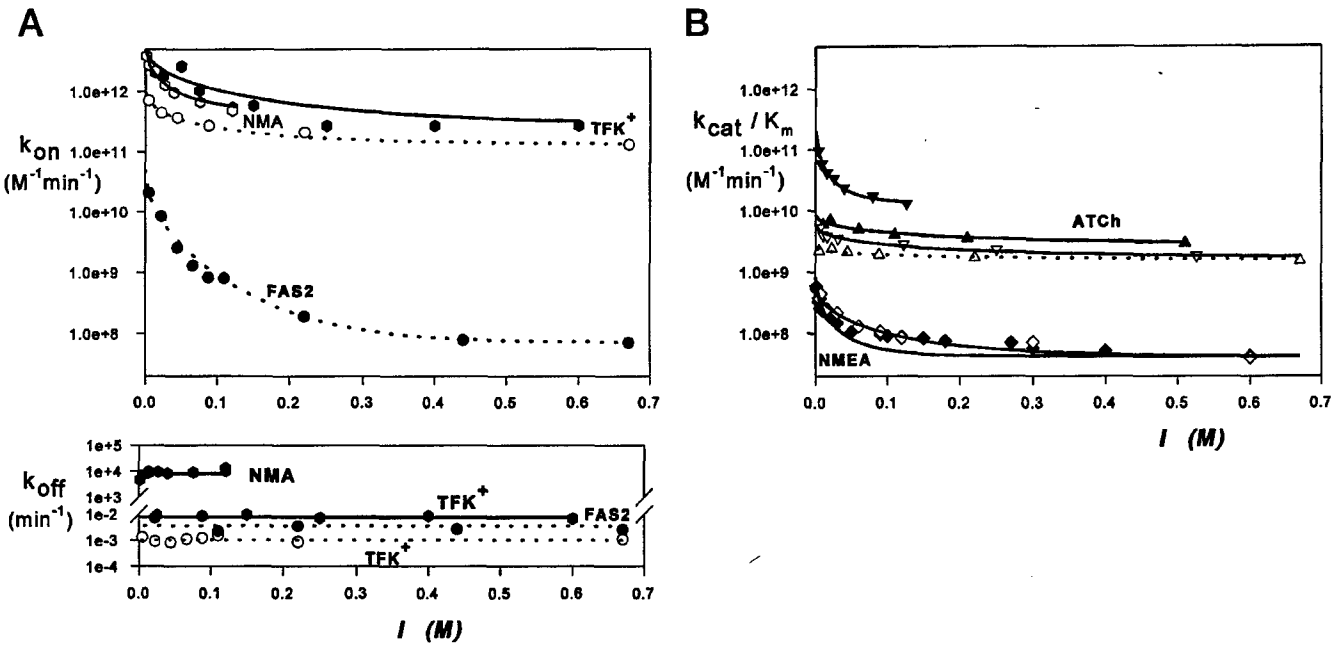

FIG. 8. **Literature data on ionic strength dependence of rate constants for ligands and various wild-type AChEs***Curves* were calculated as a best fit of data to Eq. 2. Evaluated constants and source of experimental data are given in Table IX*Dashed lines* represent data from this study. *A*, association (k_{on}) and dissociation (k_{off}) rate constants for TFK^+ with *T. californica* (★) and mouse AChE (○); *N*-methylacridinium (*NMA*) with *E. electricus* AChE (●) and FAS2 with mouse AChE (●). *B*, the second-order turnover constants (k_{cat}/K_m) of substrates ATCh with *E. electricus* (▼), *T. californica* (▲), human (▽), and mouse AChE (△); 2-(*N*-methylmorpholinium)ethyl acetate (*NMEA*) with *E. electricus* (◇) and cobra venom AChE (◆).

TABLE IX

Ionic strength dependence of rate constants for association and dissociation of inhibitors and for turnover of substrates with different wild-type AChEs

Constants were calculated using data from references cited below and from this paper (mouse AChE) k_{on}^0 and k_{on}^H are inhibitor second-order association rate constants at 0 and 670 mM ionic strengths, respectively. $(k_{cat}/K_m)^0$ and $(k_{cat}/K_m)^H$ are second-order reaction rate constants for substrate turnover at 0 and 670 mM ionic strengths, respectively. z_E and z_I are charges of the enzyme and ligand, respectively, involved in the interaction. Constants k_{on}^0 for inhibitors $(k_{cat}/K_m)^0$ for substrates and z_E were obtained by nonlinear regression analysis of Equation 2 using fixed values of k_{on}^H $(k_{cat}/K_m)^H$ and z_I. The first-order dissociation rate constant k_{off} was calculated as a mean of values obtained at different ionic strengths.

Ligand	Enzyme	k_{on}^0	k_{on}^H	z_I	z_E	k_{off}
		$10^9\ M^{-1}\ min^{-1}$	$10^9\ M^{-1}\ min^{-1}$			$10^{-3}\ min^{-1}$
NMA^+	*E. electricus* (1)	5400	480	+1	−3.9	$8.7 \cdot 10^6$
TFK^+	*T. californica* (2)	5100	270	+1	−2.1	9.4
	Mouse	980	130	+1	−2.3	1.1
FAS2	Mouse	49	0.088	+4	−1.2	4.4

Substrate	Enzyme	$(k_{cat}/K_m)^0$	$(k_{cat}/K_m)^H$	z_I	z_E
		$10^9\ M^{-1}\ min^{-1}$	$10^9\ M^{-1}\ min^{-1}$		
ATCh	*E. electricus* (1)	210	13	+1	−5.5
	T. californica (45)	8.5	2.9	+1	−1.4
	Human (1)	5.8	1.6	+1	−1.5
	Mouse	2.5	1.5	+1	−1.1
NMEA	*E. electricus* (46)	0.65	0.040	+1	−2.7
	Cobra venom (46)	0.83	0.027	+1	−4.9

Of the three anionic residues within the active center gorge, D74N appears to contribute the most to the ligand trapping or orientation, whereas Glu-202 has a negligible effect. Thus Asp-74 may play a role in orientation of TFK^+ similar to that shown for enantiomeric organophosphate inhibitors containing a charged, thiocholine leaving group (37). The specific role of Asp-74 is partially the consequence of its unique location in the gorge, close to the rim, and in a position to interact with incoming ligands. This residue has also been shown to assist in stabilization of peripheral site ligands (16, 19). In contrast to the behavior with the active center ligands, the rate of reaction of the large peptide, FAS2, with the interactive surface located at the rim of AChE gorge is affected similarly by both active center and surface anionic residues.

The reaction rates for the cationic ligands show a marked dependence on ionic strength consistent with electrostatic dipole vector guiding diffusion into the gorge for TFK^+ and to the rim of the gorge for FAS2. FAS2 shows a greater ionic strength dependence than TFK^+, consistent with its multiple net positive charges. However, if analyzed on a unit charge basis, z_E is smaller for FAS2 than TFK^+, a finding in accord with the lower density of interacting anionic residues at the rim of the gorge. The increase in FAS2 reaction rates of more than 2 orders of magnitude observed at low ionic strength yields rate constants of the magnitude expected for diffusion-limited reactions. The acceleration in rate at low ionic strength is virtually eliminated upon a 6-fold substitution of anionic residues at the AChE surface. However, the magnitude of the free energy change ($\Delta\Delta G^{\ddagger}$, Fig. 7) imparted by ionic strength is only 4-fold larger for FAS2 than for TFK^+ and is linearly dependent on the

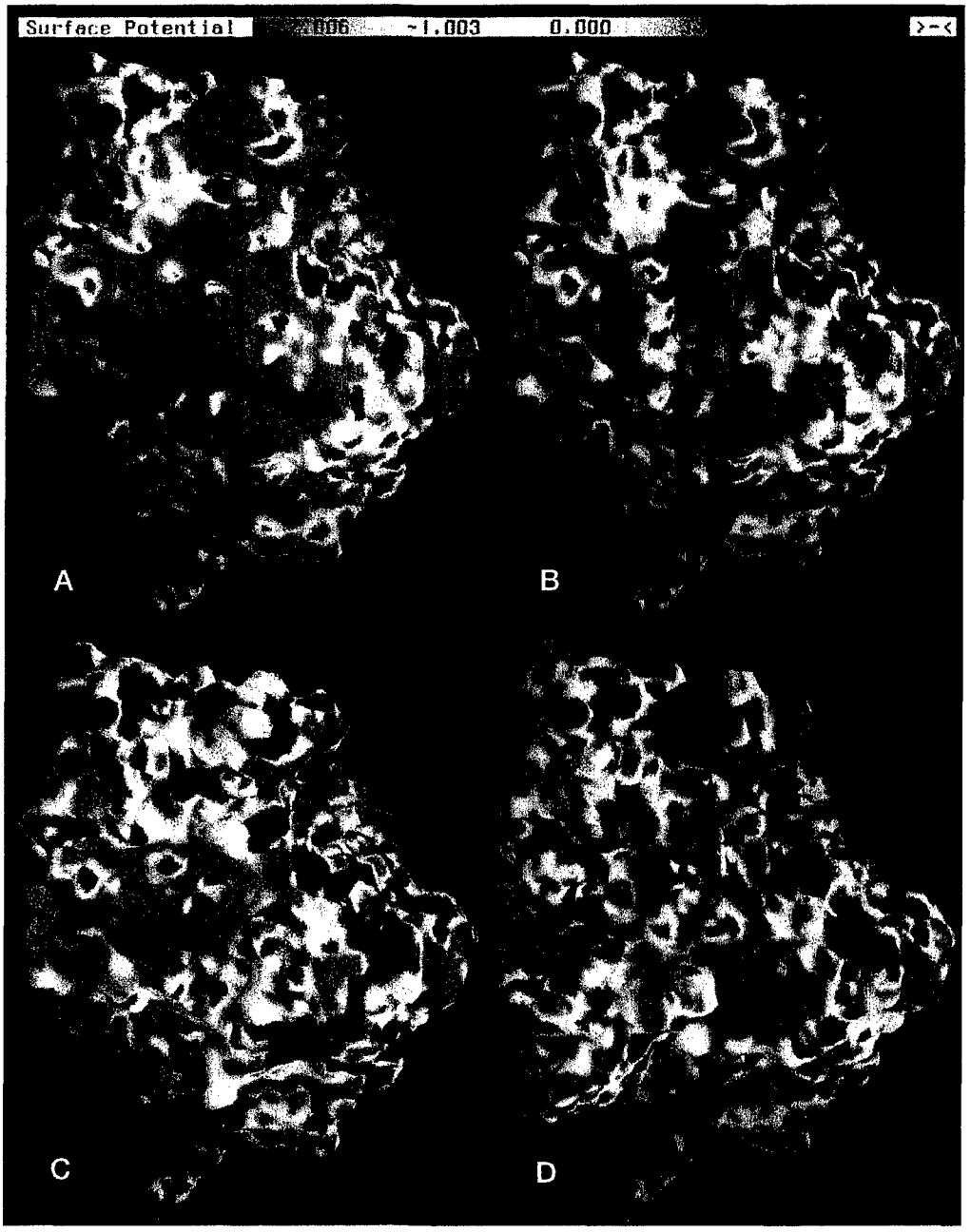

FIG. 9. **GRASP representation of electrostatic potential generated by UHBD for the following: *A*, wild-type mouse AChE; *B*, D74N/E202Q/E450Q mouse AChE mutant; *C*, E84Q/E91Q/D280V/D283N/E292Q/D372N mouse AChE mutant; *D*, wild-type mouse AChE·FAS2 complex.** The opening of the active center gorge is visible as an indentation located in the center of the molecule.

number of mutated residues (Fig. 7, Table VIII). The difference in free energy between TFK^+ and FAS2 is consistent with the difference in net charge for the two cationic ligands.

Rate constants for ligand association and dissociation can be related to the transition state in forming the complex by Equations 3 and 4.

$$k_{on} = \kappa(kT/h)e^{-\Delta G^{\ddagger}_{on}/RT} \quad \text{(Eq. 3)}$$

$$k_{off} = \kappa(kT/h)e^{-\Delta G^{\ddagger}_{off}/RT} \quad \text{(Eq. 4)}$$

where $\Delta G^{\ddagger}_{on} = G^{\ddagger} - G_{E+I}$, $\Delta G^{\ddagger}_{off} = G^{\ddagger} - G_{EI}$, k is Boltzmann's constant, h is Planck's constant, T is the absolute temperature, and κ is the transmission coefficient.

The insensitivity of dissociation of TFK^+ or FAS2, k_{off}, to ionic strength indicates that the energetic relationship between the transition state and the stabilized complex is not altered by solvent changes. Hence dissociation processes are not influenced by the electric field on AChE and intervening ions in the solvent. By contrast, association kinetics of TFK^+ and FAS2 show that the diminished activation barrier for restricted diffusion into the gorge imparted by the electrostatic attraction is partly masked by increasing the ionic strength. The same masking is evident when TFK^+ diffuses into the gorge of the FAS2·AChE complex; however, in this case, the masking accelerates the reaction. Accordingly, a unique repulsive electrostatic influence is evident as TFK^+ traverses an altered activation barrier in the FAS2 complex. Since this phenomenon is not replicated by simple charge neutralization on AChE, it likely arises from the close apposition of the TFK^+ cation

with a domain of cationic charges in FAS2 during TFK^+ entry into the gorge.

Shown in Fig. 9 are potential energy maps of wild type, a mutant with the three anionic side chains in the gorge neutralized, a mutant with six surface residues neutralized, and a FAS2-wild-type AChE complex. For the surface residues mutant, reduction of the overall charge is evident, yet a negative sector in the 9 o'clock position to the gorge entrance remains. Neutralization of the three active center gorge residues results in a locus of positive charge deep within the gorge.

Shafferman and colleagues (12) have previously analyzed human AChEs substituted with amidated amino acids for Asp and Glu at seven surface positions outside the gorge and examined substrate hydrolysis kinetics and edrophonium binding at two ionic strengths. They demonstrated a minimal influence of surface charge on acetylthiocholine hydrolysis kinetics and the reversible binding of edrophonium. However, association rates for the ligands were not examined in these studies as is possible for the more potent inhibitors, FAS2 and TFK^+. Also, as considered below, substrate hydrolysis kinetics in human AChE and edrophonium binding are likely not to be diffusion-limited and therefore not fully reveal the electrostatic influences on the critical diffusion step.

AChEs from *T. californica* and *E. electricus* have higher turnover numbers for ATCh than the mammalian AChEs, and their substrate kinetics appear to approach the diffusion limit (3, 4) as suggested by a compilation of data on the ionic strength dependence of AChE catalysis and inhibition (Fig. 8 and Table IX). Similar to hydrolysis by human AChE, the rates of ATCh hydrolysis catalyzed by mouse enzyme defined by k_{cat}/K_m are only moderately dependent on ionic strength, and therefore, diffusion is not the prevailing rate-limiting step. The rate constants for association of cationic ligands TFK^+ and FAS2 with this enzyme approach the diffusion limit, providing more sensitive tools for monitoring structural elements involved in controlling rates of access of cationic ligands to AChE.

Early kinetic observations on the role of electrostatic interactions in AChE catalysis (1) have been reinforced by both theoretical considerations (9, 10, 13) and analysis of charge and ionic strength presented in this study. We are able to distinguish two types of electrostatic interactions of mouse AChE with cationic ligands. First, acceleration of the initial encounter rates of the cation with the enzyme by anionic residues, which is diminished upon sequential substitution of up to six anionic residues on the enzyme surface or upon increasing the ionic strength of reaction medium. Second, the acceleration of cation reaction rates, seen at all ionic strengths, result from trapping of the ligand and/or optimizing the reactive orientation of the ligand in the active center. While both surface and active center anionic residues contribute similarly to the acceleration of cation encounter, only active center anionic residues, in particular Asp-74, show a pronounced influence on trapping and/or orientation of cationic ligands. Other theoretical and experimental data suggest that in addition to Coulombic interactions, significant contributions to ligand orientation may come from interactions of cations with aromatic residues in the enzyme (23, 38, 39). Similar short range electrostatic interactions are likely involved in the interactions between cationic ligands and three aromatic residues at the AChE peripheral site (19, 39).

The FAS2·AChE complexes still exhibit capacities for residual ester substrate hydrolysis (23, 40, 41), for acylation by organophosphates (23, 40), and for hemiketal formation at the active serine (23). The binding of the reversible inhibitor, *N*-methylacridinium, shows a 1000-fold reduction in rates of association and dissociation with FAS2-AChE; yet the compensatory influence of FAS2 on the opposing rates still leaves a relatively high affinity complex (42). The degree of reduction in k_{on} is in reasonable agreement to 100-fold reduction in k_{on} for smaller TFK^+, measured under the same experimental conditions (*cf.* Fig. 6). Charge neutralization by FAS2 in its AChE complex is globally equivalent to removal of four anionic charges by site mutagenesis. Since the complex still retains a net negative charge of −4, the inverted ionic strength dependence uniquely seen for TFK^+ association in the FAS2·AChE complex and not in the corresponding charge neutralized enzyme can best be explained by TFK^+ traversing a path close to the bound FAS2 upon entering the gorge. Upon approaching the active center in the AChE·FAS2 complex, TFK^+ experiences about 10-fold slow down due to steric limitations and close to 100-fold slow down due to the electrostatic barrier. The surface area of Van der Waals contact at the FAS2-AChE interface extends over 1100 $Å^2$, and no gap between the FAS2 plug and gorge rim for substrate entry is evident in the crystal structures of the FAS2·AChE complexes (8, 43) (*cf.* Fig. 9*D*). Hence extensive breathing of the complex or a major conformational change would be expected to be required to accommodate substrate entry. However, to date, the nature of the conformational change or molecular motion has not been revealed through study of alternative crystal forms or conformational dynamics.

Electrostatic considerations appear to take on an increasingly important role in functioning of proteins involved in neurotransmission. A recent description of an "electrostatic switch" in synaptotagmin-mediated neurotransmitter release from synaptic vesicles (44), the suggestion of electrostatics influencing the subunit interface for neurotransmitter binding to the nicotinic acetylcholine receptor (47), and the guidance of an electric field in AChE to accelerate clearance of neurotransmitter in the synapse point to involvement of electrostatics in the precise temporal control of synaptic transmission. This mechanism has the virtue of high speed and low energy cost when compared with conformational changes.

Acknowledgments—The assistance of students Dinah Misner and Alexander Zambon in generation of some of multiple AChE mutants and help of Snjezana Radić in completion of kinetic experiments is appreciated. P. D. K. thanks Dr. Adrian H. Elcock for his help in setting up the mouse AChE system used in the Brownian dynamics simulations and for many useful discussions. We also thank Dr. Gabi Amitai for helpful suggestions in the initial phase of this work.

REFERENCES

1. Nolte, H.-J., Rosenberry, T. L. & Neumann, E. (1980) *Biochemistry* **19,** 3705–3711
2. Quinn, D. M., Seravalli, J., Nair, H. K., Medhekar, R., Husseini, B., Radić, Z., Vellom, D. C., Pickering, N. & Taylor, P. (1995) in *Enzymes of the Cholinesterase Family* (Quinn, D. M., Balasubramanian, A. S., Doctor, B. P. & Taylor, P., ed) pp. 203–207, Plenum Publishing Corp., New York
3. Rosenberry, T. L. (1975) *Adv. Enzymol. Relat. Areas Mol. Biol.* **43,** 103–218
4. Quinn, D. M. (1987) *Chem. Rev.* **87,** 955–979
5. Antosiewicz, J., Briggs, J. M., Elcock, A. H., Gilson, M. K. & McCammon, J. A. (1996) *J. Comput. Chem.* **17,** 1633–1644
6. Antosiewicz, J., McCammon, J. A. & Gilson, M. K. (1996) *Biochemistry* **35,** 7819–7833
7. Sussman, J. L., Harel, M., Frolow, F., Oefner, C., Goldman, A., Toker, L. & Silman, I. (1991) *Science* **253,** 872–879
8. Bourne, Y., Taylor, P. & Marchot, P. (1995) *Cell* **83,** 503–512
9. Tan, R. C., Truong, T. N., McCammon, J. A. & Sussman, J. L. (1993) *Biochemistry* **32,** 401–403
10. Ripoll, D. R., Faerman, C. H., Axelsen, P. H., Silman, I. & Sussman, J. (1993) *Proc. Natl. Acad. Sci. U. S. A.* **90,** 5128–5132
11. Porschke, D., Creminon, D., Cousin, X., Bon, C., Sussman, J. & Silman, I. (1996) *Biophys. J.* **70,** 1603–1608
12. Shafferman, A. Ordentlich, A., Barak, D., Kronman, C., Ber, R., Bino, T., Ariel, N., Osman, R. & Velan, B. (1994) *EMBO J.* **13,** 3448–3455
13. Antosiewicz, J., McCammon, J. A., Wlodek, S. T. & Gilson, M. K. (1995) *Biochemistry* **34,** 4211–4219
14. Antosiewicz, J., Wlodek, S. T. & McCammon, J. A. (1996) *Biopolymers* **39,** 85–94
15. Taylor, P. & Lappi, S. (1975) *Biochemistry* **14,** 1989–1997
16. Radić, Z., Duran, R., Vellom, D. C., Li, Y., Cervenansky, C. & Taylor, P. (1994) *J. Biol. Chem.* **269,** 11233–11239

17. Epstein, D. J., Berman, H. A. & Taylor, P. (1979) *Biochemistry* **18,** 4749–4754
18. Barak, D., Ordentlich, A., Bromberg, A., Kronman, C., Marcus, D., Lazar, A., Ariel, N., Velan, B. & Shafferman, A. (1995) *Biochemistry* **34,** 15444–15452
19. Radić, Z., Pickering, N. A., Vellom, D. C., Camp, S. & Taylor, P. (1993) *Biochemistry* **32,** 12074–12084
20. Karlsson, E., Mbugua, P. M. & Rodriguez-Ithurralde, D. (1984) *J. Physiol. (Paris)* **79,** 232–240
21. Nair, H. K. & Quinn, D. M. (1993) *Bioorg. & Med. Chem. Lett.* **3,** 2619–2622
22. Ellman, G. L., Courtney, K. D., Andres, V., Jr. & Featherstone, R. M. (1961) *Biochem. Pharmacol.* **7,** 88–95
23. Radić, Z., Quinn, D. M., Vellom, D. C., Camp, S. & Taylor, P. (1995) *J. Biol. Chem.* **270,** 20391–20399
24. Glasstone, S., Laidler, K. J. & Eyring, H. (1941) *The Theory of Rate Processes,* McGraw-Hill Inc., New York
25. Molecular Simulations Inc. (1996) San Diego, CA 92121–4777
26. MacKerell, A. D., Wiorkiewicz-Kuczera, J. & Karplus, M. (1995) *CHARMM 22 Parameter Set,* Harvard University, Cambridge, MA
27. Gilson, M. K., Straatsma, T. P., McCammon, J. A., Ripoll, D. R., Faerman, C. H., Axelsen, P. H., Silman, I. & Sussman, J. L. (1994) *Science* **263,** 1276–1278
28. Antosiewicz, J., Gilson, M. K. & McCammon, J. A. (1994) *Isr. J. Chem.* **34,** 151–158
29. Antosiewicz, J., Gilson, M. K., Lee, I. H. & McCammon, J. A. (1995) *Biophys. J.* **68,** 62–68
30. Madura, J. D., Davis, M. E., Gilson, M. K., Wade, R. C., Luty, B. A. & McCammon, J. A. (1994) *Rev. Comput. Chem.* **5,** 229–267
31. Ermak, D. L. & McCammon, J. A. (1978) *J. Chem. Phys.* **69,** 1352–1360
32. McCammon, J. A., Northrup, S. H. & Allison, S. A. (1986) *J. Phys. Chem.* **90,** 3901–3905
33. Madura, J. D., Briggs, J. M., Wade, R. C., Davis, M. E., Luty, B. A., Ilin, A., Antosiewicz, J., Gilson, M. K., Bagheri, B., Scott, L. R. & McCammon, J. A. (1995) *Comp. Phys. Commun.* **91,** 57–95
34. Davis, M. E., Madura, J. D., Luty, B. A. & McCammon, J. A. (1991) *Comput. Phys. Commun.* **62,** 187–197
35. Nair, H. K., Seravalli, J., Arbuckle, T. & Quinn, D. M. (1994) *Biochemistry* **33,** 8566–8576
36. Harel, M., Quinn, D. M., Nair, H. K., Silman, I. & Sussman, J. L. (1996) *J. Am. Chem. Soc.* **118,** 2340–2346
37. Hosea, N. A., Radić, Z., Tsigelny, I., Berman, H. A., Quinn, D. M. & Taylor, P. (1996) *Biochemistry* **35,** 10995–11004
38. Dougherty, D. A. (1996) *Science* **271,** 163–168
39. Ordentlich, A., Barak, D., Kronman, C., Flashner, Y., Leitner, M., Segall, Y., Ariel, N., Cohen, S., Velan, B. & Shafferman, A. (1993) *J. Biol. Chem.* **268,** 17083–17095
40. Marchot, P., Khelif, A., Ji, Y.-H., Mansuelle, P. & Bougis, P. E. (1993) *J. Biol. Chem.* **268,** 12458–12467
41. Eastman, J., Wilson, E. J., Cerveñansky, C. & Rosenberry, T. L. (1995) *J. Biol. Chem.* **270,** 19694–19701
42. Rosenberry, T. L., Rabl, C.-R. & Neumann, E. (1996) *Biochemistry* **35,** 685–690
43. Harel, M., Kleywegt, G. J., Ravelli, R. B., Silman, I., Sussman, J. L. (1995) *Structure* **3,** 1355–1366
44. Shao, X., Li, C., Fernandez, I., Zhang, X., Sudhof, T. C. & Rizo, J. (1997) *Neuron* **18,** 133–142
45. Berman, H. A. & Leonard, K. (1990) *Biochemistry* **29,** 10640–10649
46. Tougu, V., Pedak, A., Kesvatera, T. & Aaviksar, A. (1987) *FEBS Lett.* **225,** 77–81
47. Tsigelny, I., Sugiyama, N., Sine, S. & Taylor, P. (1997) *Biophys. J.* **73,** 52–66

Enantiomer, Vol. 2, pp. 249–260
Reprints available directly from the publisher
Photocopying permitted by license only

Determining Ligand Orientation and Transphosphonylation Mechanisms on Acetylcholinesterase by Rp, Sp Enantiomer Selectivity and Site-Specific Mutagenesis

PALMER TAYLOR[a,*], NATILIE A. HOSEA[a], IGOR TSIGELNY[a], ZORAN RADIĆ[a] and HARVEY A. BERMAN[b]

[a]*Department of Pharmacology, 0636 University of California, San Diego, La Jolla, CA 92093, U.S.A.;* [b]*Department of Biochemical Pharmacology, State University of New York at Buffalo Buffalo, NY 14260, U.S.A.*

(Received 25 June 1996; In final form 8 August 1996)

Acetylcholinesterase, an enzyme of the serine hydrolase family, catalyzes the rapid hydrolysis of certain carboxyl esters. Other acyl esters efficiently transacylate the enzyme with a subsequent, slow deacylation step. Of these, the phosphoryl and phosphonyl esters are perhaps of greatest mechanistic interest since individual enantiomers of known absolute stereochemistry can be isolated and their interactions with the dissymmetric enzyme active site examined. We describe here studies of a series of enantiomeric Rp- and Sp-alkylphosphonates interacting with mouse acetylcholinesterase. Since the acetylcholinesterase is generated by recombinant DNA methods, mutant enzymes can be made with specific replacements of individual amino acid side chains. Individual amino acid replacements in the acyl pocket, the choline subsite and at the active center gorge entry have been generated, and the reaction kinetics of the mutant enzymes analyzed. These studies have shown that substitution of aliphatic amino acids for phenylalanines 295 and 297 in the acyl pocket diminishes, and in some cases, actually inverts chiral preferences. The combined structure-activity approach, where both ligand and enzyme are modified systematically, has enabled us to show that the restricted dimensions of the acyl pocket in the active center dictate enantiomeric selectivity. Moreover, the reactions of compounds of known absolute stereochemistry show three requirements for efficient transphosphonylation: (a) apposition of the phosphate with the γ-oxygen on Ser 203 to form a pentavalent, presumed trigonal bipyramidal intermediate, (b) polarization of the phosphonyl oxygen bond by its positioning in the oxyanion hole, and (c) positioning the leaving group towards the gorge exit.

Keywords: Acetylcholinesterase, Phosphonates, Enantiomeric Inhibitors, Site-specific Mutagenesis, Serine Phosphonylation

INTRODUCTION

Cloning and sequence determination of the cholinesterases have shown that these enzymes belong to a large family of serine hydrolases [1,2] whose tertiary structure is characterized by an α,β hydrolase fold [3,4]. Included within this family are not only a large number of serine hydrolases, but several proteins that appear to serve non-hydrolytic functions. The first identi-

*Corresponding author. Tel.: 619-534-1366. Fax: 619-534-8248.

fied homologous protein, thyroglobulin [1] serves as a precursor for thyroid hormone. Subsequently, a series of proteins which appear to be involved in heterologous cell contacts and synaptogenesis (the glutactins, neurotactins, gliotactins and neuroligins) have been identified. The proteins with hydrolase activity contain a serine, glutamate (occasionally aspartate) and histidine forming a catalytic triad, with the residues found in that sequence order. The glutamate and histidine residues render the catalytic serine nucleophilic. The proteins of this family also contain at least two characteristic disulfide loops. Figure 1 details the sequence identities and residue positions in this family of proteins.

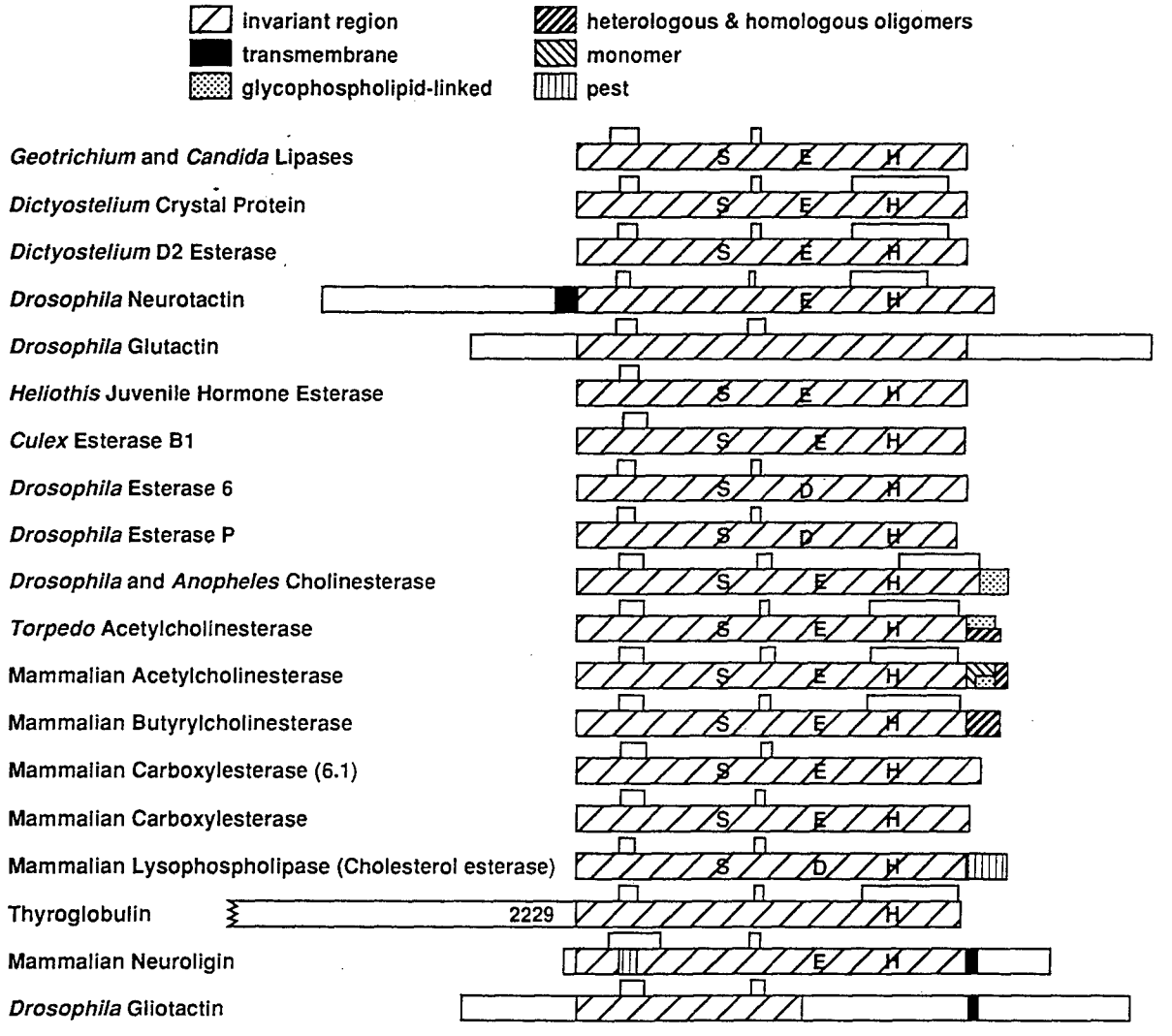

FIGURE 1 The cholinesterase superfamily is composed of an expanding number of proteins with documented homology in sequence but diverse and eclectic functions. Shown by the various hatch and stippled markings are the regions of sequence identity and specialized and/or alternatively spliced regions of sequence. The bars above each linear sequence denote conserved cysteines and intra-subunit disulfide bonds. The S, E (D) and H symbols denote the essential serine, glutamate (aspartate) and histidine in each catalytic triad. Note that the glutactins, neurotactins, gliotactins, thyroglobulins and neuroligins do not contain all three essential residues, consistent with their lack of catalytic activity (cf: [1], [26], [27]).

The determination of the three-dimensional structure of first the *Torpedo* [4], and then the mammalian acetylcholinesterase (AChE) [5], provided essential structural templates for the analysis of the catalytic mechanism. The catalytic triad resides at the base of a narrow gorge, 18–20Å in depth, which is heavily lined with aromatic residues. The active center containing this catalytic triad is located nearly centrosymmetric to the subunit.

The cholinesterases show considerable diversity in the catalysis of hydrolytic reactions and are well known for their high catalytic efficiency (k_{cat} approaching 10^4 molecules of acetylcholine per molecule of enzyme per sec). In addition to hydrolysis of carboxyl esters, such as in the natural substrate and neurotransmitter-acetylcholine, phosphoryl, phosphonyl, sulfonyl and carbamoyl esters or halides also react with the enzyme to form the corresponding acyl enzymes. With the latter compounds enzyme deacylation is slow, and hence they may be thought of as hemisubstrates. Since the hemisubstrates block access of acetylcholine to AChE, they are effective inhibitors of the enzyme and are employed therapeutically for this purpose (cf: [2]). Trifluoroacetophenones also conjugate with the active center serine, leading to the formation of hemiketals [6,7].

The carboxyl esters, the carbamoyl esters and the trifluoroacetophenones are all planar, with the moieties attached to the electrophilic carbon in a trigonal geometry. Hence substrate enantiomers at the reactive carbon do not exist, and the planar configuration confers minimal steric constraints for exit of a leaving group in a gorge of limited dimensions. By virtue of their tetrahedral configuration, the phosphonates contain an asymmetric phosphorus atom when it is surrounded by chemically different groups. Such asymmetry, and the observation of a measurable chiral preference in reaction with AChE, permits direct inferences on the nature (steric; electrostatic charge) of amino acid residues within the active center of the enzyme. Moreover, the capacity to alter structure in a precise manner through site-directed mutagenesis, allowed us to manipulate, not only the structure of the organic moiety undergoing reaction with the enzyme, but selected amino acid residues within the reactive pocket of the enzyme.

The studies that we describe employ enantiomeric methylphosphonates containing organic residues surrounding the asymmetric phosphorus. These agents were synthesized through reaction of *l*-(−)-ephedrine with methylphosphonothioic dichloride to form separable diastereomers, (2Rp,4S,5R)- and (2Sp,4S,5R)-2,3,4-trimethyl-5-phenyl-1,3,2-oxazaphospholidine-2-thione (Scheme 1; **1a,b**) [10–12]. These individual diastereomers were resolved through column chromatography, and were then subjected to reaction with an alcohol, subsequent hydrogenolysis, and then final reaction with an appropriate alkyl halide. Each chemical step in this procedure yields a predictable stereochemical outcome. This factor, coupled with resolution of a common precursor (**1a,b**) during an early step in

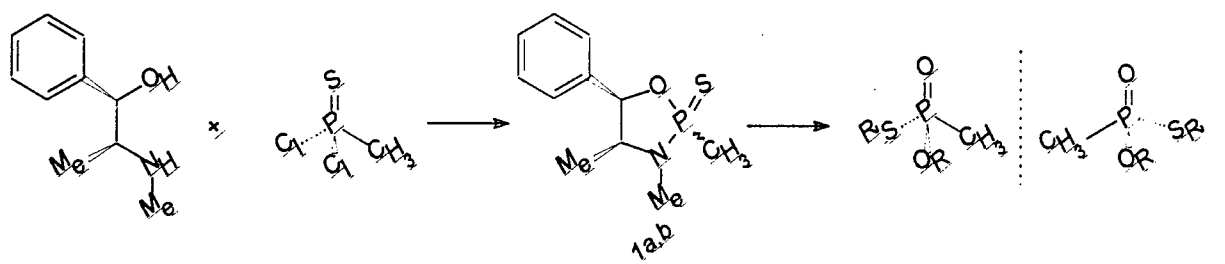

SCHEME 1

the synthetic scheme, afforded unambiguous assignment of configuration of the final products.

Three families of agents were synthesized: enantiomeric cycloheptyl-, isopropyl-, and 3,3-dimethylbutyl methylphosphonothioates containing thiomethyl-, thioethyl-, and thiocholine leaving groups (see Table I). The phosphonyl ester moieties, comprising cyclic and acyclic

TABLE I Structures of compounds employed. CHMP, iPrMP and DMBMP refer to cycloheptyl-, isopropyl- and 3,3-dimethylbutyl-methylphosphonyl

Sp	Rp
CHMP thiocholine	
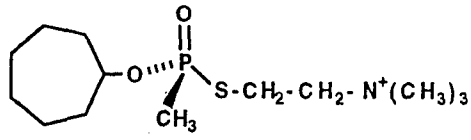	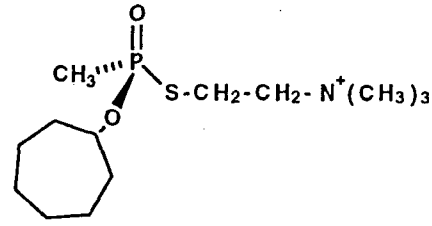
iPrMP thiocholine	
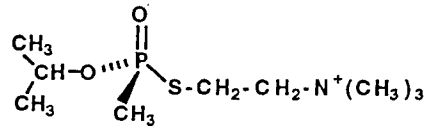	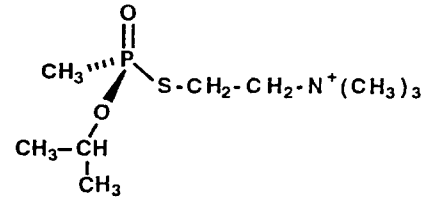
DMBMP thiocholine	
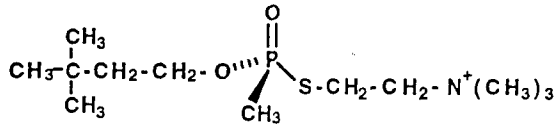	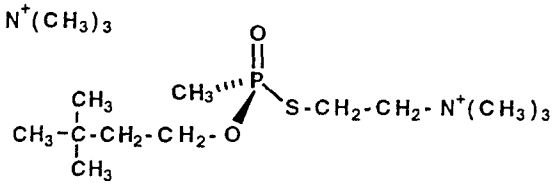
CHMP thiomethylate	
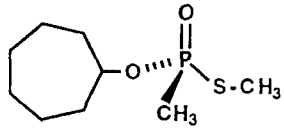	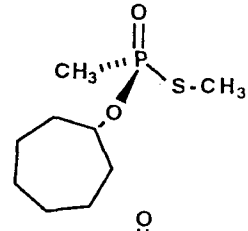
CHMP thioethylate	
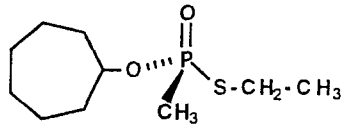	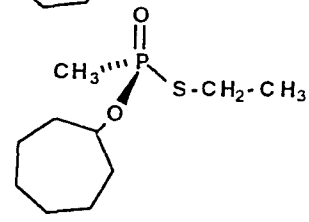

branched alkyl groups, are seen to differ in their hydrophobicity and the steric properties with which they interact with the enzyme surface. Of particular interest are the enantiomeric 3,3-dimethylbutyl methylphosphonyl thiocholines. For these agents, since the space-filling properties of the leaving group and the alkyl ester are similar, inversion of configuration is not expected to engender substantial steric interference to binding.

Thus, analysis of the reaction of tetrahedral phosphonates with the cholinesterases adds another dimension to structure-activity considerations of ligands interacting at a target site. Herein, we examine the specificity for AChE of Rp and Sp enantiomeric phosphonates containing uncharged and charged leaving groups.

METHODS

The procedures for site-specific mutagenesis, transfection of expression plasmids containing the cDNA of interest, selection of stable transfectants, expression of mouse AChE in human embryonic kidney cells, isolation and purification of the recombinant wild-type and mutant enzymes, and kinetic analyses have been presented previously [8,9]. The synthesis, modeling and characterization of the enantiomeric phosphonates (Table I) have also been documented previously [10–12].

RESULTS

Studies on ligand specificity for the cholinesterases, when coupled with the recent findings from X-ray crystallography [4,5] and site-specific mutagenesis [13–15], reveal three distinct domains on the enzyme: (a) the acyl pocket of the active center, (b) the choline binding site in the active center, and (c) a peripheral anionic site residing near the rim of the gorge. Ligands interacting with these sites and the residues that have an important involvement at these sites are detailed below [13–16].

AChE has phenylalanines at positions 295 and 297 which extend towards the substrate binding site and, as such, delimit the dimensions of this site. Butyrylcholinesterase contains leucine and isoleucine at the corresponding positions, and this accounts for its capacity to catalyze the hydrolysis of the larger substrate butyrylcholine as rapidly as acetylcholine (Figure 2). Mutation of Phe 295 and Phe 297 in AChE to Leu and Ile, respectively, results in an enzyme with butyrylcho-

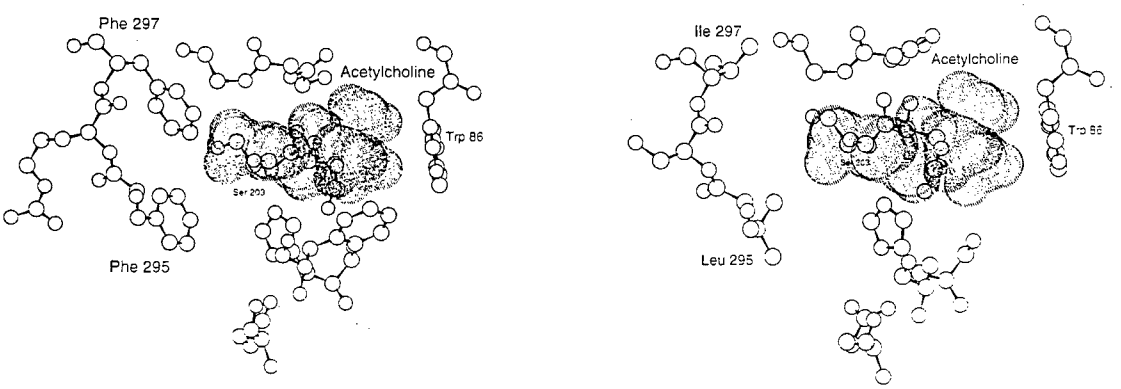

FIGURE 2 Positions of acetylcholine in native (A) and in Phe295Leu; Phe297Ile (B) acetylcholinesterases. Structures were developed from the crystallographic coordinates of *Torpedo* AChE [4] and are based on the probable positioning of the substrate.

linesterase specificity [13–16], as well as substrate activation, a characteristic of butyrylcholinesterase [15]. Examination of the chiral preference of a series of Rp- and Sp-alkylmethylphosphonyl thiocholines, containing cycloheptyl, isopropyl or 3,3-dimethylbutyl ester moieties shows that up to a 230-fold enantiomeric selectivity is achieved for AChE (Table II). The chiral preference appears greater for the more bulky alkyl groups and for secondary rather than primary alkyl groups. Replacement of the Phe with Leu and Ile at these positions results in a loss of enantiomeric selectivity and, in fact, upon replacement at the 297 position, the 230-fold preference for the Sp enantiomer reverts to a slight preference for the Rp enantiomer.

Since the absolute stereochemistry of the phosphonates is known [10], the Rp and Sp enantiomers of the phosphonates can be positioned within the active center, either by docking as an initial tetrahedral complex or as a pentavalent, trigonal bipyramidal intermediate; the latter would simulate the putative transition state for an associative mechanism. In addition to the apposition of the γ-oxygen of the catalytic serine (Ser 203) with the phosphorus, there is substantial evidence for the placement of the phosphonyl oxygen in the oxyanion hole as a requirement for transphosphonylation [6,17–19]. In particular, the crystal structure of a phosphonylated intermediate with a *Candida* lipase, an enzyme homologous to AChE, shows the insertion of its phosphonyl oxygen in the oxyanion hole [20]. Upon positioning the phosphorus in bonding distance with the serine and the phosphonyl oxygen in the oxyanion hole, neither the leaving group nor the bulky alkoxyl groups can fit into the acyl pocket of limited dimensions; only the methyl group on the phosphonate should be devoid of steric hindrance in the acyl pocket. Accordingly, the orientation permits the Sp enantiomer to have the thiocholine leaving group pointed out towards the gorge entrance; whereas in the Rp enantiomer, the thiocholine is oriented behind the cycloheptyl group. Consequently, the cycloheptyl moiety is directed out of the gorge with the respective orientations of the alkoxyl and thioalkyl groups interchanged. In this configuration the leaving group would suffer from two orientational constraints: (a) the leaving group is pointed in the wrong direction and it must traverse around the bulky cycloheptyl group for exit from the gorge; (b) an apical positioning of the serine and leaving group would be limited by dimensional constraints of the gorge wall. Hence the higher reactivity of the Sp enantiomer can be explained on these grounds. However, the data are less informative regarding the reactive orientation of the less active, Rp, enantiomer during the transphosphonylation reaction.

To shed further light on this issue, we have expanded our structural considerations to include uncharged thioates, as well as examined additional mutations in the enzyme. Although the uncharged thioates with methanethiol and ethanethiol as leaving groups are about 1000-fold less reactive with both the *Torpedo* [10,12]

TABLE II Rates[a] of transphosphonylation by Rp- and Sp-alkyl methylphosphonyl thiocholine with wild-type and acyl pocket mutations of mouse acetylcholinesterase

Enzyme	Alkyl Group								
	Cycloheptyl			Isopropyl			3,3-Dimethylbutyl		
	Sp	Rp	Sp/Rp	Sp	Rp	Sp/Rp	Sp	Rp	Sp/Rp
AChE (wild type)	190,000	820	230	16,000	140	110	360,000	19,000	19
Phe 295 Leu	66,000	8,700	7.6	3,400	1,200	3	140,000	10,000	14
Phe 297 Ile	16,000	62,000	0.3	950	1,200	0.8	56,000	12,000	5

[a]Rate constants given as 10^3/Mmin; the standard error of the mean from typically three experiments was 10–15%. Data were obtained from reference [8].

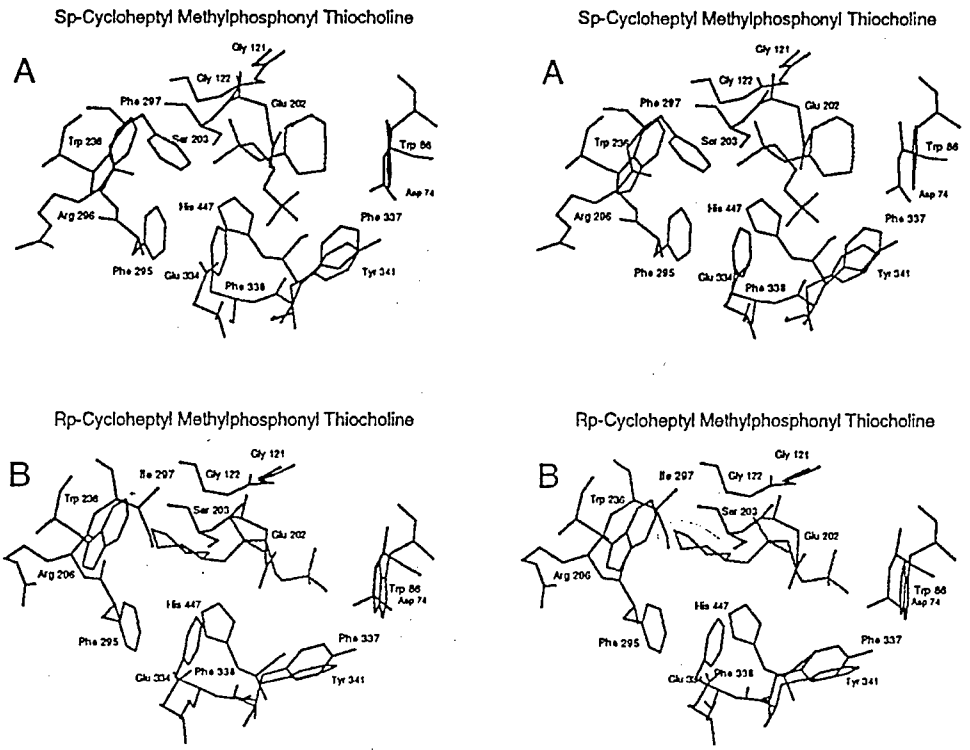

FIGURE 3 Stereoviews of Sp- and Rp-cycloheptyl methylphosphonothiocholine docked in the active center of native (A) and Phe297Ile (B) acetylcholinesterase. Residues of the acyl pocket (Phe 295 and 297), choline binding subsite (Trp 86, Tyr 337, Glu 202) are shown (cf: ref. [8] for details).

and mouse AChEs (Tables II and III), the enantiomeric selectivities for the wild-type and mutant AChEs are virtually the same as the charged compounds. This would suggest, but not prove, that the additional charge and volume of the thiocholine have little influence on the reactive orientations of the Rp and Sp phosphonates. In addition, the comparison of reaction rates for charged and uncharged phosphonates shows residues in the acyl pocket do not account for their reactivity differences.

Having established the above principles on ligand position, we have gone on to modify charge within the active center gorge at the positions of Glu 202, Glu 450, and Asp 74 by isosteric replacement to form the corresponding carboxamides. Glu 202 and Glu 450 reside deep within the gorge and may be involved in facilitating the polarization of the phosphonyl oxygen. Their influence on the transphosphonylation reaction shows no preference for the charged or uncharged leaving group. Moreover, these mutations do not affect appreciably the chiral preference (Table IV). However, the isosteric mutation of Asp 74 to the neutral Asn, results in a marked reduction of transphosphonylation for the charged phosphonates but not the uncharged compounds. In fact, there appears to be a slight increase in the rate of transphosphonylation for the uncharged compounds (Table IV).

Despite the great reductions in rate of phosphonates of the cationic enantiomers, enantiomeric preference for the Rp and Sp phosphonylation does not change with the Asp74Asn mutation. This suggests that the trimethylammonio moieties in the Rp and Sp enantiomers reside at similar distances from Asp 74 in the transition state; otherwise, it is unlikely that the Coulom-

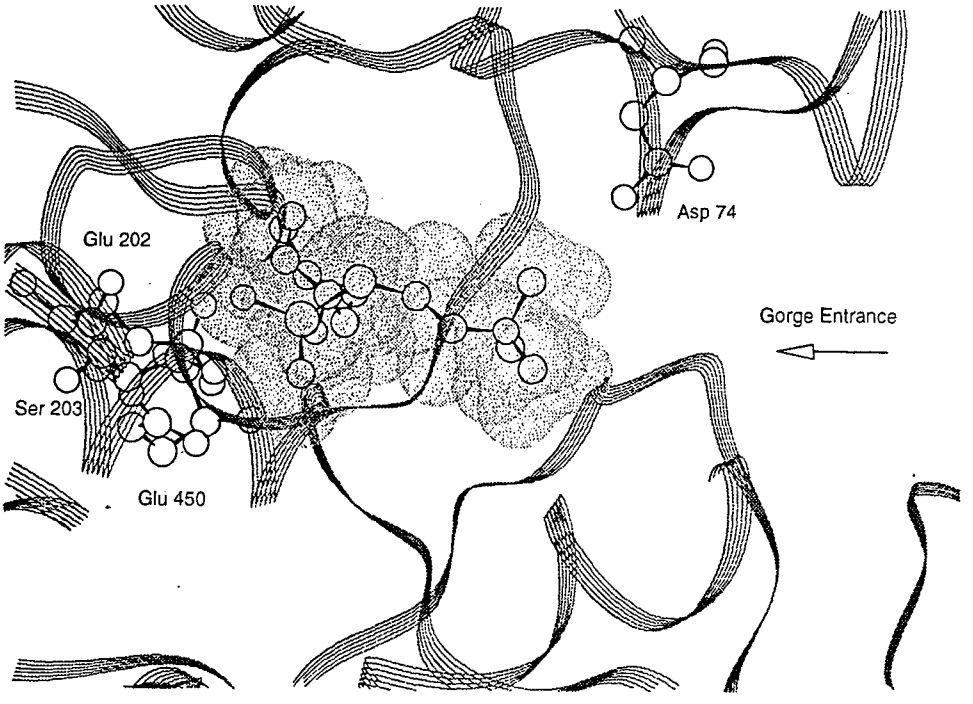

FIGURE 4 Sp-cycloheptyl methylphosphonothiocholine docked in the active center of acetylcholinesterase. The view is a 90° side view from Figure 3 to show the orientation of the thiocholine moiety with respect to the gorge exit and Asp 74. A portion of the cholinesterase molecule is cut away in order to show an unobstructed view of the inhibitor (cf: refs. [8,9] for details).

bic influence would be virtually identical for the two enantiomers.

DISCUSSION

The findings reviewed here show two distinct linkage relationships. Chiral preference is dependent on the dimensions of the acyl pocket which are governed by the amino acid side chains directed towards the active center. Thus, chiral selectivity is largely independent of the charge and apparent dimensions of the leaving group. By contrast, the anionic side chain (Asp 74) near the gorge entry is linked to the charge on the leaving group and the enhanced reactivity of the cationic alkylphosphonates is eliminated by the isosteric substitution of an Asn at

TABLE III Rates[a] of transphosphonylation by Rp- and Sp-cycloheptyl methylphosphonyl thioate possessing charged leaving groups

	Leaving Group					
	-S-CH_3			-S-CH_2-CH_3		
Enzyme	Sp	Rp	Sp/Rp	Sp	Rp	Sp/Rp
AChE (wild type)	310	1.7	180	74	0.16	460
Phe 295 Leu	340	2.9	120	160	1.0	160
Phe 297 Ile	55	22	2.5	55	26	2.1

[a]Rate constants are given as 10^3/Mmin; the standard error of the mean from typically three experiments was 10–15%. Data were obtained from reference [8].

this position. Although this substitution affects rates of reaction markedly, chiral selectivity is largely unaffected.

The diminished reactivity of the Rp enantiomer results from steric constraints precluding the simultaneous (a) positioning of the phosphorus to enable attack by the γ-oxygen of the serine, (b) insertion of the oxygen in the oxyanion hole, and (c) positioning the leaving group to extend out the gorge exit. Mutation of Phe 297 to Ile eliminates the apparent steric hindrance, and this would account for the greatly increased reactivity of the Rp compound.

Recently, it was shown that the boundary region to the active center contains a rather thin wall and a conformational change might yield a "back door" opening suitable for product removal [21]. This region outlines a portion of the choline binding site. Should such an alternative portal exist, it would be better situated for the thiocholine exit of the Rp enantiomers, yet we find the Rp enantiomers acylate some 230-fold more slowly than the Sp enantiomers. Hence, the transphosphonylation rates do not lend support to a "back door" hypothesis for removal of a thiocholine moiety.

Over sixty years ago, Eason and Stedman proposed that stereospecificity in drug action and in catalytic processes was a consequence of a three-point attachment between the chiral compound and a dissymmetric macromolecular surface [22]. Although the original binding site was often modeled on a planar surface, the hypothesis has withstood the tests of time to explain stereospecificity of drug action. Even with the addition of three-dimensional structures as templates for the interaction of small ligands, the principle of a *minimal* three-point attachment can be shown to be applicable to chiral ligands and AChE.

Shown in Figure 5 is an analysis of docking of a pentavalent transition state for the Rp and Sp enantiomers of cycloheptyl methylphosphonothiocholine using molecular dynamics with further minimization to achieve a low-energy conformation of the docked ligand [9]. Three dimensions can be considered here. The first is in the reaction bond distance and is displayed in the Z-axis direction; this becomes fixed for the γ-oxygen on serine 203 attacking the phosphorus. Although the precise transition state cannot be described, it is assumed that the attacking serine and the leaving group adopt apical positions. In turn, the three remaining groups would be equatorially disposed around the phosphorus. Hence the plane of phosphorus and the three equatorial groups define the Z dimension. A fixed optimal reaction distance should hold irrespective of whether we consider the transition state for transphonylation to be associative or dissociative in nature. The remaining two positions, the oxygen in the oxyanion hole and the leaving group directed out of the gorge, are then analyzed in the docked low-energy conformations minimized following molecular dy-

TABLE IV Rates[a] of transphosphonylation by Rp- and Sp-cycloheptyl methylphosphonyl thioate possessing charged and uncharged leaving groups

	Leaving Group								
	$-S-CH_2-CH_2-N^+(CH_3)_3$			$-S-CH_3$			$-S-CH_2-CH_3$		
Enzyme	Sp	Rp	Sp/Rp	Sp	Rp	Sp/Rp	Sp	Rp	Sp/Rp
AChE (wild type)	190,000	820	230	310	1.7	180	74	0.16	460
Asp 74 Asn	1,400	8.0	180	530	2.3	230	190	0.41	460
Glu 202 Gln	21,000	130	160	14	0.060	230	2.3	0.014	160
Glu 450 Gln	1,400	23	61	9	0.050	180	14	0.018	780

[a]Rate constants are given as 10^5/Mmin; the standard error of the mean from typically three experiments was 10–15%. Data were obtained from reference [9].

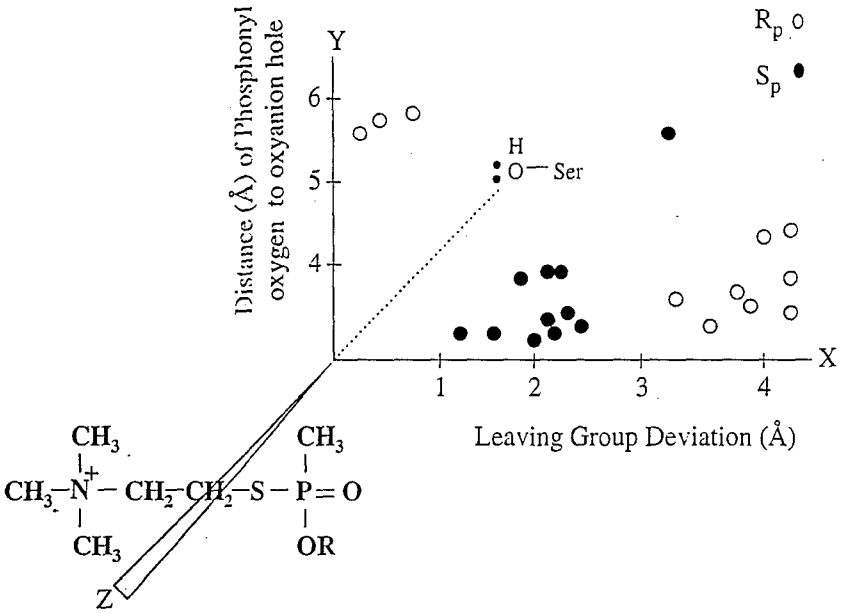

FIGURE 5 Molecular dynamics simulation followed by energy minimization of a docked Sp (closed circles) and Rp (open circles) cycloheptyl methylphosphonothiocholine in a reversible complex with acetylcholinesterase. The phosphorus group is docked within bonding distance with the γ-oxygen of serine 203 in the enzyme. This position along the Z-axis then becomes defined by the plane X,Y. A productive conformation is assumed to require: (a) the appropriate Ser-O-P distance on the Z axis; (b) insertion of the phosphonyl oxygen in the oxyanion hole (Y axis)—a mean hydrogen bonding distance of 3–4 Å from the amide backbone hydrogens of Gly 121, Gly 122 and Ala 204; and (c) an orientation of the leaving group directed towards gorge entrance. The ideal position is assumed to be 180° from the attacking serine oxygen placing the serine oxygen and the leaving group in apical positions and the remaining three groups in equatorial positions. The deviations reflect the difference in distances for the quaternary nitrogen between the energy minimized position and that expected for apical positioning (180°) of the serine γ-oxygen and the leaving group (9).

namics. Clearly, only the Sp enantiomer reproducibly yields the simultaneous optimization of positions for the phosphonyl oxygen and the leaving group. In the case of the oxyanion hole, interaction is dependent on hydrogen bonding distances between the three candidate donor hydrogens (amide hydrogens on Gly121, Gly122 and Ala201) and the phosphonyl oxygen. Data in Figure 5 are represented as an average of the three distances for these potential hydrogen bonds. For the thiocholine leaving group, we show the data as a deviation from the apical position which would be 180° from the γ-oxygen of the serine. Hence, this analysis and the positioning of the three critical groups are compatible with the overall kinetics.

Our examination of enantiomeric selectivity is part of a larger investigation of ligand interactions with the active center of the cholinesterases. Site-specific mutations have been made at other positions on AChE and the kinetics analyses for three classes of charged and uncharged congeneric ligands have been examined [8,9]. The trifluoroketones conjugate directly with the active center serine to form a hemiketal [6,7] without loss of a leaving group. Their reaction with AChE approaches the diffusion limitation. Second, the alkylphosphonates, sulfonates and carbamoyl esters form relatively stable phosphonyl, sulfonyl and carbamoyl esters with the active center serine, with the loss of a leaving group. The stability of the newly formed acyl

serine intermediate typically allows for direct study of the acylation step. Third, the carboxyl esters show rapid turnover because of the near diffusion-controlled acylation step and a rapid deacylation. Under physiologic concentrations it is thought that the acylation and deacylation steps are of comparable magnitude allowing for a fractional build up of acylenzyme intermediate [23]. Only steady-state kinetics for catalysis of the carboxyl esters can be readily monitored, and the characterization of intermediate species has proven more elusive.

Enantiomeric selectivity of the alkylphosphonates is of considerable practical significance. The toxic nerve gas soman contains two chiral centers, one on the phosphorus and one on the attached carbon substituent yielding four diastereomers. The four diastereomers have very different rates of reaction and overall stability in the body [24]. Similarly, the widely used insecticide malathion possesses a chiral center on a carbon side chain. By virtue of rearrangement around the phosphorus, it can form diastereomers possessing distinct toxicities [25].

Such enantiomeric or diastereomeric selectivity can be understood on the basis of fundamental steric and electrostatic properties of the groups surrounding the asymmetric phosphorus, and the interactions they encounter with the side chains of amino acids in spatial proximity with the reactive serine. As seen here, the chemistry of organophosphorus agents in combination with techniques of site-directed mutagenesis allow not only estimation of the prevalent physical interactions at play, but the identification of the individual amino acids that govern such interactions.

Acknowledgment

This work was supported by USPHS and DAMD Grants: GM 18360, ES 03085 and 17-95-1-5027.

References

[1] Schumacher, M., Camp, S., Maulet, Y., Newton, M., MacPhee-Quigley, K., Taylor, S. S., Friedmann, T. and Taylor, P. **(1986)**. Primary structure of *Torpedo californica* acetylcholinesterase deduced from cDNA sequence. *Nature*, 319, 407–409.

[2] Taylor, P. and Radić, Z. **(1994)**. The cholinesterases: from genes to proteins. *Ann. Rev. Pharmacol. & Toxicol.*, 34, 281–320.

[3] Cygler, M., Schrag, J. D., Sussman, J. L., Harel, M., Silman, I., Gentry, M. K. and Doctor, B. P. **(1993)**. Relationship between sequence conservation and three-dimensional structures in a large family of esterases, lipases and related proteins. *Protein Science*, 2, 366–382.

[4] Sussman, J. L., Harel, M., Frolow, F., Oefner, C., Goldman, A., Toker, L. and Silman, I. **(1991)**. Atomic structure of acetylcholinesterase from *Torpedo californica*: a prototypic acetylcholine-binding protein. *Science*, 253, 872–879.

[5] Bourne, Y., Taylor, P. and Marchot, P. **(1995)**. Acetylcholinesterase inhibition by fasciculin: crystal structure of the complex. *Cell*, 83, 503–512.

[6] Nair, H. K., Seravalli, J., Arbuckle, T. and Quinn, D. M. **(1994)**. Molecular recognition in acetylcholinesterase catalysis: free-energy correlations for substrate turnover and inhibition by trifluoroketone transition state analogs. *Biochemistry*, 33, 8566–8576.

[7] Harel, M., Quinn, D. M., Nair, H. K., Silman, I. and Sussman, J. L. **(1996)**. The X-ray structure of a transition state analog complex reveals the molecular origins of catalytic power and substrate specificity of the cholinesterases. *J. Am. Chem. Soc.*, 118, 2340–2346.

[8] Hosea, N. A., Berman, H. A. and Taylor, P. **(1995)**. Specificity and orientation of trigonal carboxyl esters and tetrahedral alkylphosphonyl esters in cholinesterases. *Biochemistry*, 34, 11528–11536.

[9] Hosea, N. A., Radić, Z., Tsigelny, I., Berman, H. A., Quinn, D. M. and Taylor, P. **(1996)**. Aspartate 74 as a primary determinant in acetylcholinesterase governing specificity to cationic organophosphonates. *Biochemistry*, 35, 10995–11004.

[10] Berman, H. A. and Leonard, K. **(1989)**. Chiral reactions of acetylcholinesterase probed with enantiomeric methylphosphonothioates: non-covalent determinants of enzyme chirality. *J. Biol. Chem.*, 264, 3942–3950.

[11] Berman, H. A. and Decker, M. M. **(1986)**. Kinetic, equilibrium and spectroscopic studies on dealkylation of alkylorganophosphonyl acetylcholinesterase. *J. Biol. Chem.*, 261, 10646–10652.

[12] Berman, H. A. and Decker, M. M. **(1989)**. Chiral nature of covalent methylphosphonyl conjugates of acetylcholinesterase. *J. Biol. Chem.*, 264, 3951–3956.

[13] Vellom, D. C., Radić, Z., Li, Y., Pickering, N. A., Camp, S. and Taylor, P. **(1993)**. Amino acid residues controlling acetylcholinesterase and butyrylcholinesterase specificity. *Biochemistry*, 32, 12–17.

[14] Ordentlich, A., Barak, D., Kronman, C., Flashner, Y., Leitner, M., Segall, Y., Ariel, N., Cohen, S., Velan, B. and Shafferman, A. **(1993)**. Dissection of the human acetylcholinesterase active center determinants of substrate specificity. *J. Biol. Chem.*, 268, 17083–17095.

[15] Radić, Z., Pickering, N. A., Vellom, D. C., Camp, S. and

Taylor, P. **(1993)**. Three distinct domains in the cholinesterase molecule confer selectivity for acetyl- and butyrylcholinesterase inhibitors. *Biochemistry*, 32, 12074–12084.

[16] Harel, M., Sussman, J. L., Krejci, E., Bon, S., Chanal, P., Massoulié, J. and Silman, I. **(1992)**. Conversion of acetylcholinesterase to butyrylcholinesterase, modeling and mutagenesis. *Proc. Natl. Acad. Sci. USA*, 89, 10827–10831.

[17] Taylor, P. and Jacobs, N. M. **(1974)**. Interaction between *bis*-quaternary ammonium ligands and acetylcholinesterase—complex formation studies by fluorescence quenching. *Mol. Pharmacol.*, 10, 93–107.

[18] Grochulski, P., Bouthillier, F., Kazlauskas, R. J., Serreqi, A. N., Schrag, J. D., Ziomek, E. and Cygler, M. **(1994)**. Analogs of reaction intermediates identify a unique substrate binding sites in *Candida rugosa*. *Biochemistry*, 33, 3494–3500.

[19] Zhao, Q., Kovach, I. M., Bencsura, A. and Papathanassia, A. **(1994)**. Enantioselective and reversible inhibition of trypsin and alpha-chymotrypsin by phosphonate esters. *Biochemistry*, 33, 8128–8138.

[20] Cygler, M., Grochulski, P., Kazlauskas, R. J., Schrag, J. D., Bouthillier, F., Rubin, B., Serreqi, A. N. and Gupta, A. K. **(1994)**. A structural basis for the chiral preferences of lipases. *J. Am. Chem. Soc.*, 116, 3180–3186.

[21] Gilson, M. K., Straatsma, J. P., McCammon, J. A., Ripoll, D. R., Faerman, C. H., Axelsen, P. H., Silman, I. and Sussman, J. L. **(1994)**. Open "back door" in a molecular dynamics simulation of acetylcholinesterase. *Science*, 263, 1276–1278.

[22] Eason, L. M. and Stedman, E. **(1933)**. Studies on the relation between chemical constitution and physiological action. *Biochem. J.*, 27, 1257–1266.

[23] Froede, H. C. and Wilson, I. B. **(1984)**. Direct determination of acetyl enzyme intermediate in the acetylcholinesterase-catalyzed hydrolysis of acetylcholine and acetylthiocholine. *J. Biol. Chem.*, 259, 11010–11013.

[24] de Jong, L. P., van Dijk, C., Berhitoe, D. and Benschop, H. P. **(1993)**. Hydrolysis and binding of a toxic stereoisomer of soman in plasma and tissue homogenates. *Biochem. Pharm.*, 46, 1413–1419.

[25] Berkman, C. E., Thompson, C. M. and Perrin, S. R. **(1993)**. Synthesis, absolute configuration and analysis of malathion, malaoxon and isomalathion enantiomers. *Chem. Res. Toxicol.*, 6, 718–723.

[26] Auld, V. J., Fetter, R. D., Broadie, K. and Goodman, C. S. **(1995)**. Gliotactin, a novel transmembrane protein on peripheral glia, is required to form the blood-brain barrier in *Drosophila*. *Cell*, 81, 757–767.

[27] Ichtchenko, K., Nguyen, T. and Sudhof, T. C. **(1996)**. Structures, alternative splicing and neurexin binding of multiple neuroligins. *J. Biol. Chem.*, 271, 2676–2682.

Biochemical Pharmacology, Vol. 54, pp. 269–274, 1997.

ELSEVIER

ISSN 0006-2952/97/$17.00 + 0.00
PII S0006-2952(97)00180-9

Mutant Acetylcholinesterases as Potential Detoxification Agents for Organophosphate Poisoning*

Ashima Saxena,†‡ Donald M. Maxwell,§ Daniel M. Quinn,‖ Zoran Radić,¶ Palmer Taylor¶ and B. P. Doctor†

†Walter Reed Army Institute of Research, Washington, DC 20307, U.S.A.; §U.S. Army Medical Research Institute of Chemical Defense, Aberdeen Proving Ground, MD 21010; ‖University of Iowa, Iowa City, IA 52242, U.S.A.; and ¶University of California at San Diego, La Jolla, CA 92093, U.S.A.

ABSTRACT. It has been demonstrated that cholinesterases (ChEs) are an effective mode of pretreatment to prevent organophosphate (OP) toxicity in mice and rhesus monkeys. The efficacy of ChE as a bioscavenger of OP can be enhanced by combining enzyme pretreatment with oxime reactivation, since the scavenging capacity extends beyond a stoichiometric ratio of ChE to OP. Aging has proven to be a major barrier to achieving oxime reactivation of acetylcholinesterase (AChE) inhibited by the more potent OPs. To further increase the stoichiometry of OP to ChE required, we have sought AChE mutants that are more easily reactivated than wild-type enzyme. Substitution of glutamine for glutamate (E_{199}) located at the amino-terminal to the active-site serine (S_{200}) in *Torpedo* AChE generated an enzyme largely resistant to aging. Here we report the effect of the corresponding mutation on the rate of inhibition, reactivation by 1-(2-hydroxyiminomethyl-1-pyridinium)-1-(4-carboxyaminopyridinium)-dimethyl ether hydrochloride (HI-6), and aging of mouse AChE inhibited by C(+)P(−)- and C(−)P(−)-epimers of soman. The E_{202} to Q mutation decreased the affinity of soman for AChE, slowed the reactivation of soman-inhibited AChE by HI-6, and decreased the aging of mutant AChE. These effects were more pronounced with C(−)P(−)-soman than with C(+)P(−)-soman. *In vitro* detoxification of soman and sarin by wild-type and E_{202}Q AChE in the presence of 2 mM HI-6 showed that, E_{202}Q AChE was 2–3 times more effective in detoxifying soman and sarin than wild-type AChE. These studies show that these recombinant DNA-derived AChEs are a great improvement over wild-type AChE as bioscavengers. They can be used to develop effective methods for the safe disposal of stored OP nerve agents and potential candidates for pre- or post-exposure treatment for OP toxicity. BIOCHEM PHARMACOL 54;2:269–274, 1997. © 1997 Elsevier Science Inc.

KEY WORDS. organophosphate; acetylcholinesterase inhibition; aging; stereoisomers of soman; reactivation; bioscavenger

OP** reacts with AChE (EC 3.1.1.7) and BChE (EC 3.1.1.8) to produce phosphylated enzyme conjugates with the active-center serine (S_{200}) [1, 2]. These conjugates, while relatively slow in turnover, have two dominant modes of reaction [2–7]. Spontaneous reactivation results from cleavage of the serine—O—P bond and results in the regeneration of active-site serine. ChEs inhibited by OPs can also be reactivated by various oxime nucleophiles such as 2-PAM and HI-6. However, they are only effective if the ChE–OP complex has not undergone a prior aging reaction [2]. The capacity of an oxime to regenerate active enzyme depends on the structure of inactivating OP, the structure of oxime, and the source of ChE [8].

Aging results from cleavage of the alkoxy—O—P bond, forming the corresponding P—O^- containing conjugates that can no longer be reactivated [2, 3, 8]. The rate of aging depends on the structure of OP, the source of enzyme, pH, temperature, and ionic strength of the solution [3, 9, 10]. Analysis of the kinetics and pH profiles of aging suggests two potential mechanisms for aging: a general acid-catalyzed reaction and one catalyzed by a nucleophile/activated H_2O. The acid or low pH-catalyzed rate of aging appears most rapid with OP–AChE conjugates containing tertiary alkoxy groups, followed by secondary and primary alkoxy groups. This suggests that a carbonium ion may serve as an intermediate [2, 4, 11].

In particular, ChEs inhibited by the nerve agent soman are refractory to reactivation by oximes because they age very rapidly [3]. Studies of the pH dependence of the dealkylation reaction of soman-inhibited AChE indicated participation of a residue with pK 4.5 and another residue with pK 6.0 [3, 10]. Based on the X-ray crystal structure of

* A portion of this report was presented at the Fifth International Symposium on 'Chemical and Biological Warfare Agents' held 11–16 June 1995, in Stockholm, Sweden.

‡ Corresponding author. Tel. (202) 782-0087; FAX (202) 782-6304.

** *Abbreviations:* BChE, butyrylcholinesterase; ChE, cholinesterase; FBS AChE, fetal bovine serum acetylcholinesterases; HI-6, 1-(2-hydroxyiminomethyl - 1 - pyridinium) - 1 - (4 - carboxyaminopyridinium)-dimethyl ether hydrochloride; OP, organophosphate; 2-PAM, 2-(hydroxyiminomethyl)-1-methylpyridinium iodide; sarin, O-isopropyl methylphosphonofluoridate; and soman, O-pinacolyl methylphosphonofluoridate.

Received 29 July 1996; accepted 14 February 1997.

Torpedo AChE, these residues were proposed to be E_{199} and H_{440}. Molecular modeling and site-directed mutagenesis studies with *Torpedo* AChE suggested that electrostatic interactions between the carbonium ion and the carboxylate of E_{199} could facilitate the dealkylation reaction [12, 13].

Besides aging, steric hindrance may also be important in the reactivation reaction [13, 14]. Due to the presence of two chiral centers, one at the α-carbon atom of the pinacolyl moiety and the other at the phosphorus atom, soman is a mixture of four stereoisomers. The *in vitro* toxicologic and anticholinesterase properties of the isomers of soman are very different [15]. Of the four stereoisomers, only the two P(−)-epimers are potent inhibitors of AChE [16, 17]. *In vivo* studies with mice challenged with a dose of one LD_{50} of racemic soman showed that toxicity arose primarily from the C(−)P(−)-epimer [17]. *In vitro* inhibition and reactivation studies with C(+)P(−)- and C(−)P(−)-soman-inhibited AChE indicated that the two diastereomeric-enzyme conjugates had different rates of reactivation, which depend on the source of the enzyme [18].

Recently we showed that mutation of glutamate (E_{199}) located at the amino-terminal to the active-site serine (S_{200}) in *Torpedo* AChE generated a mutant AChE that was largely resistant to aging [12]. The loss of charge appeared to affect the intrinsic rate of aging of mutant AChE, suggesting that the negative charge on E_{199} facilitated the removal of the alkoxy group. Here we have extended these studies using mouse $E_{202(199)}Q^*$ AChE to determine the effect of this mutation on the rate of inhibition, reactivation by HI-6, and aging of mouse AChE inhibited by the two P(−)-epimers of soman. The *in vitro* detoxification of soman and sarin by wild-type and $E_{202}Q$ AChE in the presence of 2 mM HI-6 was also studied.

MATERIALS AND METHODS

Materials

Wild-type and $E_{202}Q$ mutant of mouse AChE were expressed, purified, and characterized with respect to catalytic parameters as described [20]. One nanomole of wild-type AChE was equivalent to 132 units, and 1 nmol of $E_{202}Q$ mutant AChE was equivalent to 60 units. Soman was obtained from the Chemical Research, Development and Engineering Center (Aberdeen Proving Ground, MD). Soman used in these experiments was 98.6% pure when analyzed by [^{31}P] nuclear magnetic resonance. The two P(−)-epimers of soman were obtained as described previously [21]. Concentrations of soman solutions were determined by titration of the solution with a known amount of FBS AChE and measurement of residual activity (1 nmol of FBS AChE is equivalent to 400 units). The oxime, HI-6, was obtained from the Division of Experimental Therapeutics, Walter Reed Army Institute of Research (Washington, DC).

Titration of AChE with Soman

Dilutions of racemic soman, or C(+)P(−)-soman, or C(−)P(−)-soman, in saline (1–10 μL), were added to wild-type or $E_{202}Q$ mutant AChE (0.5 U/mL) in 10 mM sodium phosphate, pH 8.0, containing 0.05% BSA. Samples were incubated for 30 min at room temperature and assayed for residual enzyme activity using the Ellman assay [22]. Residual AChE activity was plotted against the concentration of soman added to the reaction mixture to ascertain the stoichiometry between AChE and soman.

Inhibition of AChE with Soman

Inhibition of mouse wild-type AChE (0.1 U/mL; 0.76 nM) by soman, run in 50 mM sodium phosphate, pH 8.0, containing 0.05% BSA, was initiated by adding racemic soman (2.2 to 4.4 nM) or the two P(−)-epimers of soman (0.55 to 2.2 nM) and measuring enzyme activity at various time intervals. A similar procedure was used for $E_{202}Q$ AChE (0.1 U/mL; 1.67 nM) except that the amount of racemic soman and the two P(−)-epimers used was 4.4 to 17.6 and 2.2 to 8.8 nM, respectively. Experiments were carried out with at least four different concentrations of soman. The apparent bimolecular rate constants for the inhibition reactions measured under second-order conditions were determined by non-linear regression of the plot of $\{AChE_t/(OP_0 - [AChE_0 - AChE_t])\}$ versus time at different inhibitor concentrations [23], where $AChE_t$ is the enzyme concentration at time t, $AChE_0$ is the initial enzyme concentration at time t = 0, and OP_0 is the initial concentration of OP.

Reactivation of Soman-Inhibited AChE with HI-6

Mouse wild-type (8.0 U/mL) and $E_{202}Q$ AChE (12 U/mL) in 50 mM Tris · HCl, pH 9.5, were inhibited with stoichiometric amounts of soman or one of its P(−)-epimers for 15 min at 4°. Reactivation was started by mixing 10 μL of the soman–AChE conjugate with 90 μL of sodium phosphate, pH 8.0, containing HI-6 at a final concentration of 2 mM at 25°. Enzyme activity of aliquots of the reactivation mixture were measured at intervals of 0.5, 1, 2, 3, 4, 6, and 24 hr using the Ellman method [22]. Data for the time-course of reactivation reactions were analyzed by nonlinear regression analysis using the equation [14]:

$$\%(AChE_{reac})_t = A[1 - e^{-kt}] \quad (1)$$

where A is the percent-amplitude of the reactivatable form of soman-inhibited AChE and k is the pseudo first-order rate constant for reactivation.

* The dual numbering system gives the residue number in the species designated followed by the corresponding residue in *Torpedo* AChE [19].

pH Profile for the Aging of AChE

Mouse wild-type (8 U/mL) and $E_{202}Q$ AChE (12 U/mL) in 50 mM Tris · HCl, pH 9.5, were inhibited with stoichiometric amounts of soman or one of its P(−)-epimers for 15 min at 4°. Fifty microliters of soman–AChE conjugate was diluted into 450 μL of one of the 50 mM buffer solutions at different pH values at 25°, and the pH of all samples was monitored using the pH meter. The following buffer solutions were used: sodium acetate at pH 5.0 and 5.5; sodium phosphate at pH 6.0, 6.5, 7.0, 7.5, and 8.0; and Tris · HCl at pH 8.5. Parallel samples without soman were used to monitor the stability of enzyme at each pH. Aliquots (40 μL) were removed at various time intervals and transferred to tubes containing 10 μL of 10 mM HI-6 in 50 mM sodium phosphate, pH 8.0. Samples were incubated overnight at room temperature before assay for AChE activity using the Ellman method [22].

In Vitro Detoxification of OPs by Mouse Wild-Type and $E_{202}Q$ Mutant AChE

The incubation mixture in 50 mM sodium phosphate, pH 8.0 (total volume 0.5 mL), contained 0.05% BSA, 0.011 nmol mouse wild-type or $E_{202}Q$ AChE, 2 mM HI-6, and 0.275 nmol soman. Tubes of buffer containing enzyme alone, enzyme with HI-6, and enzyme with soman were incubated as controls. After incubating for 30 min, 10-μL aliquots from each tube were assayed for inhibition of AChE activity. Samples (10 μL) were assayed after 6 hr to measure recovery of AChE activity. The addition of soman (final concentration of 0.275 nmol) to the tube containing soman and HI-6, and buffer to the control samples followed by measurement of AChE activity was repeated until the AChE activity decreased to 10% of its original value. The detoxification of sarin by wild-type and $E_{202}Q$ AChE was conducted using a similar procedure except that the addition of 1.8 nmol of sarin was repeated every 24 hr. Residual enzyme activity was plotted against the cumulative amount of soman or sarin present in the reaction mixture.

RESULTS AND DISCUSSION

The crystal structure of the *Torpedo* AChE shows E_{199} to reside at the base of the active-center gorge, and its van der Waals surface appears to reside within 1.5 Å of that of the quaternary ammonium group of the substrate or inhibitor bound to the active center of the enzyme [24, 25]. Molecular modeling studies of the adducts of *Torpedo* AChE with the two P(−)-epimers of soman indicated that E_{199} was located at a distance of 3.3 Å from the chiral carbon of the pinacolyl moiety. Therefore, the carboxylate side chain could participate in the stabilization of the carbonium ion in the transition state for dealkylation [13]. These models were substantiated by site-directed mutagenesis studies using *Torpedo* and human AChE [12, 23].

Figure 1 shows the titration of mouse wild-type and

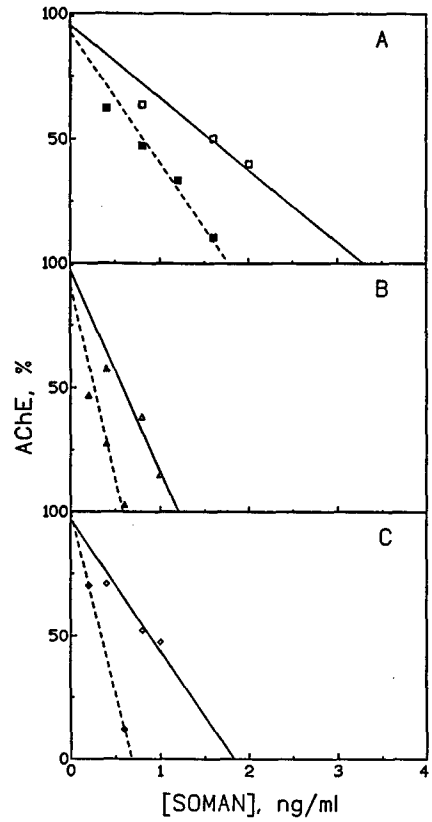

FIG. 1. Titration of mouse wild-type and $E_{202}Q$ mutant AChE with the stereoisomers of soman. Increasing amounts of racemic soman (A), or C(+)P(−)-soman (B), or C(−)P(−)-soman (C), in 1- to 10-μL aliquots, were added to wild-type (0.5 U/mL; 3.8 nM) or $E_{202}Q$ mutant AChE (0.5 U/mL; 8.35 nM) in 50 mM sodium phosphate, pH 8.0. The final concentrations of soman were 2–20 nM. Samples were incubated for 30 min and assayed for residual enzyme activity using the Ellman assay [22]. Data for wild-type (---) and $E_{202}Q$ (—) AChE were plotted as percent of residual AChE activity at various concentrations of soman. The data shown are representative of three experiments.

$E_{202}Q$ AChE with racemic soman (panel A) and its two P(−)-epimers (panels B and C). At the concentrations of soman employed, the approach to inhibition appeared practically stoichiometric for wild-type and mutant AChE. Differences in the titration curves for wild-type and $E_{202}Q$ AChE with racemic soman, C(+)P(−)-soman, and C(−)P(−)-soman reflect the 2-fold difference in the k_{cat} for acetylthiocholine hydrolysis between wild-type and mutant enzymes.

To examine the role of $E_{202(199)}$ in the stereoselectivity of AChE for the two P(−)-epimers of soman, we compared the bimolecular rate constants for the inhibition of wild-type and $E_{202}Q$ AChE by racemic soman and the two P(−)-epimers of soman (Table 1). Racemic soman is a mixture of four stereoisomers of which only the two P(−)-epimers are potent inhibitors of AChE [16, 17]. Therefore, the values for the bimolecular rate constants for wild-type and mutant AChE with racemic soman should be effectively twice that reported in Table 1. A 2-fold difference in the bimolecular rate constant of wild-type AChE

TABLE 1. Bimolecular rate constants for the inhibition of mouse acetylcholinesterase by stereoisomers of soman

Inhibitor	$k \times 10^{-8}$ (M^{-1} min^{-1})	
	Wild-type	$E_{202}Q$
Racemic soman	0.48 ± 0.06	0.048 ± 0.002
C(+)P(−)-Soman	1.20 ± 0.27	0.200 ± 0.017
C(−)P(−)-Soman	0.69 ± 0.09	0.044 ± 0.004

Values for the bimolecular rate constants of inhibition, k, were measured under second-order reaction conditions as described in Materials and Methods. Values are the means ± SD from three experiments.

for the two P(−)-epimers was observed compared with a 4.5-fold difference observed for $E_{202}Q$ AChE. Previous inhibition studies with stereoisomers of soman also showed that the C(+)P(−)-soman was a slightly more potent inhibitor than the C(−)P(−)-epimer. Bovine erythrocyte AChE exhibited a 6-fold difference in the bimolecular rate constants for the two P(−)-epimers as compared with a 1.6-fold difference observed for electric eel AChE [17, 18]. The difference in the bimolecular rate constants of wild-type and $E_{202}Q$ AChE for racemic soman, C(+)P(−)-soman, and C(−)P(−)-soman was 10-, 6-, and 16-fold, respectively. These results suggest that the loss of charge on E_{202} decreased the reactivity of soman for mutant AChE and the reactivity of C(−)P(−)-soman was affected more than that of the C(+)P(−)-epimer.

The influence of E_{202} to Q mutation on HI-6-induced reactivation of wild-type and $E_{202}Q$ AChE inhibited by the two P(−)-epimers of soman was also studied. For AChE inhibited with racemic soman or either of the two P(−)-epimers, the rate of reactivation of wild-type AChE was 7- to 8-fold faster than that of $E_{202}Q$ AChE (Table 2 and Fig. 2A–C). For both enzymes, C(−)P(−)-inhibited AChE reactivated at about half the rate of C(+)P(−)-inhibited AChE. Similar studies with racemic 7-(methylethoxyphosphinyloxy)-1-methylquinolinium iodide (MEPQ)-inhibited mouse AChE showed that the mutation of E_{202} to Q resulted in a 16- to 33-fold reduction in the rate of reactivation of the enzyme by 2-PAM and HI-6 [14]. Reactivation of wild-type AChE inhibited with either epimer of soman was rapid and virtually complete (Fig. 2, panels B and C), as compared with $E_{202}Q$ AChE, which could be reactivated to about 70% from the AChE-C(−)P(−)soman conjugate (Fig. 2C). The mutation affects the rate of reactivation as well as the extent of reactivation especially for C(−)P(−)-soman-AChE. These results are consistent with molecular modeling studies, which showed that steric hindrance between the methyl group at the chiral carbon of C(−)P(−)-soman and H_{440} can reduce the efficiency of nucleophilic reactivation of C(−)P(−)-soman-AChE compared with C(+)P(−)-soman-AChE [13]. The results are also consistent with *in vitro* studies with human, electric eel, and plaice AChE, which demonstrated that reactivation of C(+)P(−)-soman-AChE by HI-6 was more effective than the reactivation of C(−)P(−)-soman-AChE [17, 18, 26, 27].

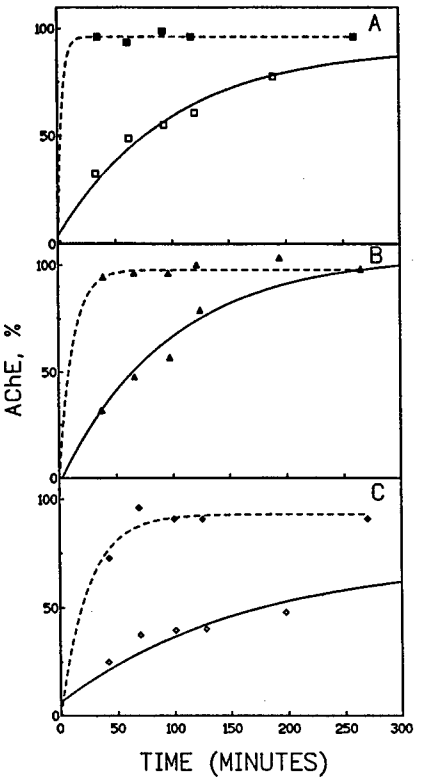

FIG. 2. Time–course for the reactivation of soman-inhibited mouse wild-type and $E_{202}Q$ mutant AChE with 2 mM HI-6. Mouse wild-type and $E_{202}Q$ AChE (60 nM; 10 U/mL) in 50 mM Tris · HCl, pH 9.5, were inhibited with stoichiometric amounts of racemic soman (A) or C(+)P(−)-soman (B) or C(−)P(−)-soman (C). Reactivation was started by mixing 10 μL of the soman–AChE conjugate with 90 μL of sodium phosphate, pH 8.0, containing HI-6 at a final concentration of 2 mM. Enzyme activity of aliquots of the reactivation mixture were measured at intervals of 0.5, 1, 2, 3, 4, 6, and 24 hr using the Ellman method [22]. Data for wild-type (---) and $E_{202}Q$ (—) AChE were plotted as percent of AChE control activity without soman. The data shown are representative of three experiments.

A reaction that counteracts reactivation of soman-inhibited AChE is aging. We examined the pH dependence of aging of wild-type and $E_{202}Q$ mutant AChE inhibited by soman and the two P(−)-epimers by their incubation at various pHs and subsequent measurement of the extent of reactivation by 2 mM HI-6 at pH 8.0. Unlike *Torpedo* $E_{199}Q$ AChE and human $E_{202}Q$ AChE, the rate constants

TABLE 2. Rate constants for the reactivation of soman-inhibited mouse acetylcholinesterase by 2 mM HI-6

Inhibitor	k (min^{-1})	
	Wild-type	$E_{202}Q$
Racemic soman	0.07 ± 0.02	0.01 ± 0.002
C(+)P(−)-Soman	0.08 ± 0.01	0.01 ± 0.002
C(−)P(−)-Soman	0.04 ± 0.01	0.006 ± 0.001

Values for the rate constants for the reactivation of soman-inhibited AChE, k, were obtained by analyzing the data for the time course of the reactivation reactions using equation 1 [14]. Values are the means ± SD from three experiments.

TABLE 3. pH Dependence of the rate constants for the aging of mouse wild-type and $E_{202}Q$ mutant acetylcholinesterases

	k (min^{-1})*					
	Racemic soman		C(+)P(−)-Soman		C(−)P(−)-Soman	
pH	Wild-type	$E_{202}Q$	Wild-type	$E_{202}Q$	Wild-type	$E_{202}Q$
5.0	0.39 ± 0.04†	0.11 ± 0.02†	0.27 ± 0.04†	0.066 ± 0.01	0.35 ± 0.05†	0.04 ± 0.01
6.2	0.23 ± 0.01†	0.04 ± 0.01	0.33 ± 0.05†	0.035 ± 0.01	0.27 ± 0.04†	0.02 ± 0.002
6.5	0.19 ± 0.02†	0.05 ± 0.01	0.19 ± 0.01†	0.025 ± 0.005	0.25 ± 0.04†	0.01 ± 0.003
6.8	0.21 ± 0.03†	0.04 ± 0.014	0.21 ± 0.03†	0.024 ± 0.007	0.19 ± 0.02†	0.022 ± 0.016
7.3	0.07 ± 0.01	0.003 ± 0.001	0.066 ± 0.01	0.006 ± 0.001	0.09 ± 0.01	0.003 ± 0.001
7.9	0.023 ± 0.005	0.003 ± 0.001	0.036 ± 0.01	0.003 ± 0.001	0.05 ± 0.01	ND‡
8.5	0.03 ± 0.008	ND	0.02 ± 0.006	ND	0.04 ± 0.01	ND

* Determined by non-linear regression analyses of kinetic data. Values are averages ± the range from two experiments.
† Estimates from the residual portion of the kinetic profiles.
‡ ND: Aging not detected over a 24-hr period.

for the aging of mouse $E_{202}Q$ mutant AChE were only 8- to 24-fold lower at pH 7.0 to 7.5 than wild-type AChE [12, 23]. At pH values below 7.3, aging of the wild-type enzyme was too rapid to measure the aging constants accurately. No differences in the rate constants for the aging of wild-type AChE inhibited with C(+)P(−)- and C(−)P(−)-soman were observed. These results are consistent with previous observations made with human, eel, and bovine erythrocyte AChE, which showed that the rate of aging was independent of the configuration at the α-carbon atom of the pinacolyl moiety of soman [17, 27]. For $E_{202}Q$ AChE, at pH 8.0 and above, the rate of aging was so slow that it could not be measured under present experimental conditions (Table 3). At pH values below 8.0, the rate of aging of C(+)P(−)-soman-$E_{202}Q$ AChE was two times faster than the rate of aging of C(−)P(−)-soman-$E_{202}Q$ AChE. Wild-type and $E_{202}Q$ AChE inhibited with soman or the P(−)-epimers showed an increase in the rate of aging with decreasing pH, consistent with an aging mechanism involving a carbonium-ion intermediate. A similar pH dependence for the soman-*Electrophorus* AChE and soman-*Torpedo* AChE conjugate was observed previously [3, 12]. The pH profile for the aging of soman-inhibited wild-type mouse AChE between pH 5.0 and 8.5 indicated the participation of a residue with an estimated pK ~6.4, which is in agreement with a previously reported value of 6.4 for electric eel AChE [3] and 6.0 for bovine erythrocyte AChE [10].

Aging has proven to be the major barrier to achieving oxime reactivation of AChE inhibited by the more potent OPs [28]. Recombinant enzymes without this liability would confer a superior characteristic in the development of catalytic scavengers of OPs. To test this possibility, we carried out *in vitro* detoxification of sarin and soman by wild-type and $E_{202}Q$ AChE in the presence of 2 mM HI-6 as shown in Figure 3. In the presence of 2 mM HI-6 (the extrapolated sarin/AChE ratio was 2800 for wild-type AChE and 7200 for $E_{202}Q$ AChE), the same amount of wild-type and $E_{202}Q$ AChE could neutralize 2800- and 7200-fold molar excess of sarin, respectively (Fig. 3A). Similarly, the extrapolated soman/AChE ratio was 135 for wild-type AChE and 225 for $E_{202}Q$ AChE, suggesting that in the presence of 2 mM HI-6, the same amount of wild-type and $E_{202}Q$ AChE could detoxify 135- and 225-fold molar excess of soman, respectively (Fig. 3B). The overall effect of the reduced reactivity of $E_{202}Q$ AChE with soman and reduced rates for the reactivation and aging of soman-inhibited $E_{202}Q$ AChE is a 2- to 3-fold increase in detoxification of soman and sarin compared with wild-type

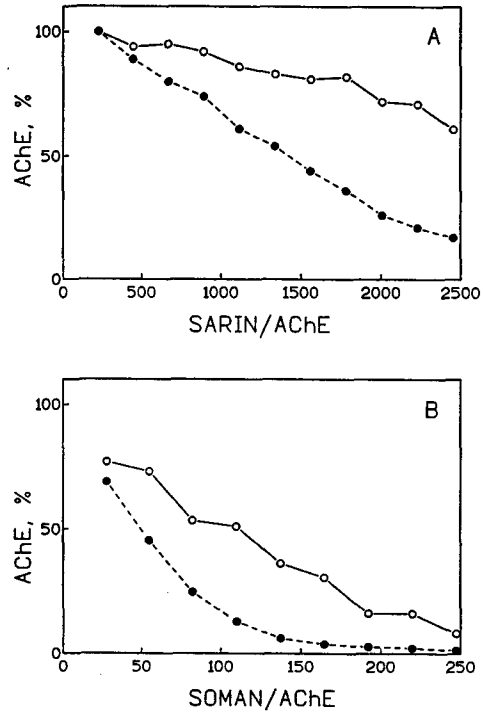

FIG. 3. *In vitro* detoxification of sarin or soman by mouse wild-type and $E_{202}Q$ mutant AChE in the presence of HI-6. The reactivation of mouse wild-type (●) and $E_{202}Q$ (○) AChE (0.011 nmol) was carried out in the presence of 50 mM sodium phosphate, pH 8.0, containing 0.05% BSA and 2 mM HI-6 after repeated additions of sarin (1.8 nmol, panel A) at 24-hr intervals, or soman (0.275 nmol, panel B) at 6-hr intervals. Residual enzyme activity was plotted against the cumulative amount of soman or sarin present in the reaction mixture. The data shown are representative of three experiments.

AChE. These results suggest that such recombinant DNA-derived AChEs, in which the glutamate located at the amino-terminal to the active-site serine is substituted by glutamine, are a great improvement over wild-type AChE as bioscavengers. These recombinant enzymes can be used to develop effective methods for the safe disposal of stored OP nerve agents and appropriate formulations for medical, surgical, and skin decontaminants and also for decontamination of materials, equipment, and the environment. The major requirements for an enzyme to be an effective bioscavenger for OP toxicity are: (a) relatively long half-life in circulation, (b) relatively high turnover number, (c) immunocompatibility, and (d) availability in sufficient quantities for use as a pretreatment drug. These recombinant DNA-derived ChEs have to fulfill these criteria before they can be tested as bioscavengers.

References

1. Froede HC and Wilson IB, Acetylcholinesterase. In: *The Enzymes* (Ed. Boyer PD), pp. 87–114. Academic Press, New York, 1971.
2. Aldridge WN and Reiner E, Enzyme inhibitors as substrates. In: *Frontiers of Biology* (Eds. Neuberger A and Tatum EL), pp. 8–36. North-Holland, Amsterdam, 1972.
3. Michel HO, Hackley BE, Berkowitz L, List G, Hackley EB, Gillilian W and Pankau M, Ageing and dealkylation of soman (pinacolylmethylphosphonofluoridate)-inactivated eel cholinesterase. *Arch Biochem Biophys* **121:** 29–34, 1967.
4. Berends F, Posthumus CH, van der Sluys I and Deierkauf FA, The chemical basis of the "aging process" of DFP-inhibited pseudocholinesterase. *Biochim Biophys Acta* **34:** 576–578, 1959.
5. Levy D and Ashani Y, Synthesis and *in vitro* properties of a powerful quaternary methylphosphate inhibitor of acetylcholinesterase. *Biochem Pharmacol* **35:** 1079–1085, 1986.
6. de Jong LPA and Kossen SP, Stereospecific reactivation of human brain and erythrocyte acetylcholinesterase inhibited by 1,2,2-trimethylpropyl methylphosphonofluoridate (soman). *Biochim Biophys Acta* **830:** 345–348, 1985.
7. Berman HA and Decker MM, Kinetic, equilibrium, and spectroscopic studies on dealkylation ('aging') of alkyl organophosphonyl acetylcholinesterase. *J Biol Chem* **261:** 10646–10652, 1986.
8. Segall Y, Waysbort D, Barak D, Ariel N, Doctor BP, Grunwald J and Ashani Y, Direct observation and elucidation of the structures of aged and nonaged phosphorylated cholinesterases by ^{31}P NMR spectroscopy. *Biochemistry* **32:** 13441–13450, 1993.
9. Keijer JH, Wolring GZ and de Jong LPA, Effect of pH, temperature and ionic strength on the aging of phosphorylated cholinesterases. *Biochim Biophys Acta* **334:** 146–155, 1974.
10. Schoene K, Steinhanses J and Wertmann A, Aging of soman-inhibited acetylcholinesterase: pH-Rate profiles and temperature dependence in absence and in presence of effectors. *Biochim Biophys Acta* **616:** 384–388, 1980.
11. Aldridge WN, Survey of major points of interest about reactions of cholinesterases. *Croatica Chem Acta* **47:** 215–233, 1975.
12. Saxena A, Doctor BP, Maxwell DM, Lenz DE, Radic Z and Taylor P, The role of glutamate-199 in the aging of cholinesterase. *Biochem Biophys Res Commun* **197:** 343–349, 1993.
13. Qian N and Kovach IM, Key active site residues in the inhibition of acetylcholinesterases by soman. *FEBS Lett* **336:** 263–266, 1993.
14. Ashani Y, Radić Z, Tsigelny I, Vellom DC, Pickering NA, Quinn DM, Doctor BP and Taylor P, Amino acid residues controlling reactivation of organophosphonyl conjugates of acetylcholinesterase by mono- and bisquaternary oximes. *J Biol Chem* **270:** 6370–6380, 1995.
15. Benschop HP, Berends F and de Jong LPA, GLC-analysis and pharmacokinetics of the four stereoisomers of Soman. *Fundam Appl Toxicol* **1:** 177–182, 1981.
16. Benschop HP, Konings CAG and de Jong LPA, Gas chromatographic separation and identification of the four stereoisomers of 1,2,2-trimethylpropyl methylphosphonofluoridate (soman): Stereospecificity of *in vitro* "detoxification" reactions. *J Am Chem Soc* **103:** 4260–4262, 1981.
17. Benschop HP, Konings CAG, van Genderen J and de Jong LPA, Isolation, anticholinesterase properties, and acute toxicity in mice of the four stereoisomers of the nerve agent soman. *Toxicol appl Pharmacol* **72:** 61–74, 1984.
18. de Jong LPA and Wolring GZ, Stereospecific reactivation by some hagedorn-oximes of acetylcholinesterases from various species including man, inhibited by soman. *Biochem Pharmacol* **33:** 1119–1125, 1984.
19. Massoulié J, Sussman JL, Doctor BP, Soreq H, Velan B, Cygler M, Rotundo R, Shafferman A, Silman I and Taylor P, Recommendations for nomenclature in cholinesterases. In: *Multidisciplinary Approaches to Cholinesterase Functions* (Eds. Shafferman A and Velan B), pp. 285–288. Plenum Press, New York, 1992.
20. Hosea NA, Radić Z, Tsigelny I, Berman HA, Quinn DM and Taylor P, Aspartate 74 as a primary determinant in acetylcholinesterase governing specificity to cationic organophosphonates. *Biochemistry* **35:** 10995–11004, 1996.
21. Benschop HP and de Jong LPA, Nerve agent stereoisomers: Analysis, isolation and toxicology. *Acc Chem Res* **21:** 368–374, 1988.
22. Ellman GL, Courtney KD, Andres V Jr and Featherstone RM, A new and rapid colorimetric determination of acetylcholinesterase activity. *Biochem Pharmacol* **7:** 88–95, 1961.
23. Ordentlich A, Kronman C, Barak D, Stein D, Ariel N, Marcus D, Velan B and Shafferman A, Engineering resistance to 'aging' of phosphylated human acetylcholinesterase. Role of hydrogen bond network in the active center. *FEBS Lett* **334:** 215–220, 1993.
24. Sussman JL, Harel M, Frolow F, Oefner C, Goldman A, Toker L and Silman I, Atomic structure of acetylcholinesterase from *Torpedo californica*: A prototypic acetylcholine binding protein. *Science* **253:** 872–879, 1991.
25. Sussman JL, Harel M and Silman I, Three dimensional structure of acetylcholinesterase. In: *Multidisciplinary Approaches to Cholinesterase Function* (Eds. Shafferman A and Velan B), pp. 95–108. Plenum Press, New York, 1992.
26. Keijer JH and Wolring GZ, Stereospecific ageing of phosphonylated cholinesterases. *Biochim Biophys Acta* **185:** 465–468, 1969.
27. Bucht G and Puu G, Aging and reactivatability of plaice cholinesterase inhibited by soman and its stereoisomers. *Biochem Pharmacol* **33:** 3573–3577, 1984.
28. Caranto GR, Waibel KH, Asher JM, Larrison RW, Brecht KM, Schutz MB, Raveh L, Ashani Y, Wolfe AD, Maxwell DM and Doctor BP, Amplification of the effectiveness of acetylcholinesterase for detoxification of organophosphorus compounds by bis-quaternary oximes. *Biochem Pharmacol* **47:** 347–357, 1994.